Climate Modelling User Group

Deliverable 3.1

Quality Assessment Report

Centres providing input: Met Office, MPI-M, ECMWF, MétéoFrance, IPSL, BSC

Revision nr.	Date	Status
0.1	26 July 2019	Agreed outline and scope of content with ESA
0.2	9 Sept. 2019	First input from partners of activity and results, Met Office, IPSL, BSC
1.0	24 Sept 2019	Input from all WP3 partners, submission to ESA
1.1	21 Feb 2020	Address comments from ESA
1.2	March 2020	Accepted by ESA
1.3	August 2020	Typo corrected
2.0	8 July 2021	Update from all WP3 partners, submission to ESA
3.1	June 2022	Update from all WP3 partners, submission to ESA
3.2	22 Aug 2022	Resubmission to ESA after addressing RIDv3.1
3.3	22 Sept 2022	Resubmission to ESA after addressing RIDv3.2

CMUG CCI+ Deliverable 3.1

Quality Assessment Report

Table of Contents

Technical report on quality assessment

1. Purpose and scope of this report

This document is the first technical report on the Quality Assessment of CCI ECVs in the CCI+ phase of the initiative. Its purpose is to assess the quality of the available versions of CCI products and update feedback to ESA and the CCI teams. This assessment is being conducted by the climate modelling and reanalysis centres in the CMUG consortium using CCI Phase 2 data and includes a wide range of data and model interactions (assimilation, boundary conditions, optimisation, reanalysis, sensitivity studies etc.). This evaluation continues to examine the following top level questions:

- Are the CCI data products of 'climate quality' i.e. is their quality adequate for use in climate modelling, reanalysis and for wider research applications?
- Are the error characteristics provided by CCI products adequate?
- Do the products meet the Global Climate Observing System (GCOS) quality requirements for satellite for Essential Climate Variables (ECV)?
- Is the quality of the products sufficient for climate service applications?

2. CMUG approach for assessing quality in CCI products

This report describes the results of CMUG CCI+ Task 3 "Assessing consistency and quality of CCI products". The work is spread across twelve Work Packages (WP) listed in Table 1.1, which includes the CCI product being assessed, and the type of climate modeling experiment.

The CMUG results presented here provide information on the accuracy, consistency and usefulness of the CCI data sets. The analysis assesses the suitability of the CCI datasets for coupled climate model and reanalysis applications and evaluates the impact of the data products on model based studies, including quantification of the uncertainties associated with both the models and the observations. This information is aimed at the CCI teams producing the data but is also of use to other modelling centres which will use CCI data in the future.

Table 1.1: Main features of CMUG WP3 on assessing consistency and quality of CCI products across ECVs.

CMUG WP 3: Quality Assessment of CCI products		Lead	Experiment type	CCI ECVs	Other ECVs
3.1	Consistency between CCI LST, SM	Météo France	Reanalysis, benchmarking	LST, SM	CGLS LAI
3.2	Consistency between CCI Snow, SM	Météo France	Reanalysis, benchmarking	Snow, SM	NOAA IMS SCF
3.3	Consistency between CCI SM, PERMAFROST	Météo France	Reanalysis, benchmarking	Permafrost, SM	
3.4	Propagation of CCI(+) observational uncertainties to climate models scales	BSC	Statistical analysis	SI, Fire	
3.5	Document SM-atmosphere feedbacks in transition regions (temperature and precipitation)	IPSL	Process analysis	SM, LST	turbulent fluxes, radiation, air temp, precip.
3.6	Better constrain evapotranspiration at the scale of climate model	IPSL	Process analysis	SM, LST	Snow, LAI, radiation, air temp
3.7	The effect of Lakes on local temperatures	Met Office	Assimilation, process understanding	Lakes, LST	Lake surface temp datasets
3.8	Evaluation of the impact of an enhanced ESA Sea Ice reanalysis (EnESA-SIR) on initialization of seasonal prediction	BSC	Hindcast	SI	
3.9	Biophysical feedbacks in the global ocean	Met Office	Assimilation, reanalyses, process study	OC, SST, SI, Sea level, Salinity, Sea State	Temp, salinity, inorganic carbon
3.10	CCI/CCI+ data to constrain mineral dust simulations	BSC	Assimilation, stat. analysis	Aerosol dust, HRLC/LC	
3.11	Dust reanalysis at the regional scale	BSC	Assimilation, stat. analysis	Aerosol dust, HRLC/LC	
3.12	Integrated assimilation of the CCI+ Sentinel 3 AOD and Sentinel 5P ozone retrievals in the IFS	ECMWF	Reanalysis	Aerosol and Ozone	

The modeling experiments are described in the following sections of this report and cover the following topics: assimilation of CCI data into climate models; cross assessments of CCI data (those which have physical links/interactions); benchmarking of models against observations; applications for reanalysis; statistical analysis; hindcasting; and Earth system process studies.

3. CMUG Quality Assessment Results

3.1 Consistency between CCI LST, and SM products

Lead partner: Météo-France
Author: Jean-Christophe Calvet

Aim

The aim of this research is to assess the consistency between CCI LST and SM products. It addresses the following scientific questions:

1. How can land ECVs' consistency can be verified?
2. Are land ECVs represented well in climate and land surface models?
3. Can EO data improve land reanalyses?
4. Can EO data improve representation of extreme events (e.g., droughts)?

Summary of Work

Combined CCI SM V06.1 surface soil moisture (SSM) data were assimilated together with the Copernicus Global Land Service (CGLS) LAI V2 product version into the ISBA land surface model of Meteo-France. The LDAS-Monde tool (Land Data Assimilation System) was used to perform this task. Root-zone soil moisture (RZSM) was analysed together with leaf biomass. The impact of the assimilation on the simulated land surface temperature (LST) was assessed at a global scale using the MODIS-derived CCI LST product, from 2002 to 2019. The latest version of the MODIS LST products was downloaded in May 2021.

Publications

The modelling and data assimilation framework was described in Albergel et al. (2020).

Interactions with the ECVs used in this experiment

Interactions with the SM and LST CCI ECV teams at the quarterly CSWG meetings and the Integration meetings. Contact was established with the CCI SM project in order to decide which version of the product to use, and to learn about the beta data that CCI LST released in late 2019. Discussions with the CCI LST and with the CCI SM teams led to choosing the MODIS LST and the Combined V06.1 SM products, respectively. The simulated open-loop and analysed RZSM was shared with the CCI SM team in order to benchmark their own demonstration RZSM product

Consistency between data products

Figure 3.1.1 shows that the assimilation can have a marked impact on the model LST bias. It is shown that over Pakistan, India, and Bangladesh area, a large part of the bias is reduced by the assimilation. Areas where a warm bias is reduced correspond to irrigated areas. The month of January corresponds to the end of the crop growing time period with irrigation. Since irrigation is not accounted for by the model, and since irrigation tends to cool the land surface, the model presents a warm bias. This is corrected to some extent by the assimilation.

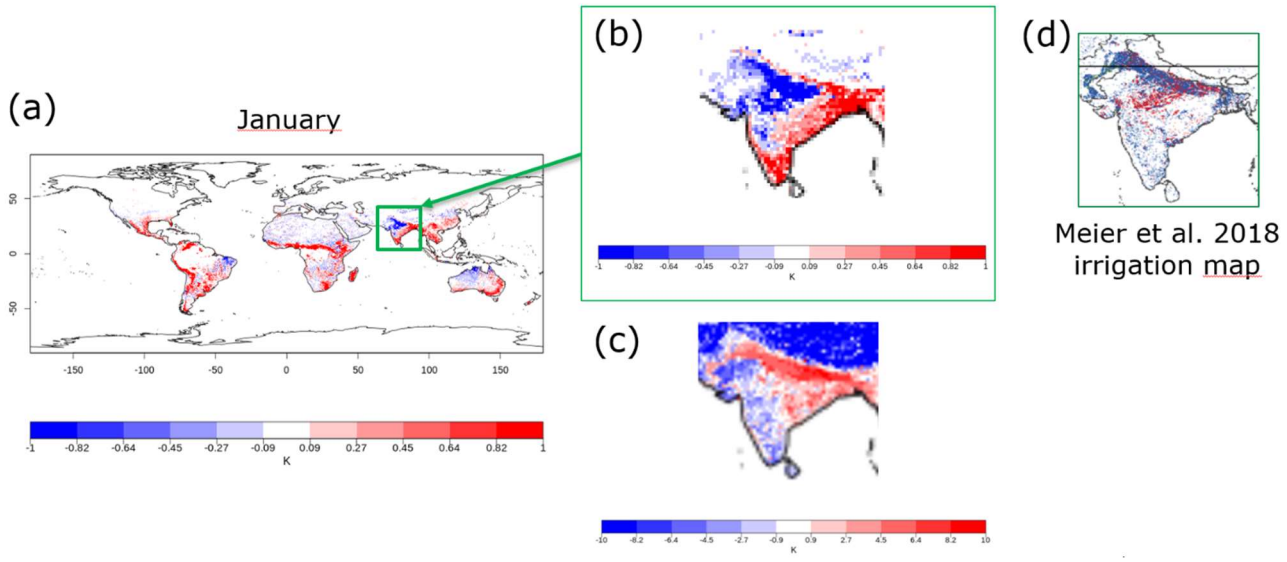

Figure 3.1.1*: Impact of assimilating CCI SM and LAI on daytime LST bias with CCI LST MODIS product in January for the 2002-2019 time period: (a) analysis minus open-loop difference in LST bias, (b) zoom of (a) over Pakistan, India, and Bangladesh, (c) open-loop LST bias, (d) extract from the irrigation map of Meier et al. (2008).*

Recommendations to the CCI ECV teams

Assimilating SSM to analyse RZSM is not sufficient. Vegetation variables such has LAI should be assimilated alone or together with SSM because assimilating LAI may have a very large impact (not shown) on RZSM and on the simulated water and carbon fluxes. Also, LAI assimilation does not present shortcomings of SSM assimilation, caused by physical decoupling between SSM and RZSM in dry conditions. The decoupling strength may vary from one model to another. It is quite strong in the multilayer soil diffusion scheme of ISBA.

3.2 Consistency between CCI Snow and SM products

Lead partner: Météo-France
Author: Jean-Christophe Calvet

Aim

The aim of this research is to assess the consistency between CCI Snow and SM products. It will address the following scientific questions:

1. How can land ECVs' consistency can be verified?
2. Are land ECVs represented well in climate and land surface models?
3. Can EO data improve land reanalyses?
4. Can EO data improve representation of extreme events (e.g. droughts)?

Summary of Work

The CCI SWE (Snow Water Equivalent) V1.1 product was assimilated in the ISBA land surface model using the LDAS-Monde tool, coupled with the CTRIP river discharge model. The experiment was conducted over Europe over the 2008-2018 time period. It was shown that the assimilation efficiently reduced the difference between SWE simulations and observations. Assimilating the CCI SWE improved the consistency between the simulated snow cover fraction (SCF) and the independent NOAA IMS SCF product. On the other hand, assimilating SWE had very little impact on the comparison between the simulated surface soil moisture (SM) and CCI SM. A hydrovalidation experiment was performed. It was based on the capability of LDAS-Monde to simulate river discharge. The comparison between simulated river discharge and in situ observations of river discharge showed that the assimilation of SWE tended to improve the simulations. The improvement was particularly large over the stations located in the Elbe river basin.

Publications

None so far.

Interactions with the ECVs used in this experiment

The snow-permafrost cross-cutting evaluation was presented at the May 2021 CSWG session and at the May 2021 Snow-CCI user workshop.

Consistency between data products

Figure 3.2.1 shows that assimilating SWE has virtually no impact on the comparison between open-loop or analysed surface soil moisture with the SM-CCI product. However, a slight improvement can be observed over Scandinavia (NW region).

Figures 3.2.2 and 3.2.3 show that assimilating SWE has a positive impact on the simulated river discharge. The impact is particularly large over the Elbe river basin.

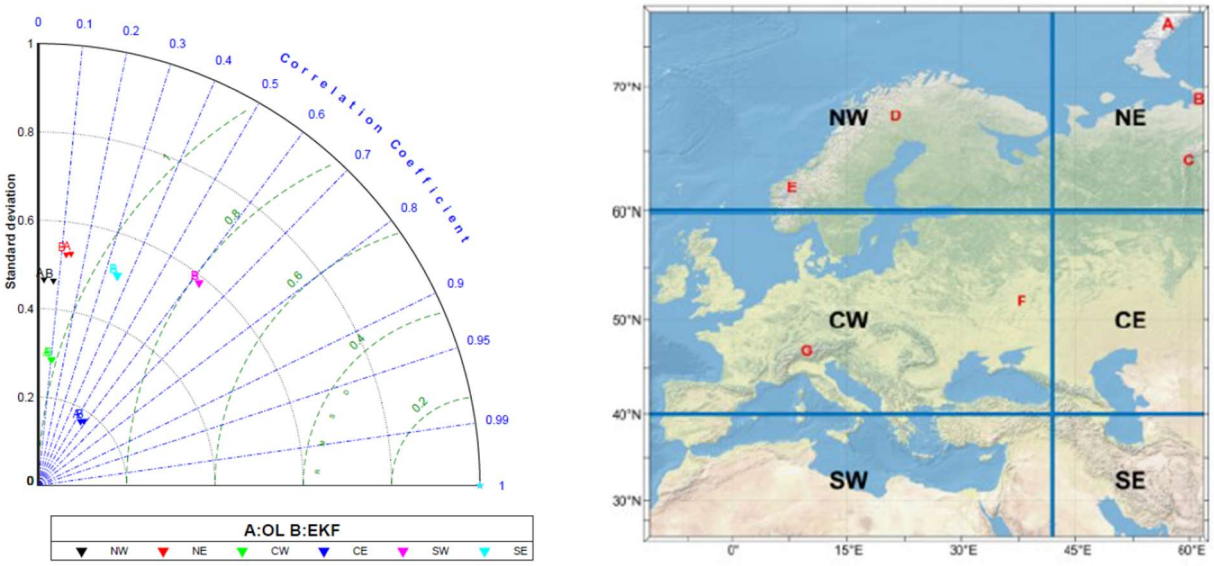

***Figure 3.2.1**: Taylor diagram comparing open-loop (OL) and analyses (EKF) of a SWE assimilation experiment in terms of surface soil moisture score. The SM-CCI V5.2 dataset is used for the comparison. Six regions are considered (right panel): NW, NE, CW, CE, SW, SE.*

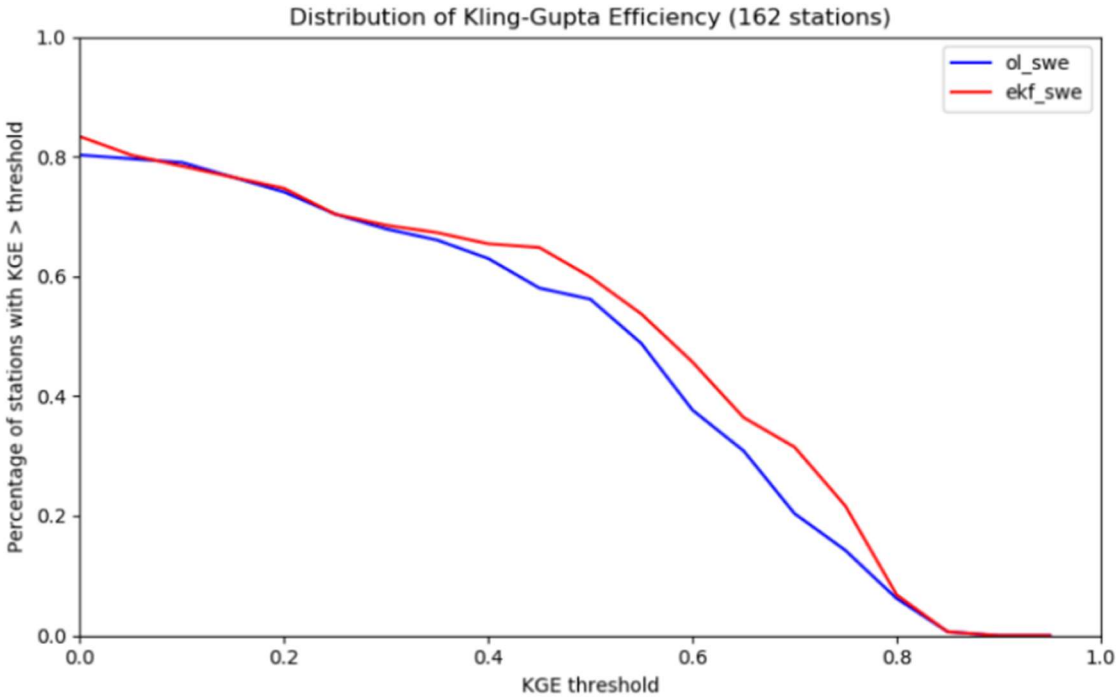

***Figure 3.2.2**: Cumulative statistical distribution function of the Kling-Gupta Efficiency score of river discharge using the open-loop simulation (blue line) and the analysis resulting from the assimilation of the SWE product (red).*

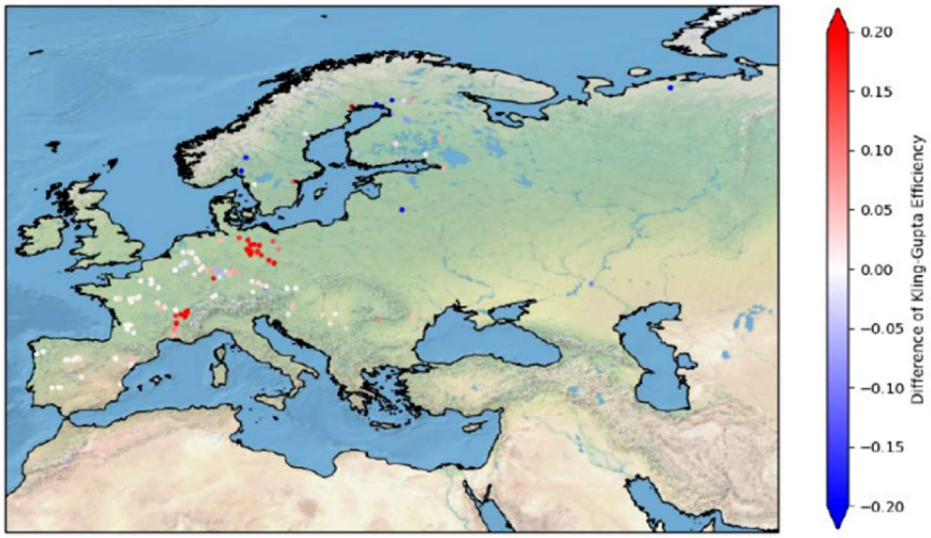

Figure 3.2.3: *Impact of assimilating SWE on the Kling-Gupta Efficiency score of river discharge over Europe.*

Recommendations to the CCI ECV teams

The lack of data over mountainous areas is an issue. The feasibility of producing at least simplified versions of snow products over mountainous areas should be investigated.

3.3 Consistency between CCI SM and PERMAFROST products

Lead partner: Météo-France
Author: Jean-Christophe Calvet

Aim

The aim of this research is to assess the consistency between CCI SM and CCI Permafrost products. It is noted that the CCI Permafrost data will be produced in a permafrost model forced with CCI SM data (amongst other data inputs) thus comparisons will be made with and without CCI SM. It will address the following scientific questions:

1. How can land ECVs consistency can be verified?
2. Are land ECVs represented well in climate and land surface models?
3. Can EO data improve land reanalyses?
4. Can EO data improve representation of extreme events (e.g. droughts)?

Summary of Work

The CCI SWE V1.1 product was assimilated in the ISBA land surface model using the LDAS-Monde tool. The experiment was conducted over Europe over the 2008-2018 time period. It was shown that the assimilation efficiently reduces the difference between SWE simulations and observations. Assimilating the CCI SWE helped reducing the model cold bias of ground temperature at all depths (1 m, 2 m, 5 m, 10 m) at high latitudes with respect to the CCI PERMAFOST mean annual ground temperature (MAGT) product.

Publications

None so far.

Interactions with the ECVs used in this experiment

The snow-permafrost cross-cutting evaluation was presented at the May 2021 CSWG session and at the May 2021 Snow-CCI user workshop. ISBA soil temperature simulations were shared with the CCI PERMAFROST team, who performed a comparison with in situ data over the Kola Peninsula (Figure 3.3.3).

Consistency between data products

No inconsistencies between ECV products were found. Figure 3.3.1 shows that assimilating the CCI SWE helped reducing the model cold bias of ground temperature at all depths (1 m, 2 m, 5 m, 10 m) at high latitudes with respect to the CCI PERMAFOST mean annual ground temperature (MAGT) product.

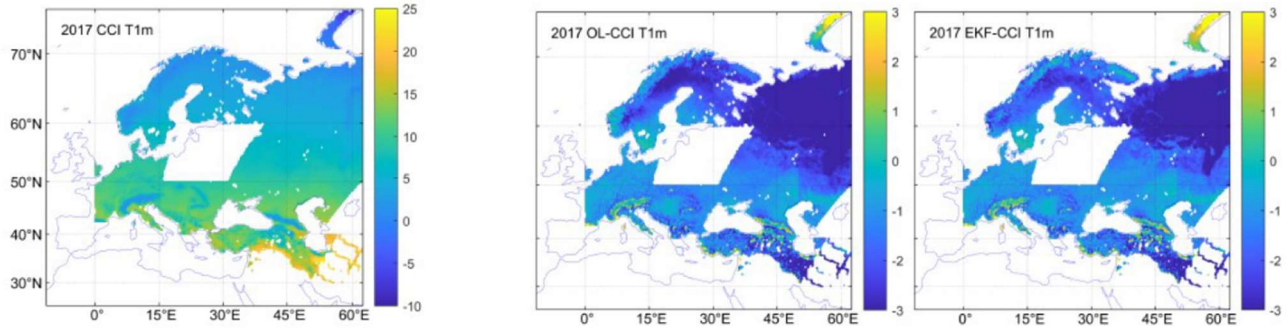

Figure 3.3.1*: Mean annual ground temperature at a depth of 1 m over Europe: (left) CCI PERMAFROST, and difference between (middle) model open-loop and CCI PERMAFROST, (right) model analysis and CCI PERMAFROST.*

Figure 3.3.2 shows that changes in the SWE annual cycle caused by the integration of SWE observations into the ISBA model had a marked impact on ground temperature at a depth of 1 m. The impact was less at 5 m but still noticeable. The larger SWE values triggered by the assimilation tended to warm the soil.

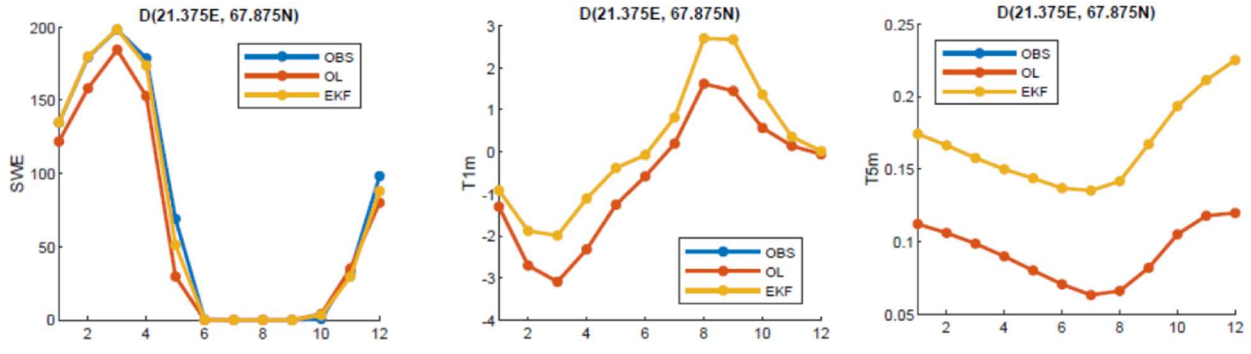

Figure 3.3.2*: Impact of (left) the assimilation of SWE on the simulated ground temperature at depths of (middle) 1 m and (right) 5 m deep soil layers over a model grid cell located at the East of Kiruna.*

However, this improvement was not observed everywhere. For example, Figure 3.3.3 shows that SWE assimilation had no impact on the model cold bias over two borehole sites in the Kola Peninsula. This could be explained by the difficulty to simulate interception of snow by trees, litter, and thermal properties of organic soils.

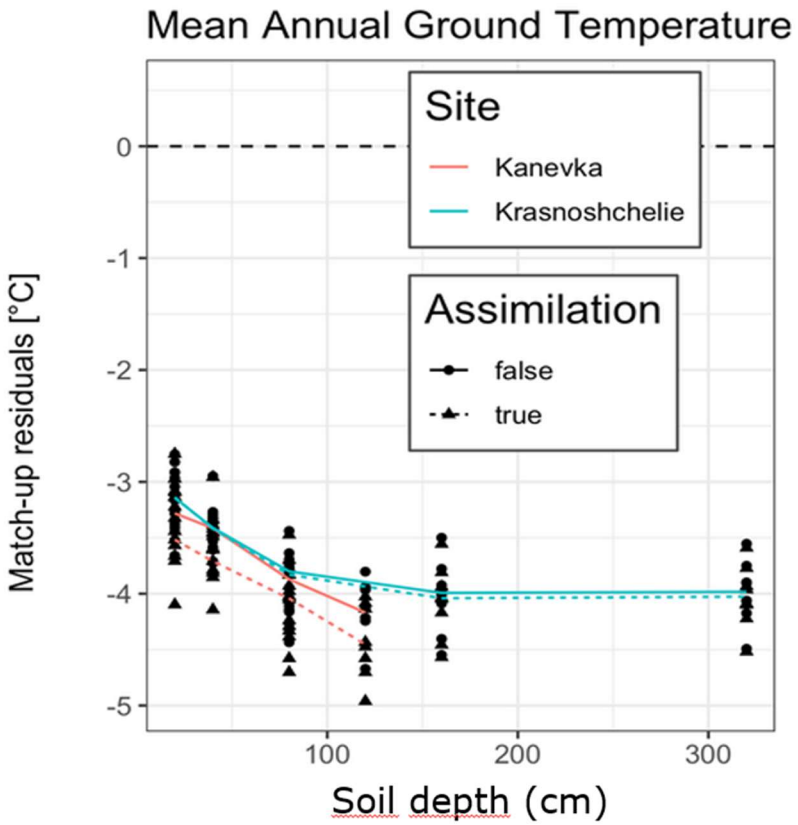

Figure 3.3.3*: Impact of the assimilation of SWE on the ISBA model bias in soil temperature at -20,-40,-80,-120,-160,-320cm depths as determined using in situ soil temperature data at two sites in the Kola peninsula, Kanevka (67.13N, 39.67E), and Krasnoshchelle (67.35N, 37.05E).*

Recommendations to the CCI ECV teams

Using the ISBA land surface model, it was shown that a long spinup of at least 200 years is needed to achieve ground temperature equilibrium in permafrost areas. The PERMAFROST dataset could be used in climate models to reduce the spinup time. The PERMAFROST ATBD (Algorithm Theoretical Basis Document) should indicate how equilibrium is achieved and to what extent it is achieved.

3.4 Propagation of CCI(+) observational uncertainties to climate model scales

Lead partner: BSC
Authors: Aude Carreric, Markus Donat, Pablo Ortega and Etienne Tourigny

Aim

Observational uncertainties originate from a cascade of errors in the retrieval process, structural uncertainties in the algorithms, and statistical uncertainties in the spatio-temporal projections (Merchant et al., 2017). These errors are correlated in space and time, due to mesoscale systems, for instance, that impact satellite retrieval on a given spatio-temporal scale. Observational uncertainties cannot therefore be averaged and scaled by the square root of the number of independent samples as for uncorrelated errors, but require the consideration of the correlation of errors in space and time. A novel approach to achieve this has been presented in Bellprat et al. (2018) and applied to the CCI sea-surface temperature (SST) dataset. This task aims at expanding this effort to other CCI ECVs (all relevant to the study of wild fires) in order to disseminate propagated observational uncertainties at daily, monthly, decadal and climatological scales as well as for different grid resolutions, regions, hemispheric and global averages. It addresses the following scientific questions:

1. How can the observational uncertainty estimates provided by CCI(+) reference datasets be translated into different spatiotemporal scales to compare to climate model simulations?
2. Are there important differences relative to the nature of the products?

Key Outcomes of CMUG Research

1. Results suggest that observational uncertainty on Arctic SICs can have a strong impact on the assessment of seasonal forecasts, larger than the uncertainty related to the limited ensemble size and the length of the forecasts.
2. An interesting region to study the effect of the propagation of errors for the fire ECV (burnt area) is North Australia.

Summary of Results

Deviation of plans:
The analysis on the propagation of errors started in the 1st July 2019, after the hiring of Aude Carreric (who has performed the analysis), and it has been centred on two ECVs: fires (i.e. burnt area) as initially planned, and sea ice (i.e. sea ice concentrations; SIC) in substitution of the originally envisaged soil moisture, for which only trajectory based L2 datasets are currently available through the CCI data portal, thus complicating the propagation into the model scales, which are gridded in space[1]. We believe that sea ice concentrations are an excellent alternative of greater utility for our ongoing activities, in which sea ice plays a central role, and the propagated errors will be more easily exploitable, as for example in the evaluation of the forecasts with the enhanced sea ice reanalysis performed in Work Package 3.8. The new ECV Land Surface Temperature has not been finally considered as the data were not available at the time the analysis started, and the allocated resources to complete this WP had already been used.

[1] CMUG acknowledge that more datasets are available than are published on the CCI data portal and CMUG always contact the ECV teams to check if such datasets are available.

Arctic Sea Ice prediction case study:
The analysis of SICs has been focused on the Barents and Kara Seas in September and October (red area in Figure 3.4.1), a region and a season in which sea ice variations have been linked with other remote impacts, including on the North Atlantic Oscillation (e.g. Ruggieri et al 2016) and the occurrence of extremes over Europe (e.g. Acosta-Navarro et al 2019).

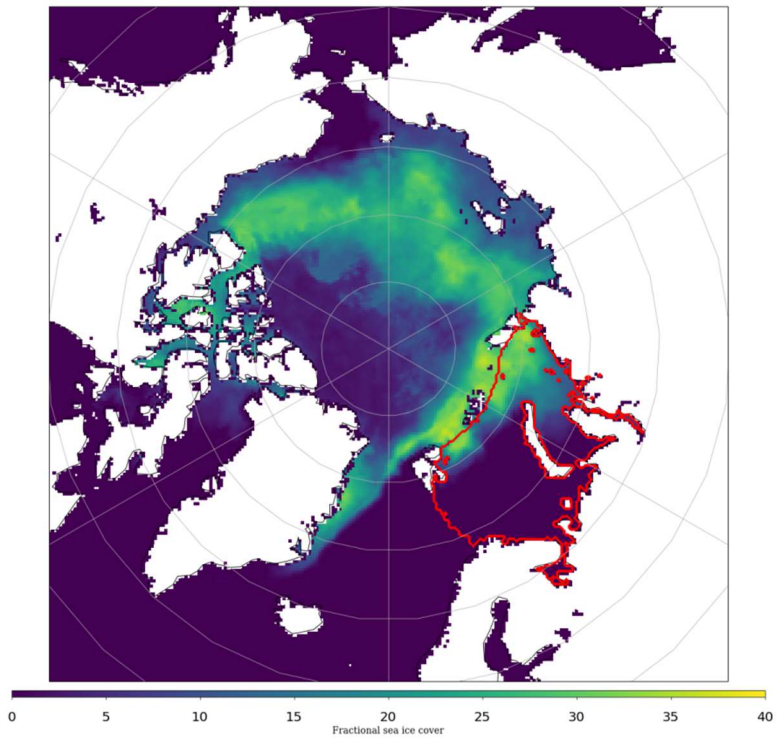

Figure 3.4.1*: Interannual standard deviation of the observed SICs (in colours) from the in August and September over the period 2003-2016. The red line encloses the Barents and Kara Seas. ESA observational data from SIC climate data record from the AMSR-E and AMSR-2 instruments at 50km grid spacing, version 2.1.*

We followed the methodology and equations in Bellprat et al. (2017) to propagate the uncertainties of SICs (from the Sea Ice Concentration climate data record from the AMSR-E and AMSR-2 instruments at 50 km grid spacing, version 2.1) into the model scales, in this case for EC-Earth 3.2 in its standard resolution (approximately 1° in the ocean). We concentrated on the average of SICs over the Barents and Kara seas and propagated the corresponding uncertainties to investigate their impact in the evaluation of skill for a seasonal prediction system with EC-Earth 3.2. This forecast was initialized every 1st May for the reforecast period 1993-2014. We also assessed the sensitivity of the skill scores, their effect compared with that of the uncertainty related to the ensemble size and the length of the forecast period (see Bellprat et al. (2017) for further details).

Figure 3.4.2 shows that the observational uncertainties have indeed a strong impact on the skill, especially for the longer lead times. In August, for example, anomaly correlation coefficients range from 0.7 (which would correspond to very good performance) to negative values close to -0.4 (which are suggestive of really poor performance). This effect is comparable to the combined effect of the ensemble size and hindcast length uncertainty. Such results thus highlight that the skill over this area

is particularly uncertain, at least for the seasonal forecasts considered. It is therefore important to identify other regions and seasons for which the skill remains high and is less sensitive to all these uncertainty sources. It is also possible that to reduce the impact of the observational uncertainty on the skill, longer reforecast periods and larger ensembles are needed, as both are expected to improve the overall skill by allowing to better constraining the predictable signals. Other potential ways to reduce the sensitivity of the skill score estimates to the observational uncertainty is to improve the initial conditions, e.g. through the assimilation of new observational products, as was done in WP3.8.

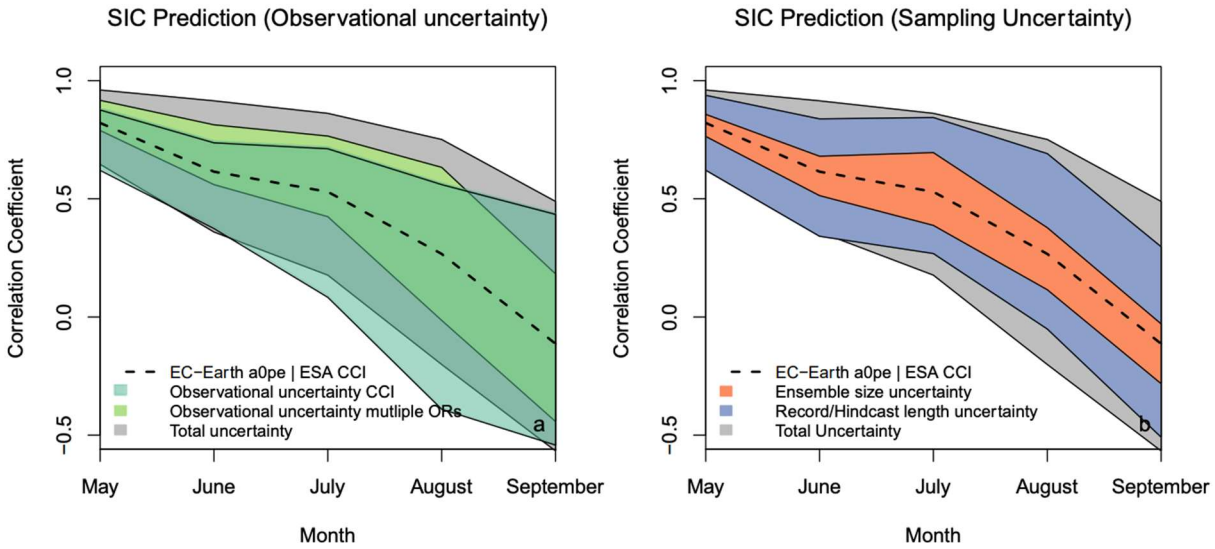

Figure 3.4.2: *Sub-seasonal to seasonal forecast skill of EC-Earth3.2 (10 members) with respect to ESA-CCI SIC (dashed line) in predicting the average sea ice concentration in the Barents and Kara Seas in a seasonal forecast system initialised on the 1st May. The areas show the 5-95% percentile range of the bootstrapped (10^6) uncertainty sources around the sample correlation skill for (left) the uncertainty in the ESA-CCI SIC observations once propagated into the model scales (blue) and the uncertainties as derived from the comparison of three other SIC products (green; NSIDC51, NSDC79 and an earlier version of ESA-CCI SIC) and (right) the sample uncertainty due to a limited ensemble size and record length of the ESA-CCI SIC product. The grey area shows the total uncertainty obtained by resampling all sources at the same time.*

Wild-fires in Australia case study:
In this study the errors were propagated into the model scales to evaluate the realism of the EC-Earth model when simulating changes in burned area.

The observational product considered for the burned area is ESA CCI (main product): version 5.1, from 01/2001 to 12/2018, 0.25º regular spatial resolution, monthly temporal resolution. This product was used to evaluate the simulated burned area in a historical experiment performed with EC-Earth and forced by the ERA5 reanalysis, for which we have accumulated annual values of burned area over a Gaussian grid that has a nominal resolution of 1°.

For the evaluation we used the fraction of burned area (and not the total burned area itself) because the analysis requires comparison of surfaces of different grids, and the regridding process (from the 0.25º regular resolution in observations to the Gaussian grid in the simulation) can introduce important interpolation errors in the computation of areas. It has been assumed that an area that has already burned does not have time to regenerate and burn again within the calendar year. The direct

consequence of this assumption is that the total burned fraction in the year cannot be more than 100%. This assumption is not entirely correct in some grid-points, such as in Northern Africa (Central African Republic, South Sudan, Ethiopia) for instance.

A simplified diagnosis of the impact of the propagation of uncertainties on the burned area fraction has been made. All observational data were annually summed to match the simulated values. The regions of the world with the largest interannual variability in burned area (Figure 3.4.3) are Africa and Australia. In the following we focus exclusively on Northern Australia as this is a region where most wild fires are rarely human induced. This is particularly interesting as only wild fires of natural origin, or with a strong natural component can be expected to be reproduced by the model.

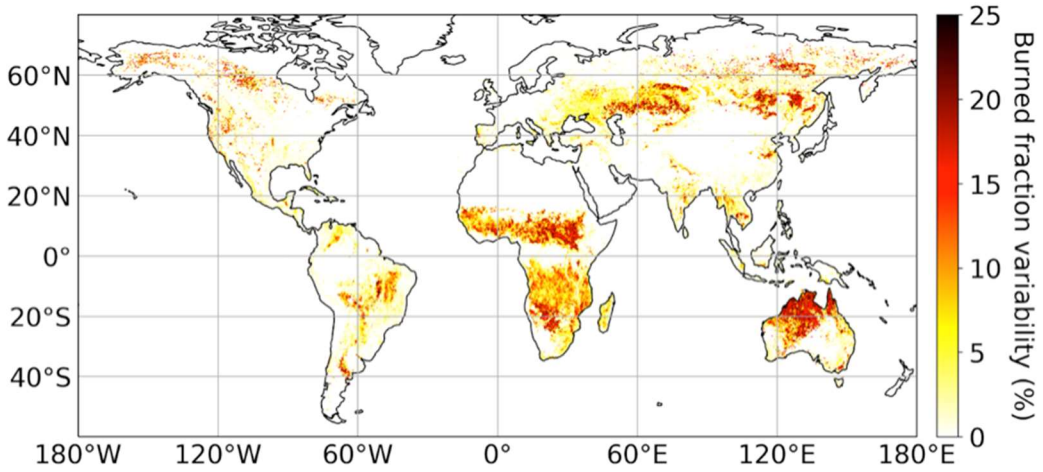

Figure 3.4.3: *Standard deviation over the 2001-2018 of the annual fraction of burned area in the CCI ESA product v5.1.*

To determine the propagation coefficient for observational the errors, their time and space decorrelation lengths are necessary. The decorrelation time of errors has been calculated from monthly errors (Figure 3.4.4), and corresponds to 1-2 months when calculated from monthly data.

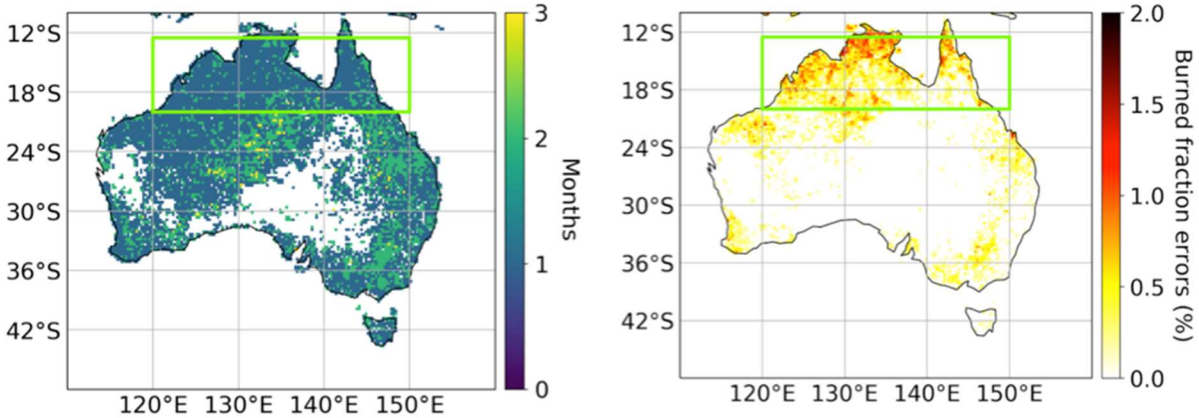

Figure 3.4.4: *(Left) Decorrelation timescales of monthly ESA CCI errors anomalies of burned area fraction, for all months (2001-2018). The decorrelation time corresponds to the first decay of an e-factor in the autocorrelation function. (Right) Observational uncertainties of the burned area fraction for the year 2015 in Australia (ESA CCI product v5.1 in its native grid).*

Since the spatial length of the decorrelation of burned area fraction errors was not provided in the documentation of the CCI dataset, we applied different choices of coherent spatio-temporal decorrelation scales to the analytical method developed in Belprat et al. (2017), that was used to compute the propagation coefficient following its Equation 3. We retained the largest (and therefore more penalising) resulting value of the propagation coefficient to perform the propagation of uncertainties to the model scales.

The propagated uncertainties (Figure 3.4.5a) were finally used to compare the climatology maps, calculated for the period 2001-2017, for the observed (Figure 3.4.5b) and simulated (Figure 3.4.5c) burned area fraction. This comparison revealed that, for all but one of the grid points, the model climatology was inconsistent with the observed one under its uncertainty range. This is a critical problem in the model that questioned its use for predictive purposes.

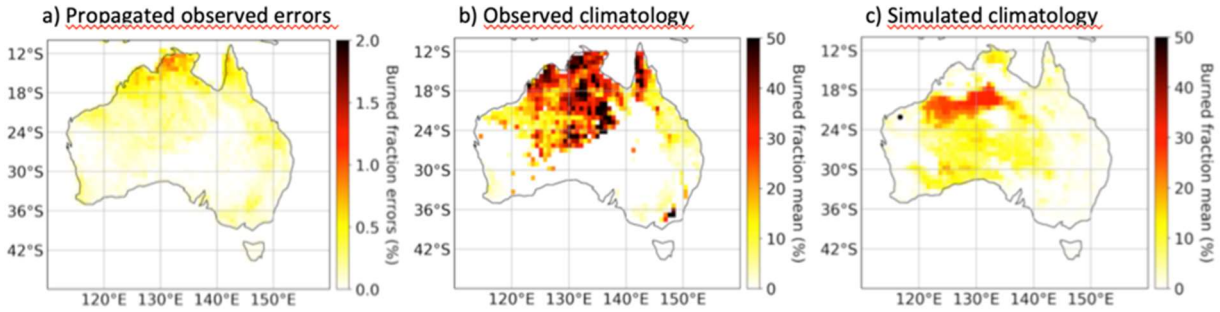

Figure 3.4.5: *a) Propagated observational errors of the fraction of burned area from the ESA CCI v5.1 product. b-c) Spatial climatology (2001-2017) of the fraction of burned area in the ESA CCI v5.1 observations and the EC-Earth historical reconstruction. The observed have been interpolated into the model grid. The black dot in panel c represents the only grid point in which the simulated mean value is consistent with the observed one when the observed uncertainty is considered.*

Publications

No new publication is envisaged of these results. The methodology applied was developed by Bellprat et al. (2017) in the previous phase of CMUG.

Interactions with the ECVs used in this experiment

During the time this work was performed there have been interactions with the SI and Fire CCI ECV teams at the quarterly CSWG meetings and the Integration meetings.

Consistency between data products

No inconsistency analysis was carried out between the two ECV products considered in this study, as each of them was used for a different application.

Recommendations to the CCI ECV teams

To reduce the numbers of assumptions made to propagate the observational errors into the model scales, and thus strengthen the confidence in the results, we would require spatio-temporal decorrelation scales of observational errors to be systematically provided for all ECV datasets.

3.5 Document SM-atmosphere feedbacks in transition regions (temperature and precipitation)

Lead partner: IPSL
Authors: Frederique Cheruy, Agnes Ducharne, Y. Zhao

Aim

The aim of this research is to examine if CCI(+) data be used to detect on observations the soil moisture/surface temperature feedback related to soil thermal inertia. It will address the following scientific question: Can the co-variations of SM, LST and precipitation be used to document the soil moisture - temperature feedback (intra-daily time scale)?

Summary of Work

Land surface temperature, soil moisture, precipitation observations have been combined on a daily basis in order to detect the contribution of soil thermal inertia which is strongly dependent on soil moisture to daily variations in night-time minimum temperature. To limit the potential sources of variation in the diurnal cycle of land surface temperature, we chose to focus on dry periods of at least 10 days at the TRMM resolution (0.25 degree) scale. In order to assess the sensitivity of the amplitude of the diurnal cycle to soil moisture during these periods we restricted the study to points where at least 16 observations per day were available. This leads us to take into account mostly cloudless days and thus limits the sources of variability of the surface temperature linked to variations in sunshine caused by the presence of clouds. The dataset used is described in Table 3.5.1: the LST pixels (0.05 degree x 0.05 degree spatial resolution) present in each TRMM grid box (0.25 degree x 0.25 degree spatial resolution) have been averaged, and data are analysed at the 0.25 degree x 0.25 degree resolution. The daily maximum LST (LST_max), daily minimum LST (LST_min) and diurnal amplitude LST (LST_amp) are calculated based on the hourly data. The dry spell requirement combined with the requirement of having at least 16 LST values in a day, strongly reduces the number of available cases for the analysis (Figure 3.5.1).

Publications

None so far.

Interactions with the ECVs used in this experiment

There have been interactions with the SM and LST CCI ECV teams at the quarterly CSWG meetings and the Integration meetings.

Consistency between data products

For each dry spell event, the changes between two consecutive days for LST_max, LST_min, LST_amp, SM and SWdn, (named ΔLST_max, ΔLST_min, ΔLST_amp, ΔSM and ΔSWdn, respectively) are computed. A linear regression coefficient between the change in LST (mean, max,

min, amplitude) and the change in the SM is evaluated for each selected dry spell event in the TRMM grid points. The possible link between the change in max LST and change in SW radiation is also explored. Mean values of the regression coefficients are reported in Figure 3.5.2. The analysis is then conducted at the scale of the three Sahel boxes depicted in Figure 3.5.2. For each case the changes in LST_max (LST_min, LST_amp) are compared to the corresponding changes in SM. Figure 3.5.3 shows the scatter plot of the standardized changes of these variables and confirms that an increase of SM tends to decrease the maximum LST (through evaporative cooling) and to increase the minimum LST, that is to say decrease the diurnal amplitude. This is consistent with the damping effect of the soil moisture on the nocturnal cooling through the impact of the soil moisture on the superficial thermal inertia, and to a contribution of this damping effect to the day-to-day variability of the LST. The changes in LST_max are well correlated with changes in downward SW radiation. The amplitude of the change of the LST_min, is modulated by the turbulence and the soil thermal properties (Cheruy et al. 2017), considering the normalized anomalies allows to minimize their impact.

Table 3.5.1: Data used for the analysis.

PRODUCT	RESOLUTION	REGION	PERIOD	PLATFORM
LST CCI SEVIRI (MSG L3U)	0.05 °, Hourly	MSG disk	2008-2010	MSG2
ESA CCI SSM COMBINED (fv0 4.5)	0.25 °, daily	Global	2008-2010	Nimbus 7, DMSP, TRMM, AQUA, Coriolis, GCOM- W1, MIRAS, ERS-1, ERS-2, METOP-A, METOP-B
TRMM V7	0.25, 3 hourly	81.125 ° W-E 50° N-S	2008-2010	TRMM
CERES, V4a	1 ° , daily	Global (interpolation to LST resolution)		

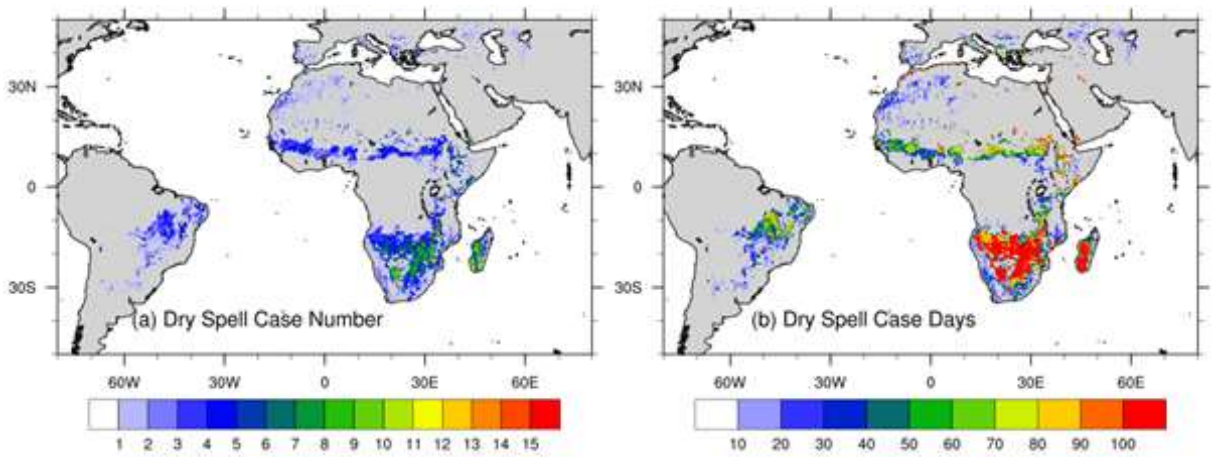

Figure 3.5.1*: Dry spell case number and number of dry spell days with at least 16 evaluations of the LST in one day (2008-2010).*

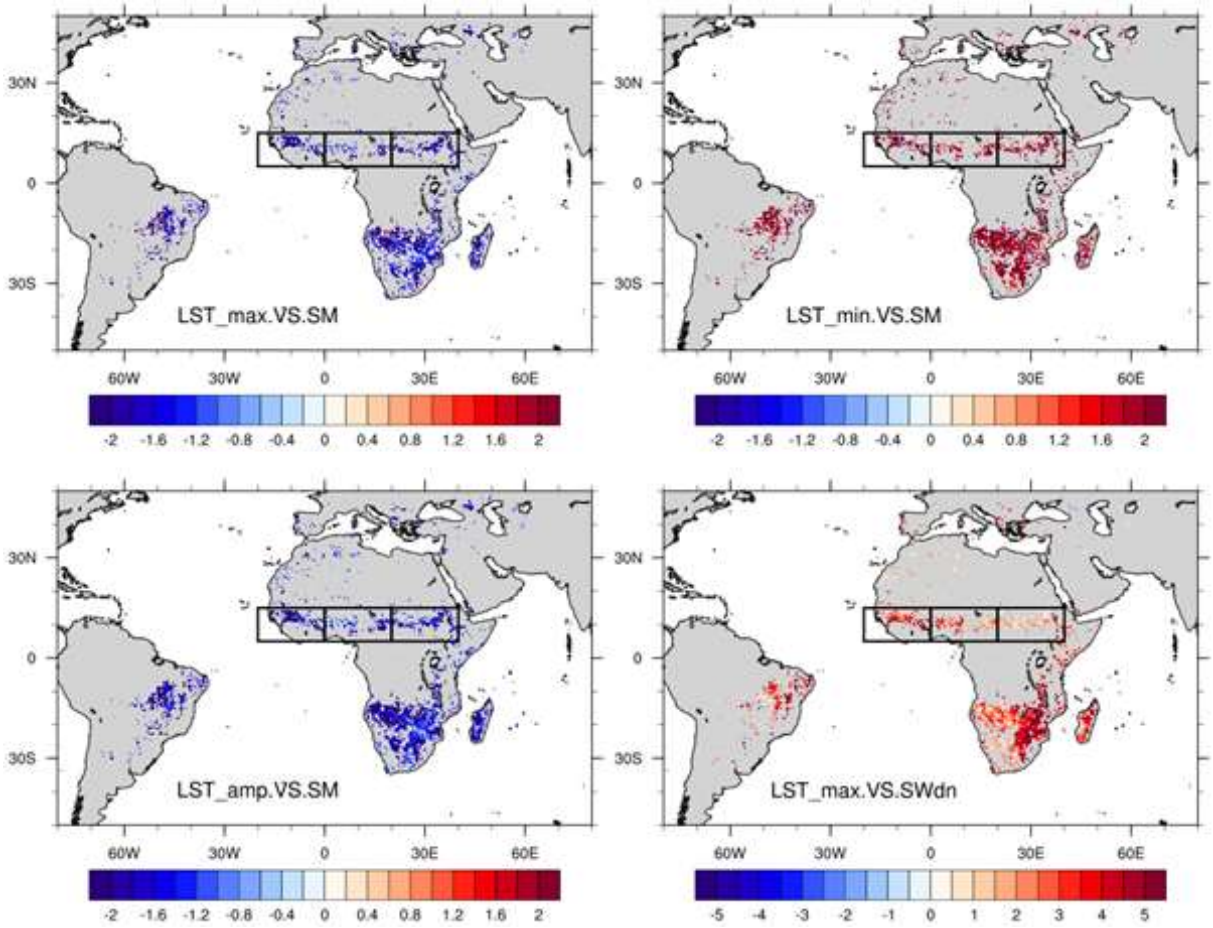

***Figure 3.5.2**: linear regression coefficient between ΔLST and ΔSM (unit: 1000×(°C×m^3)/m^3), and between ΔLST_max and ΔSWdn (unit: (°C×W)/m^2). The selected boxes over Sahel are shown.*

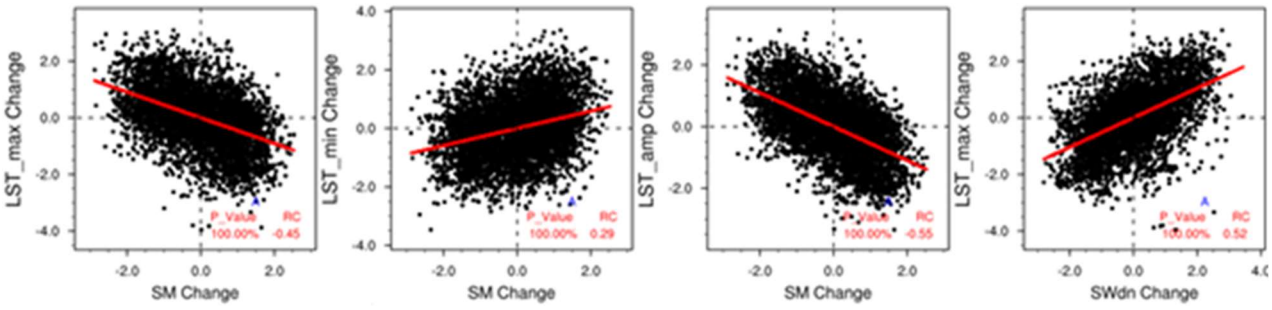

***Figure 3.5.3**: Correlation between standardized ΔSM (X axis) and ΔLST change (Y axis), and between standardized ΔSWdn (X axis) and ΔLSTmax change (Y axis) over box 1 (5-15N, -20W-0E). Standardized anomalies are calculated for each selected dry spell case.*

3.6 Constraining the evapotranspiration at the scale of climate model grid-cell

Lead partner: IPSL
Authors: Frederique Cheruy, Agnes Ducharne, Y. Zhao

Aim

The aim of this research is to explore the potential of multiple satellite derived products to better understand the land surface processes and land-atmosphere coupling, at the scale of climate model grid-cells. It will mostly focus on the water and energy budgets over land, and try to identify relationships between presumably related variables, including new ECVs such as snow cover and LST. It will address the following scientific questions:

1. Can we better constrain the controls of evapotranspiration (ET) at the scale of climate model grid-cells?
2. Do the corresponding stress functions (for soil moisture, incoming energy, atmospheric humidity, temperature) take a different form at the point and grid-cell scale?
3. Can large-scale differences between LST and air temperature provide additional information to document the behaviour of parameterizations important for the near surface climate such as turbulence, heat conduction into the soil (Ait-Mesbah et al., 2015, Wang et al., 2016)?

Summary of Work

We have shown that the evapotranspiration is better constrained with a multi-layer hydrology scheme than with a *Choisnel* type scheme, however the atmospheric forcing (in coupled mode) is decisive in terms of realisms for the regional distribution of the evapotranspiration (Figure 3.6.1). Concerning the snow, analysis has been done with Interactive Multisensor Snow and Ice Mapping System (IMS) data from NOAA since the CCI data were not yet available. A strong overestimation of the modelled snow cover inducing a marked cold bias in winter has been diagnosed on complex terrain such as the Tibetan plateau. This bias involves albedo-snow feedbacks and probably defects in modelling the snow cover on complex terrain (Cheruy et al. 2020).

Publications

Cheruy et al. (2020).

Interactions with the ECVs used in this experiment

There have been interactions with the Snow, SM and LST CCI ECV teams at the quarterly CSWG meetings and the Integration meetings. This was to be informed on data suitability for the work and data availability (direct from the CCI ECV teams or from the CCI Open Data Portal).

Consistency between data products

Figure 3.6.1 shows regional histograms computed on the monthly value of the individual grid points corresponding to the Southern Great Plains region (delimited with the Koeppen-Geiger climate classification) in JJA. Each row is dedicated to a particular variable relying on the coupling: superficial soil moisture (first row), net SW radiation at the surface (second row), evaporation (third row), and precipitation (fourth row). The first four columns correspond to the 4 reference experiments with different version of the GCM and land-surface model of IPSL. The first column corresponds to the configuration used for CMIP5 the last one to the configuration used for CMIP6, and the last two columns to the different sets of observations (indicated above the corresponding histograms). The colors depict the PDF from the minimum to first quartile (dark pink shade) from first quartile to the median (pale pink shade), from median to third quartile (cyan line) and from the third quartile to the maximum (blue line), (Cheruy et al., 2020). It can be observed that the statistical distribution of these variables is much improved in the CMIP6 model configuration. In particular, the simulated surface soil moisture presents a bimodal distribution that is consistent with the SM CCI product.

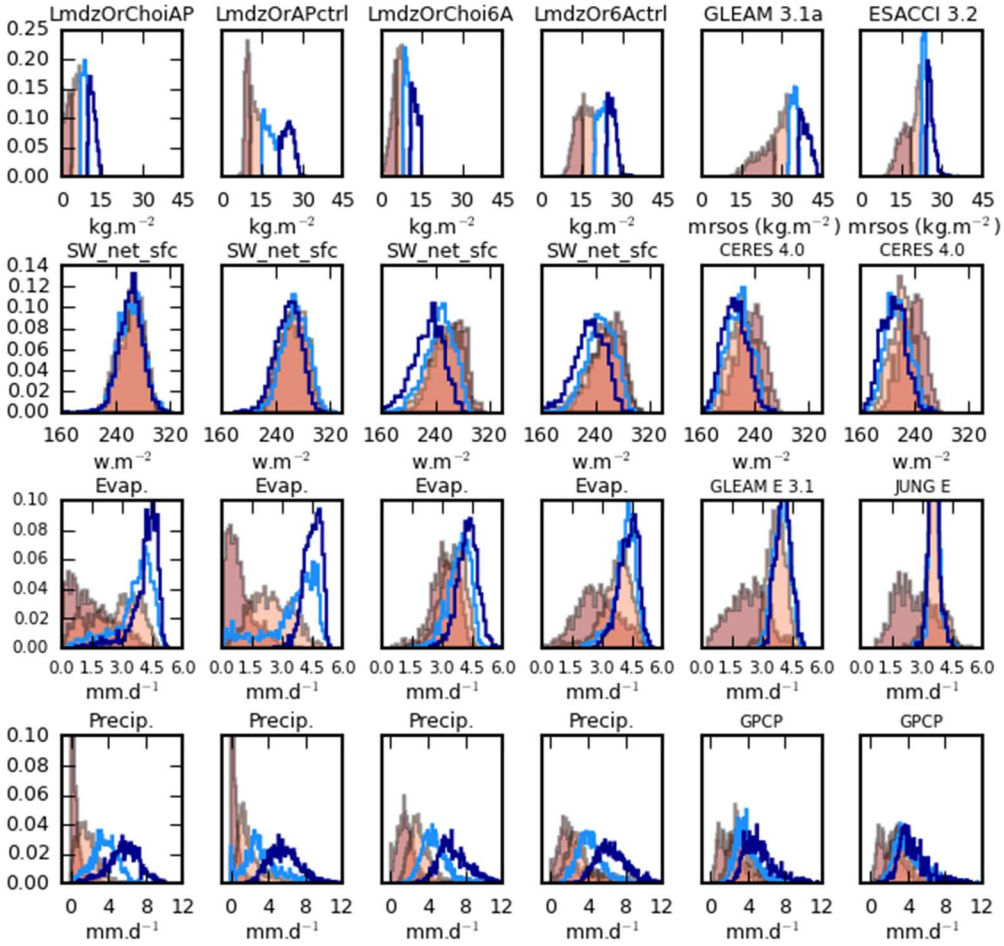

Figure 3.6.1: *Regional distribution of variables in play in the soil-atmosphere coupling, as a function of the soil moisture, modelled and observations.*

Recommendations to the CCI ECV teams

Given the importance of the Tibetan plateau thermal effects on climate simulations, it could be recommended to SNOW and SM CCI teams to consolidate the validation effort over this area.

3.7 The effect of Lakes on local temperatures

Lead partner: Met Office
Authors: Grace Jones and Erasmo Buonomo

Aim

The aim of this research is to identify and describe the interactions and relationships between lakes and their surrounding land areas. Typically, this would be around large lakes (e.g. Victoria, Great Lakes). It will address the following scientific questions:

1. What are the interactions between lakes and the surrounding land areas?
2. What effect does lake temperature (or other parameter) have on the surrounding LST?

Summary of Work

CCI ECV lake surface water temperature and lake ice cover data are not currently useable in climate model simulations due to gaps. We suggest a reconstruction like that applied to the ARC3 lake data set (MacCallum and Merchant 2012). By including lake surface water temperature/lake ice in our re-analysis driven RCM run over Europe, winter and summer surface air temperature biases over land surrounding larger lakes (> 5000km^2) are reduced compared to E-OBS observations. There are little to no changes in mean temperature or precipitation in areas surrounding smaller lakes (< 500 km^2) but this may be a feature of model resolution.

3.7.1 Introduction

Lakes are widely recognised to influence local climate. Lakes generally warm and cool more slowly than the surrounding land due to their higher heat capacity, this can lead to cooler summers and warmer winters, changes in precipitation and circulation. The impact a lake/s have on local climate is often related to lake size, with larger bodies of water having a much bigger impact than smaller ones (Rouse et al. 2008). Historically, lakes have not been well represented in global or regional climate models often due to low horizontal grid resolution and/or lack of observational data for validation. Approaches such as representing lakes as mostly land (Gordon et al. 2002), interpolating local sea surface temperatures and applying lake surface temperature climatologies have been employed (Mallard et al. 2005). More recently, simple lake models such as FLake (http://www.flake.igb-berlin.de) have been implemented, but results are generally compared to in situ data (Betts et al. 2020) which is not available for many lakes.

The Lakes CCI ECVs are filling an important data gap in climate observations and have the potential to improve the representation of lakes in climate models, particularly in locations where in situ observations are sparse. Our intention in this project was to use the daily lake surface water temperature (LSWT) and lake ice cover (LIC) ECVs as input to the HadREM3-GA7-05 regional climate model (RCM) over Europe at 12km horizontal resolution driven by ERA-Interim (Dee et al. 2011), the global atmospheric reanalysis product from the European Centre for Medium-Range Weather Forecasts (ECMWF) and prescribed daily sea surface temperature and sea ice from Reynolds et al (2020). For the RCM domain and land sea/lake mask, see Figure 3.7.1. However, as is described in the Results,

this was not possible due to the amount of missing data (likely due to cloud) currently present in the Lake ECVs. Instead, we used the daily ARC3 lake data set (MacCallum and Merchant 2012), which was developed as part of a previous ESA funded project. We then compared the output from the RCM experiment with ARC3 lake data, to an almost identical one where the lakes had been filled in. By comparing these two experiments we hope to 1) describe the interactions between the lakes and the surrounding land areas, and 2) to compare the different RCM experiments to observations to see how model performance is affected.

***Figure 3.7.1**: RCM Land Sea/Lake Mask.*

3.7.2 Methods

Observed lake data sets

The global LSWT and Lake Ice Cover LIC ECVs are thoroughly described in the documents here https://catalogue.ceda.ac.uk/uuid/3c324bb4ee394d0d876fe2e1db217378?jump=related-docs-anchor. In summary the LSWT data was created by the University of Reading using European Space Agency (ESA), European Organisation for the Exploitation of Meteorological Satellites (EUMETSAT), ECMWF daily satellite products and has an original resolution of 0.05 degrees. The LIC data was created by H20 Geomatics from ESA and National Aeronautics and Space Administration daily satellite products with a resolution of 250m.

As is described in the Results, we were not able to use the Lake ECVs as input to our regional climate model (data gaps due to cloud). Instead, we used the ARC3 lake surface temperature data set which is derived from ESA's (Advanced) Along Track Scanning Radiometers, (A)ATSRs and Sea and Land Surface Temperature Radiometers (SLSTRs) observations. This satellite data has been through a significant reconstruction process to address the cloud cover gaps. In the ARC3 data set, Empirical orthogonal function (EOF) techniques were applied to the LSWT retrievals to reconstruct a spatially and temporally complete time series of LSWT, this process is described in MacCallum and Merchant 2012. ARC3 contains 1628 lakes and is available as a spatially complete climatology or a daily time series of per lake point data (containing one night time and one day time temperature value) from 06/1995-03/2012. The climatology would be ideal as it captures the spatial variability in temperature,

but given the significant natural variability in the region, it is not appropriate for use. Figure 3.7.2 shows the ARC3 LSWT of the largest lake in Sweden (Lake Vänern, ~5600km^2) for each year in the period 1996-2011, the day on which the lake freezes/thaws (which we assume to be when the LSWT is < 273.15K) varies by ~7 weeks. As we are using a re-analysis based on observations as boundary data to our RCM, this could lead to inconsistencies between the lake state and the surrounding air. For this reason, we use the daily per lake point data. If we were running the model over significantly larger lakes (Lake Victoria, the Great Lakes) then using point data may not be appropriate.

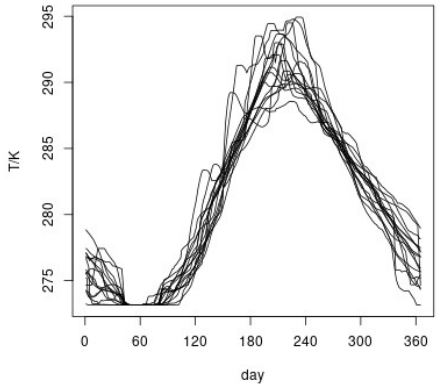

***Figure 3.7.2**: Lake Vänern daily LSWT (1996-2011) from ARC3.*

Other observations

In order to understand the impact using observed lake data has on our experiments, we compare model output for precipitation and surface air temperature to the E-OBS v20.0e data set (Cornes, et al. 2018). E-OBS is a gridded data set at 0.1 degree resolution (v20.0e) based on station observations. It has been robustly evaluated and its limitations are well described e.g. inhomogenity of stations and the underestimation of precipitation (Sevruk, 1986), it is the standard reference for RCM evaluation over Europe (Kotlarski, et al. 2019).

We also compare model land surface temperature (LST) to the Special Sensor Microwave/Imager and Special Sensor Microwave Imager/Sounder L3C v1.51 (SSM/I SSMI/S L3C) Satellite data set. The LST observations are of particular interest as they are a part of the LST ECV product, the development of which is still in progress. The product specification document can be found here https://climate.esa.int/sites/default/files/LST-CCI-D1.2-PSD%20-%20i1r11%20-%20Product%20Specification%20Document.pdf. SSMI SSMIS L3C has a spatial resolution of 0.25 and is available on annually, monthly and daily timescales. There are two passes per day at roughly 6am and 6 pm, we take the average of the two passes as our LST value at each grid point. Larger bodies of water are represented by missing data, smaller lakes are often contaminated by surrounding land but still have a significantly different temperature to land only grid boxes. One of the main benefits of this product over others is that it is an all-sky data set, so there are almost no gaps. It may be less accurate than some other products that are part of the LST ECV, but for our purpose this is more than made up for by the lack of gaps due to cloud.

Regional Model and experiment set up

The atmosphere only RCM HadREM3-GA7-05 was used to downscale ERA-interim re-analysis (Dee, et al. 2002) to 12km over Europe (see domain in Figure 3.7.1). The HadREM3-GA7-05 is the regional version of the global GC3.05 configuration of the Met Office Hadley Centre Unified Model and consists of atmosphere: GA7.0 (Walters et al. 2017) and land: GL7.0 (Walters et al. 2017) components. Sea surface temperatures and sea-ice extents are prescribed from analyses of observations (Reynolds et al., 2002). Model set up is described fully in Tucker, et al. 2021 (submitted) which also uses the same domain but uses interpolated SSTs for LSWT in Scandinavia and Northwest Russia. As far as possible we represented the location and shape of lakes realistically, but due to model resolution this was not always possible. For example, in south Finland several lakes were joined together and the LSWT was taken from the lake with the closest lat/lon point to the centre of the combined lake.

Two experiments were carried out, they were identical to each other except one replaced lakes with land points (referred to as the Filled Lakes experiment), and the other prescribed LSWT using daily night time ARC3 data (referred to as the ARC3 Lakes experiment). LIC data was not available so the assumption that when LSWT < 273.15, LIC = 1 and when LSWT > 273.15, LIC = 0 was made. The only other way the two runs differ is length, the Filled Lakes experiment ran from 12/1981-12/2012 and ARC3 Lakes ran from 06/1995-03/2012. The Filled Lakes experiment is part of the EURO-CORDEX initiative (Jacob, et al. 2014) and had to be run for a defined period. We discarded the first year of data (06/1995-06/1996) from the ARC3 Lakes run as model spin up and only compare data from 06/1996-03/2012 for both experiments.

3.7.3 Results

CCI Lake data

The RCM relies upon ancillaries, such as LSWT, containing no missing data at all. If there are one or two day stretches missing occasionally, or one or two grid boxes containing missing data, it I fairly straightforward to interpolate in space or time. However, it the case of the LSWT and LIC CCI data from this project, it quickly became clear that the gaps in data were far more extensive. Figure 3.7.3 is a histogram of the fraction of lake grid boxes (in the European RCM domain) that contain non-missing data each day in the period 1996-2011. All available LSWT data that isn't missing is counted as valid, including those flagged as bad data, worst quality and low quality, as well as that flagged acceptable and best quality. Particularly in winter when there is likely to be more days of cloud cover, there is a high proportion of days where there is little to no data. In DJF (JJA), ~63% (~28%) of days contain 0%-5% of non-missing data for LSWT. LIC tends to have fewer, but still significant gaps, in DJF (JJA), ~31% (~25%) of days contain 0%-5% non-missing data.

Whilst the picture is better in the summer, for LSWT only ~0.6% of days contain >80% non-missing data. The gaps due to cloud are often spatially variable, you might have all grid boxes containing data for one lake, but another in the domain has no data; there are also occasions where the majority of lakes contain a couple of grid boxes of data but are otherwise missing. We also looked briefly at the global picture in case our domain choice was particularly unfortunate to contain a lot of gaps, but it did not change our conclusion that at present, the LSWT and LIC are not able to be used as input to

prescribe lake surface properties in climate models, and would be of very limited use to validate RCM output or lake model output.

Given the current unsuitability of the CCI Lakes data to prescribe LSWT and LIC, we looked for alternative sources of lake data with which to run our RCM experiments. We used ARC3, developed as part of a previous ESA project. ARC3 also contained gaps due to cloud cover, but a complex reconstruction detailed in MacCallum and Merchant 2012. ARC3 demonstrates what would be possible if the gaps in the Lake CCI data were addressed. Following a positive outcome of this study, we would strongly recommend that a similar reconstruction be tested and applied by observation scientists in the next phase of the project in order to make the Lake CCI data more useful to the climate modelling community.

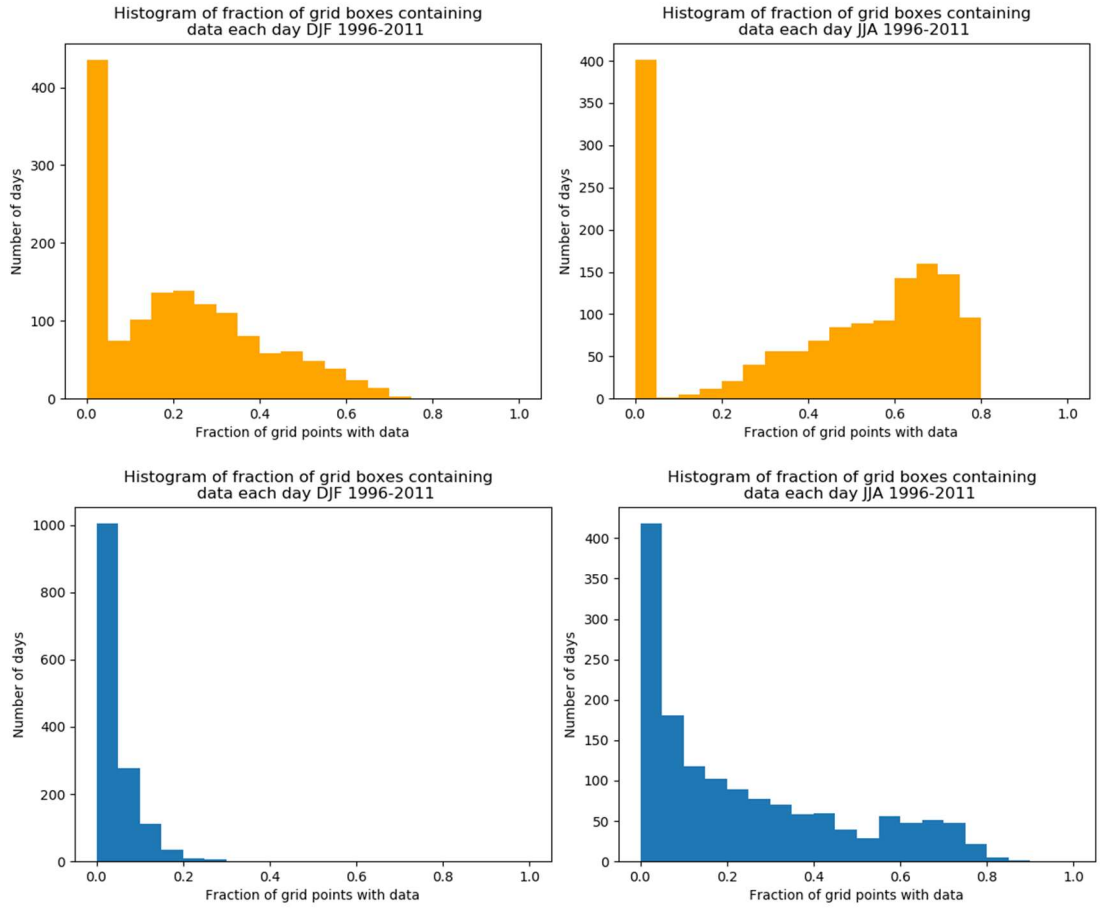

Figure 3.7.3*: histograms of the fraction of grid boxes containing data (i.e. not missing) each day in the European RCM domain for the period 1996-2011 LIC (orange) and LSWT (blue)*

RCM results

Figures 3.7.4 and 3.7.5 show the seasonal mean surface air temperature for DJF over the period 12/1996-2/2012 for E-OBS observations, the two RCM experiments (ARC3 lakes and Filled lakes), and the differences between them over the whole domain and a section which spans 54º-65ºN and 10º-39ºE. There is a ~3ºC cold bias over Norway, the Alps, Russia and North Africa with respect to E-OBS in both the ARC3 lakes and Filled lakes RCM experiments (Figure 3.7.4). We are mostly

concerned with the impact of adding lakes, but these biases are comfortably within the range of biases found ERA-interim driven RCMs over the same domain (see Kotlarski, et al, 2014 for a detailed comparison).

The bottom right plot in Figure 3.7.4 shows the difference between ARC3 lakes and Filled lakes simulations. There are large temperature differences over the lakes, with the ARC3 lakes simulation being 2ºC-5ºC warmer than Filled lakes simulation. This is mostly in line with what we would expect given the higher heat capacity of water compared to land. Over the smaller lakes (we somewhat arbitrarily define a smaller lake as those which as <500km^2), the temperature difference is generally confined to the lake itself, however over larger lakes (defined as those >5000km^2) in Sweden, South Finland and particularly Russia, the air temperature over the land surrounding the lakes is also higher. This can be seen in Figure 3.7.5, which is a section of the domain containing the largest lakes. We have masked out the lakes in order to more easily see the effect on the surrounding land. The air temperature immediately surrounding the Swedish lakes is ~0.5ºC warmer in the ARC3 lakes experiment. The air temperature around the Russian and Finnish lakes is 0.5ºC-2.5ºC warmer in the ARC3 lakes experiment, the impact on air temperature over land decreases the further you are from the lake, but it extends several hundred kilometres in each direction. The cold bias over Russia and south Finland with respect to E-OBS is reduced by up to 3º and in south Finland has become a warm bias.

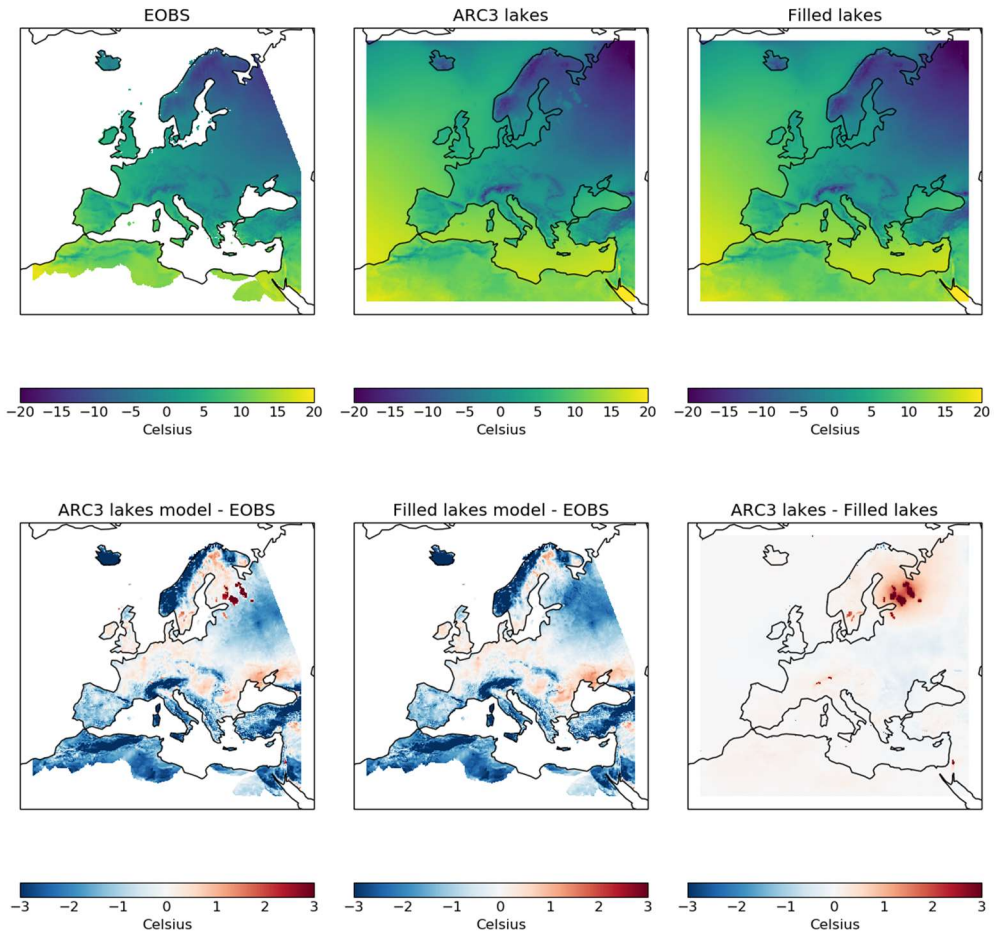

Figure 3.7.4: *DJF seasonal mean (1996-2012) surface air temperature for: E-OBS, ARC3 lakes simulation, Filled lakes simulation and the respective differences between them.*

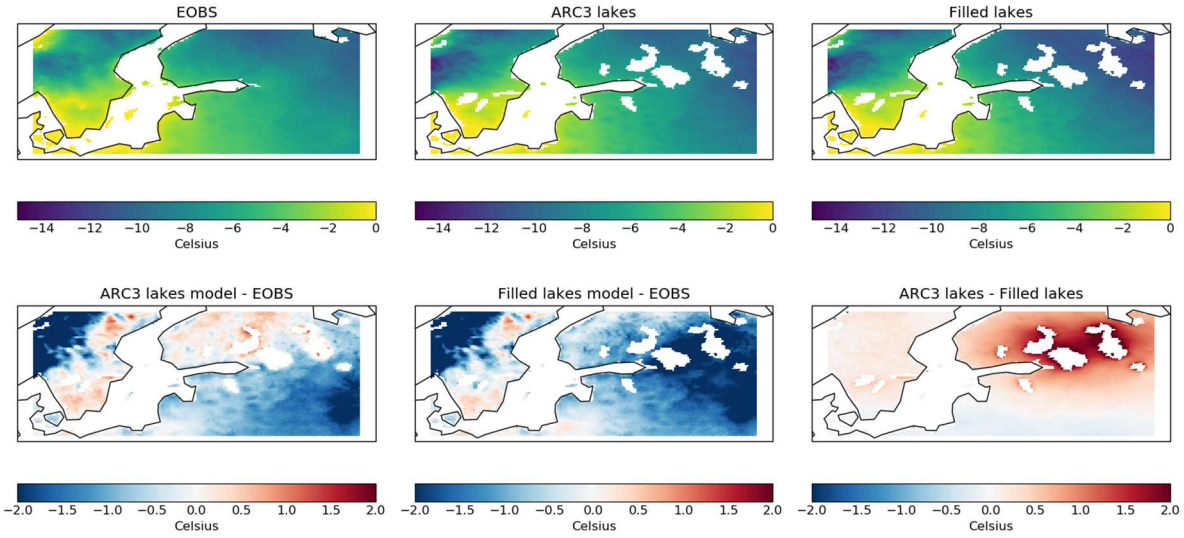

Figure 3.7.5*: DJF seasonal mean (1996-2012) surface air temperature with RCM lakes masked out for: E-OBS, ARC3 lakes simulation, Filled lakes simulation and the respective differences between them.*

Figure 3.7.6 shows the seasonal mean surface air temperature for JJA over the period 12/1996-2/2012. There is a warm bias of up to 3ºC over Southern and Central Europe and North Africa which is again within the range of biases seen when downscaling ERA-interim using an RCM (Kotlarski, et al, 2014). The air temperature difference between the ARC3 lakes and Filled lakes simulations in summer is much less pronounced than in winter, the small lakes in Italy have temperatures similar to that of the Filled lakes run. The Swedish, South Finnish and Russian lakes are cooler in the ARC3 lakes experiment by 1ºC-3ºC. The ARC3 lakes simulation is generally ~0.5ºC warmer over Central Europe than Filled lakes, this bias is currently unexplained, it could be related to the addition of lakes in a non-obvious way, or it could be due to the differing run lengths between the models.

The air temperature over land surrounding the Russian and South Finnish lakes is up to 1ºC cooler in the ARC3 lakes simulation than the Filled lakes simulation (Figure 3.7.7). This reduces the RCM's warm bias compared to E-OBS and in some areas becomes a slightly cool bias. The air temperature surrounding the Swedish lakes is very similar in both experiments, with the ARC3 simulation lakes being slightly warmer (~0.3ºC). The temperature difference between the Swedish lake region from the ARC3 lakes and Filled lakes simulations is much smaller than that of the Russian lakes from the same simulations (1ºC vs 3ºC). The greater the temperature difference between the Filled lakes and ARC3 lakes, the greater the impact on the air temperature over land.

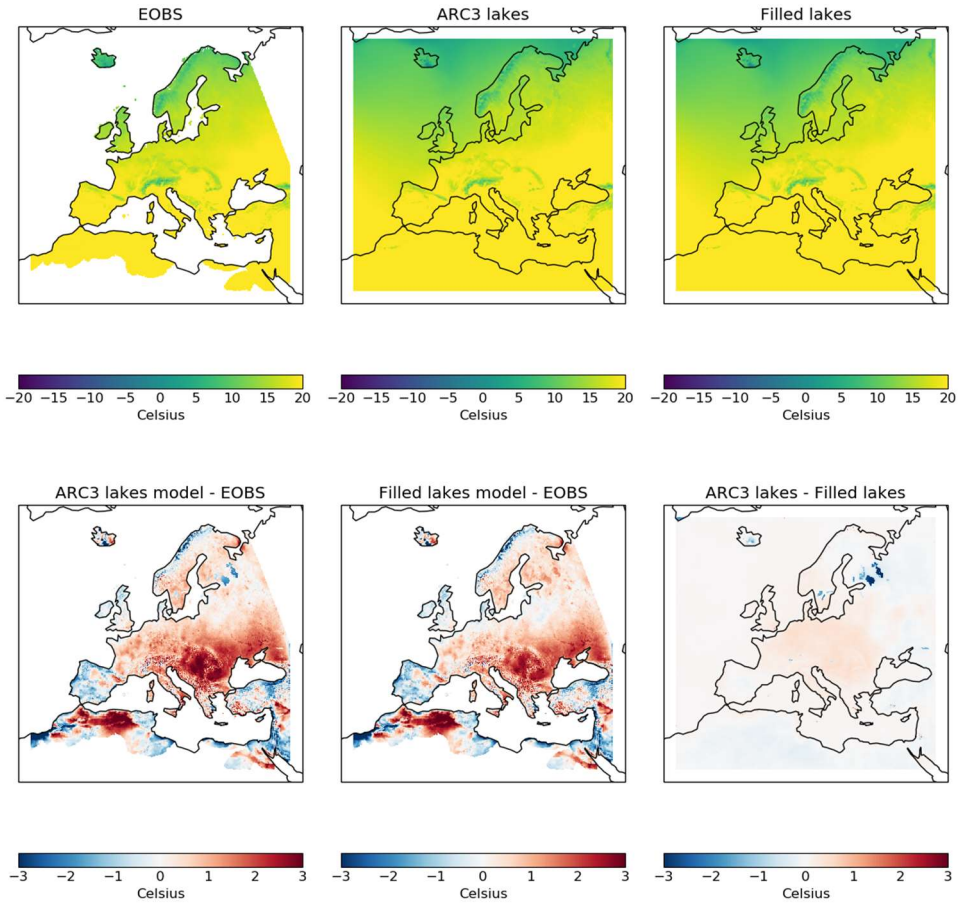

Figure 3.7.6*: JJA seasonal mean (1996-2012) surface air temperature for: E-OBS, ARC3 lakes, Filled lakes and the respective differences between them.*

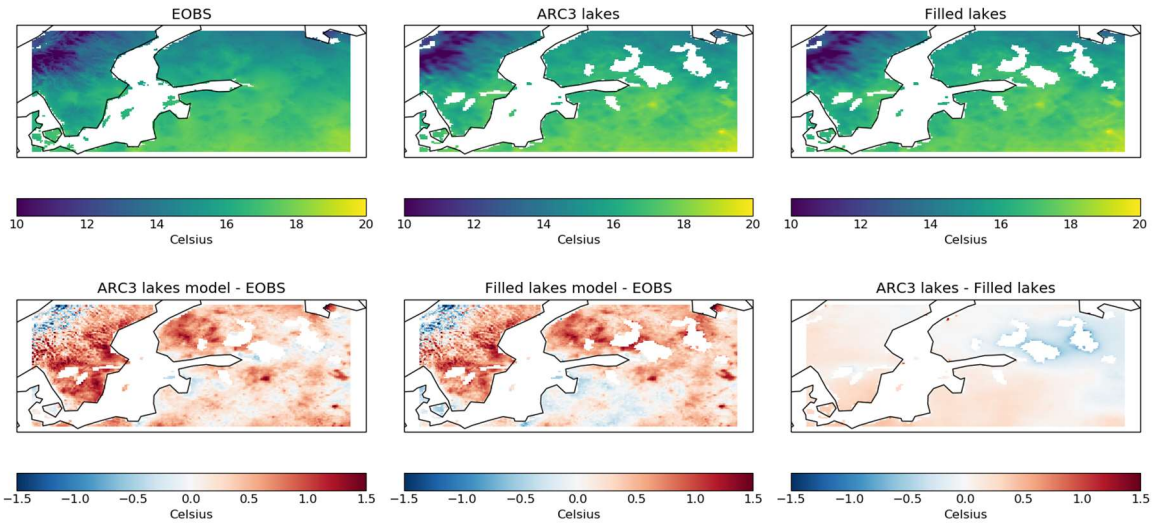

Figure 3.7.7*: JJA seasonal mean (1996-2012) surface air temperature with RCM lakes masked out for: E-OBS, ARC3 lakes simulation, Filled lakes simulation and the respective differences between them.*

Figure 3.7.8 shows the seasonal mean of winter precipitation for the larger lakes in the domain (with the lakes masked out). In the wider domain (figures not included), there is a wet bias of ~25%, and E-OBS is known to under-catch precipitation, particularly over complex orography (Kotlarski, et al. 2019). Precipitation over land surrounding the larger lakes is slightly increased (0.5-1 mm/day) in the ARC3 lakes experiment compared to the Filled lakes experiment. This makes intuitive sense given the presence of a warmer water body increasing evaporation and moisture.

The opposite is true in JJA (Figure 3.7.9), where it is generally drier over the land surrounding the lakes (up to 1mm/day). It is possible the reduction in precipitation is due to decreased evaporation (the ARC3 lakes simulation is cooler than the Filled lakes simulation), but there was not time to properly investigate the cause. This drying slightly reduces the wet bias with respect to E-OBS. In the wider domain, there is a summer wet bias in Northern Europe and over the Alps (similar magnitude to winter), and a smaller dry bias in Central Europe. There is a small increase in cloud amount (figures not included) over the larger lakes of up to ~3% in the ARC3 lakes run, but there are similar sized differences elsewhere in the domain so it is not possible to attribute these to the addition of lakes without further work for which there was not time.

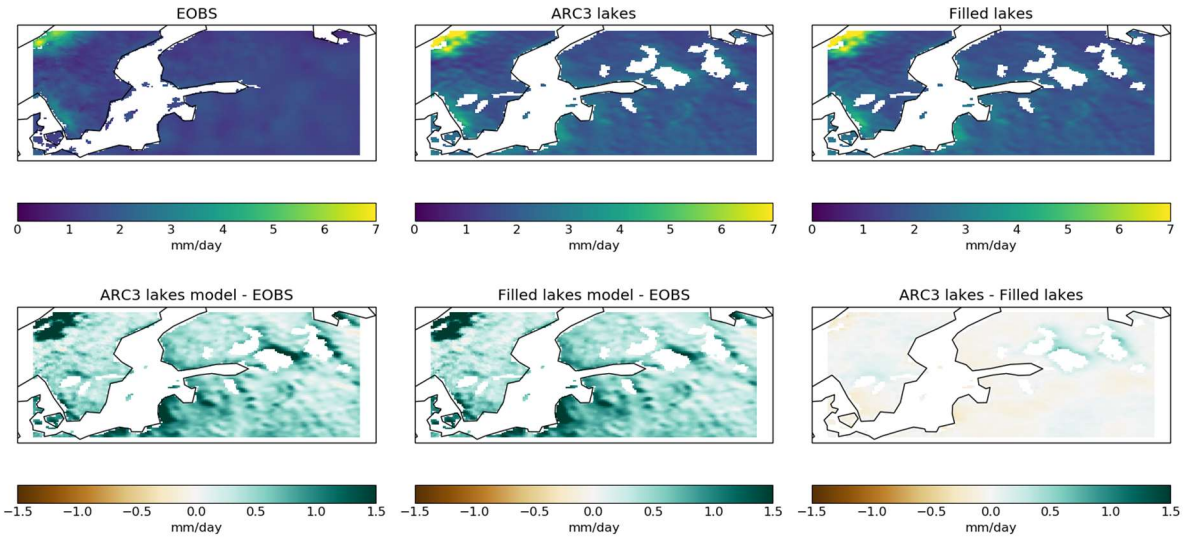

Figure 3.7.8*: DJF seasonal mean (1996-2012) precipitation with RCM lakes masked out for: E-OBS, ARC3 lakes, Filled lakes and the respective differences between them.*

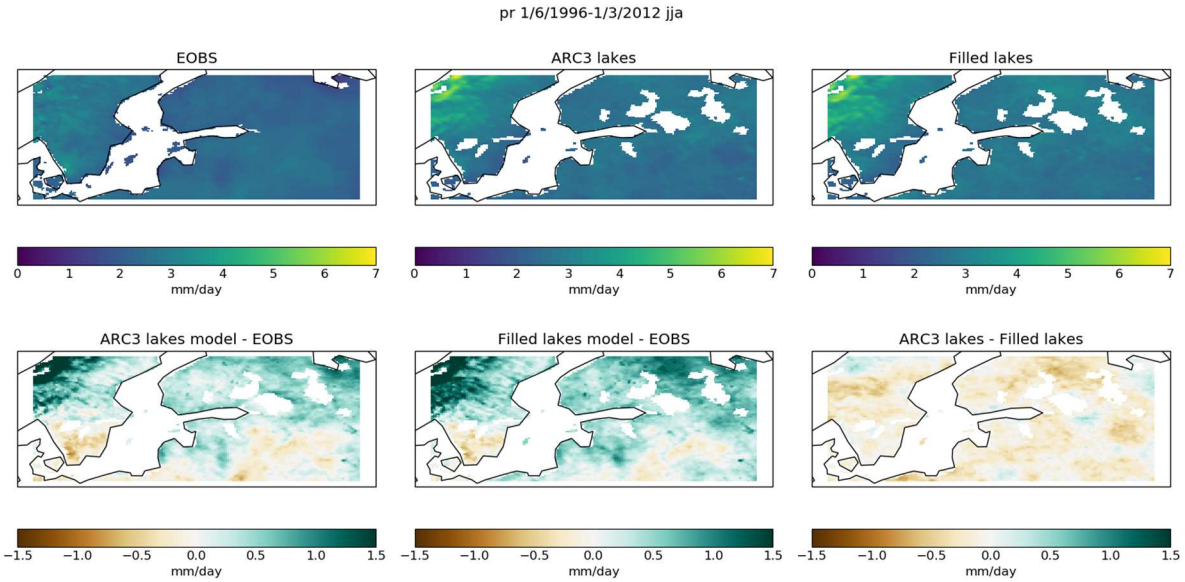

***Figure 3.7.9**: JJA seasonal mean (1996-2012) precipitation with RCM lakes masked out for: E-OBS, ARC3 lakes, Filled lakes and the respective differences between them*

A comparison of seasonal mean skin temperature (which is equivalent to SSMI SSMIS L3C land surface temperature) is shown in Figures 3.7.10 and 3.7.11. In winter there is a significant difference between the SSMI SSMIS L3C observations and the RCM experiments (Figure 3.7.10). The RCM experiments are ~4°C warmer than the observations except over the Alps, the Balkans and parts of Norway and Sweden where the RCM is cooler than the observations. This is contrary to the cool bias of winter surface air temperature in the RCM compared to E-OBS (Figure 3.7.4). Over the lakes and surrounding land areas DJF skin temperature differences between the ARC3 lakes and Filled lakes simulations are very similar to air surface temperature, with small lakes being warmer but not effecting the temperature of the surrounding land, but larger lakes, particularly in Russia and South Finland having a significant influence over surrounding land surface temperatures.
The summer skin temperature differences (Figure 3.7.11) show smaller differences between observations and RCM experiments, with a warm bias over Central Europe (similar to that seen in E-OBS surface air temperature) and bodies of water, and cool biases (~2°C) over Northern Europe, Spain, Portugal and Turkey. The cooler lakes can be seen in the observations and ARC3 lakes reduce the warm bias over them compared to the filled lakes run. For DJF the opposite is true, the lakes are warmer than the surrounding land and the warm bias with respect to SSMI SSMIS L3C is exacerbated.

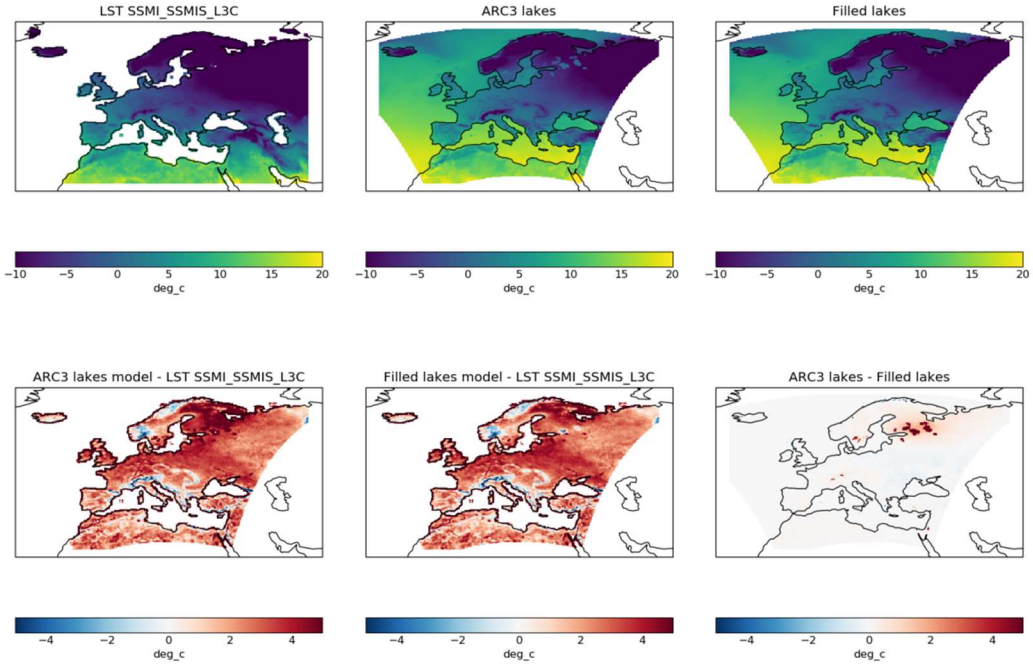

***Figure 3.7.10**: DJF seasonal mean (1996-2012) skin temperature for: SSMI SSMIS L3C, ARC3 lakes simulation, Filled lakes simulation and the respective differences between them.*

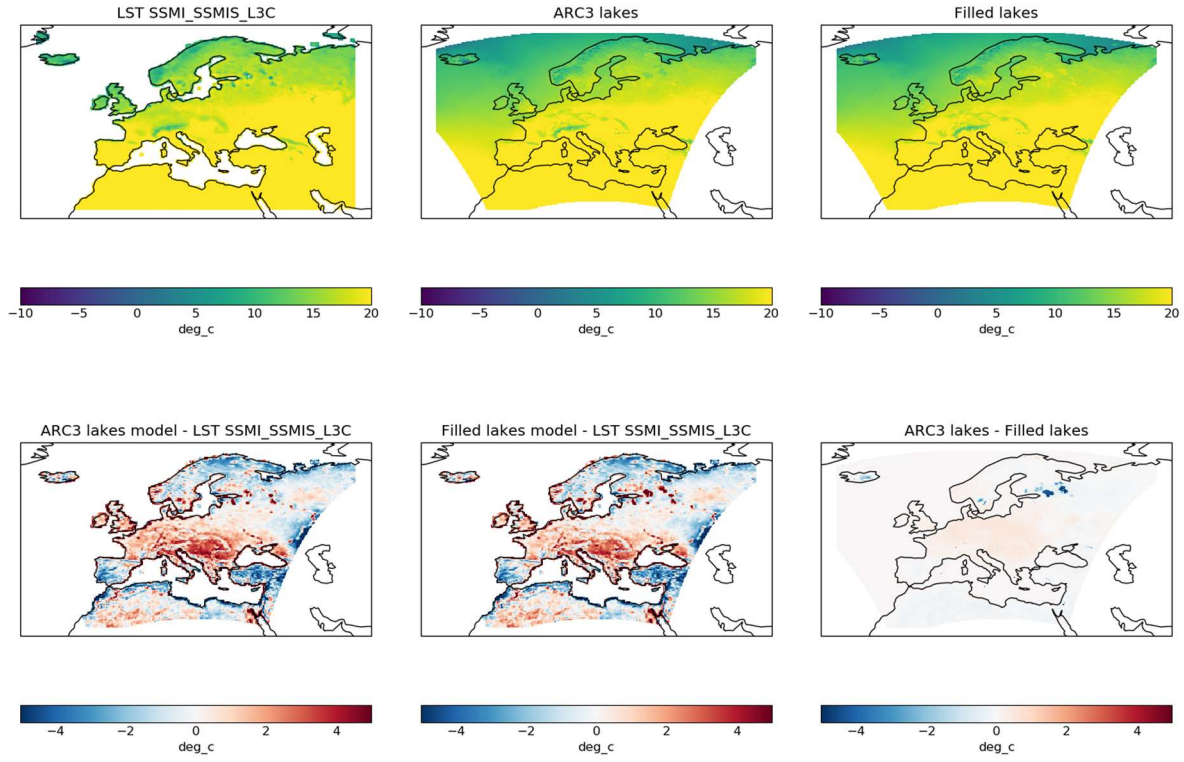

***Figure 3.7.10**: JJA seasonal mean (1996-2012) skin temperature for: SSMI SSMIS L3C, ARC3 lakes simulation, Filled lakes simulation and the respective differences between them.*

3.7.4 Summary

The current CCI LSWT and LIC datasets are of limited use to the climate modelling community due to the large amount of cloud cover gaps in the data at daily timescale. This makes them unsuitable for using as model input or for robust validation of model output. However, if a reconstruction was applied as was done to a previous ESA LSWT product (ARC3), they could prove very useful indeed. It would also be beneficial if scientifically/mathematically plausible, to try to build on ARC3 by creating a spatially coherent daily time series, rather than point data. Spatial data would be particularly useful for larger lakes.

The difference between the RCM experiments demonstrates that there is a clear impact on climatological means of the surrounding air when including prescribed LSWT and LIC data. This generally only applies to larger lakes, but this could be a function of using a 12km RCM where each grid box is 144km^2. The cold bias in surface air temperature over Russia in winter (compared to E-OBS) is reduced in the prescribed lakes run, and to a lesser extent, the warm bias in summer is also reduced. There were smaller effects on precipitation. The land surrounding the larger lakes experienced more precipitation in winter, and less in the summer in the ARC3 lakes experiment compared to the Filled lakes experiment. Unfortunately, there was not the opportunity in this study to look more deeply into the interactions between the lakes and the surrounding land areas, but this would be an area of interest if there were to be any future work. Extreme precipitation and temperature indices, not included in this analysis, could also support for the improvement of the description of lakes and their coupling with the atmosphere, another aspect which could be considered in future work.

Publications

None so far, this research could be the first step in the inclusion of a lake component in the Met Office regional model, which might lead to a publication.

Interactions with the ECVs used in this experiment

Lake ECVs team helped to understand the dataset produced by this project and suggested alternative dataset which better matched the high-frequency/completeness requirement of for using lake ECVs in a regional climate model experiment. Land surface temperature dataset also used for climate model validation.

Consistency between data products

ECV lake products from this project not used directly.

Recommendations to the CCI ECV teams

The main recommendation, discussed in the main text, is to support the work needed to fill gaps in the daily LST and Lake ice datasets by a physics-based reconstruction such as the procedure used by MacCallum and Merchant (2012).

3.8 Evaluation of the impact of an enhanced ESA Sea Ice reanalysis (EnESA-SIR) on initialization of seasonal prediction

Lead partner: BSC
Authors: Juan Camilo Acosta-Navarro, Rubén Cruz-García, Vladimir Lapin, Yohan Ruprich-Roberts, Valentina Sicardi, Pablo Ortega.

Aim

The aim of this research is to quantify the benefits on forecast skill related to an enhanced initialization of sea ice (based on a reanalysis that includes both assimilation of Sea Ice Concentrations (SIC) from ESA CCI and nudging to ocean temperature and salinity observations). This is an improved strategy to the one previously used by the BSC, which only included assimilation of ocean temperature and salinity. The EnESA-SIR now employed should improve the prediction skill over the Arctic, and has also the potential of improving the predictions in other remote regions via some observed atmospheric teleconnections. This work addresses the following scientific questions

1. What are the benefits of initializing with the new EnESA-SIR reconstruction on the seasonal climate forecast quality?
2. Is there any added-value in the assimilation of SICs?
3. Are there any benefits for the predictive skill in remote regions? If yes, can those benefits be traced back to the assimilation of Arctic SICs?

Key Outcomes of CMUG Research

Scientific outcome: The experiments performed and analysed have revealed important benefits from the assimilation of SICs, especially in the summer season, that will be described in the following section.

Technical outcome: The model capabilities developed to enable the assimilation of sea ice concentrations through nudging have been finally implemented in the CMIP6 version of the Earth System Model EC-Earth, and will be used in all new future prediction systems developed at the BSC. An additional capability to assimilate sea ice thickness data has been also developed, and could be considered in the future to further enhance the ocean reanalysis, exploiting the ESA sea ice thickness products available.

Summary of Results

Production and evaluation of the enhanced Sea Ice reanalysis:

In order to perform the reanalysis, we had first to implement some technical developments, in particular to include the nudging capabilities in the CMIP6 version of EC-Earth. The nudging module for ocean temperature and salinity was introduced in the CMIP6 version of EC-Earth at the beginning of 2019 by Valentina Sicardi and Yohan Ruprich-Robert. Later in that year, Vladimir Lapin introduced in the model an additional nudging routine to assimilate sea ice concentrations and sea ice thickness. This module was subsequently tested, with encouraging results. Figure 3.8.1 shows that, for a nudging experiment with EC-Earth that assimilates the sea ice concentrations in July-August-September (JAS) for a future Arctic/Antarctica scenario (Smith et al. 2019), the model constrains quite accurately the target fields. Indeed, when computing the difference between the simulations and the target fields, values are always below 10% for all seasons, and are particularly small in JAS in the Arctic, with errors in the order of 2%.

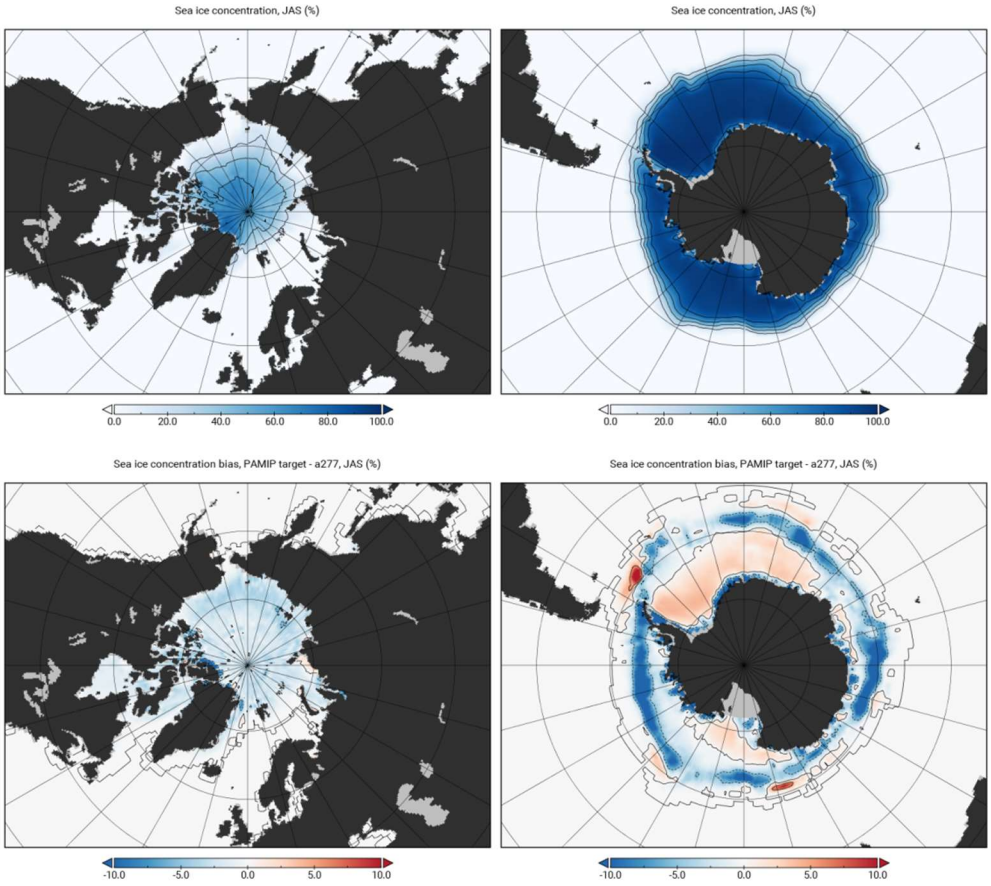

Figure 3.8.1: *(top) Average of JAS sea ice concentrations (shaded in %) in a simulation with EC-Earth3.3 that assimilates the sea ice of a future Arctic/Antarctic scenario (Smith et al. 2019; contours in increments of 20%), respectively. (bottom) Difference in JAS sea ice concentrations (in %) between the EC-Earth nudged experiment and the reference future Arctic/Antarctic sea ice concentrations, respectively.*

This same version of the model has later been used to produce two in-house reanalyses covering the period 1990-2018, one assimilating SICs, temperature and salinity (i.e., the enhanced reanalysis), and another baseline reconstruction that only assimilates temperature and salinity. In both cases the reconstructions were produced with the ocean-sea ice stand-alone version of EC-Earth, forced with surface fluxes from the ERA5 atmospheric reanalysis, and the target dataset considered for ocean temperature and salinity nudging was the ocean reanalysis ORAS5. For the enhanced sea ice reanalysis, three different members were produced, assimilating in each case a different SIC product to sample the uncertainty in the observational datasets: OSISAFv2 (recommended by the Sea Ice ECV), CERSAT and ORAS5.
Production of the seasonal predictions:

Two different sets of seasonal predictions were performed in the second half of 2020 with the coupled version of EC-Earth, the first initialised from the enhanced reanalysis, and the second from the baseline reconstruction. By construction, the comparison of both prediction systems allows to determine the impact of SIC assimilation on the seasonal predictive skill. Each system considers the re-forecast period 1992-2018 (27 years) and has 30 members, a 7-month forecast horizon and two different start months (November and May).

A first exploratory analysis revealed that SIC assimilation had a positive impact on the skill of Arctic sea ice, but mostly in the May-initialised predictions, with very marginal improvements and in some cases deteriorations of skill obtained for the November-initialised re-forecasts. This pointed to a potential issue in the nudging protocol for SIC during the winter season that is currently under investigation, and prompted us to focus the main analyses on the May initialized predictions.

Main results:
To measure the predictive skill, we use the anomaly correlation coefficient (ACC) metric. In addition, to quantify the impact of SIC assimilation on the predictive skill, we compute ACC differences between the system initialised with the enhanced reconstruction and the system initialised from the baseline reconstruction. Figure 3.8.2 shows that SIC assimilation provides clear improvements in the prediction of SIC that are visible in the first forecast month (May), in particular over the Atlantic sector of the Arctic, and persist in June and also July-August-September, when important increases in skill are visible in the Barents Sea.

Interestingly, skill improvements with SIC assimilation are also seen beyond the Arctic. The most striking improvement is a region of increased ACC in SST in the North Atlantic. The improvements start emerging during May and intensify over the subsequent months (Figure 3.8.3 top row), a result that is consistent regardless of the observational reference considered (i.e., from SST-ECV or other alternative datasets; not shown). The initial improvement in May appears to be connected with the SIC improvements, via a teleconnection mechanism between Arctic Sea Ice and the atmospheric circulation in the North Atlantic (not shown), which leads to a local improvement in the predictability of the geopotential height at 500m (GPH500; Figure 3.8.3 bottom row). This improved skill in GPH500 leads to improved predictions of the local surface atmosphere temperature, which can explain the SST improvements (Figure 3.8.3 middle row). Persistence mechanisms in the ocean amplify and maintain the skill improvements in North Atlantic SSTs at subsequent forecast months.

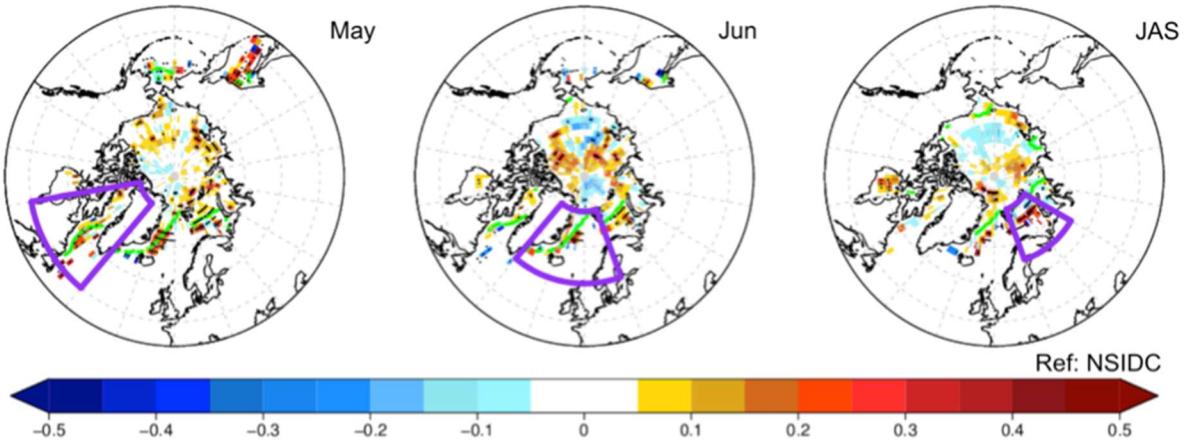

Figure 3.8.2: *Difference in the Anomaly Correlation Coefficient (ACC) for predicting the Sea Ice Concentration in May (left), June (center) and July-August-September (right) between two sets of seasonal re-forecasts, one initialised from the enhanced reconstruction and another from the baseline reconstruction. Positive values imply improved skill when SIC is assimilated. Both re-forecast systems include 30 members and cover the period 1992-2018. ACC values are computed against the observational reference NSIDC, which is independent from those considered for assimilation. Significant differences at the 95% confidence level are highlighted with stippling.*

The SST improvements have a beneficial impact on the predictability of the atmospheric circulation during the late summer and autumn (Figure 3.8.4 top row). This role of the SST is further supported by the ACC difference maps in the bottom panels of Figure 3.8.4. in which the reforecast system initialised with SIC assimilation is compared against itself, but after regressing out, from the forecasted GPH500, the variability of an SST index averaged over the North Atlantic region of the skill improvements. This SST index is computed in July-August-September to represents a leading influence on the atmospheric circulation. The differences in the bottom panel of Figure 3.8.4 thus quantify the impact of those local SSTs on the predictive skill of GPH500 several months later, and nicely show that the largest impacts occur in the same regions in which the predictions with SIC assimilation have GPH500 predictive skill (Figure 3.8.4 top panel). Further analyses have shown that the skill improvements in GPH500 also translate into higher predictive skill for surface air temperature and precipitation over Eurasia (not shown).

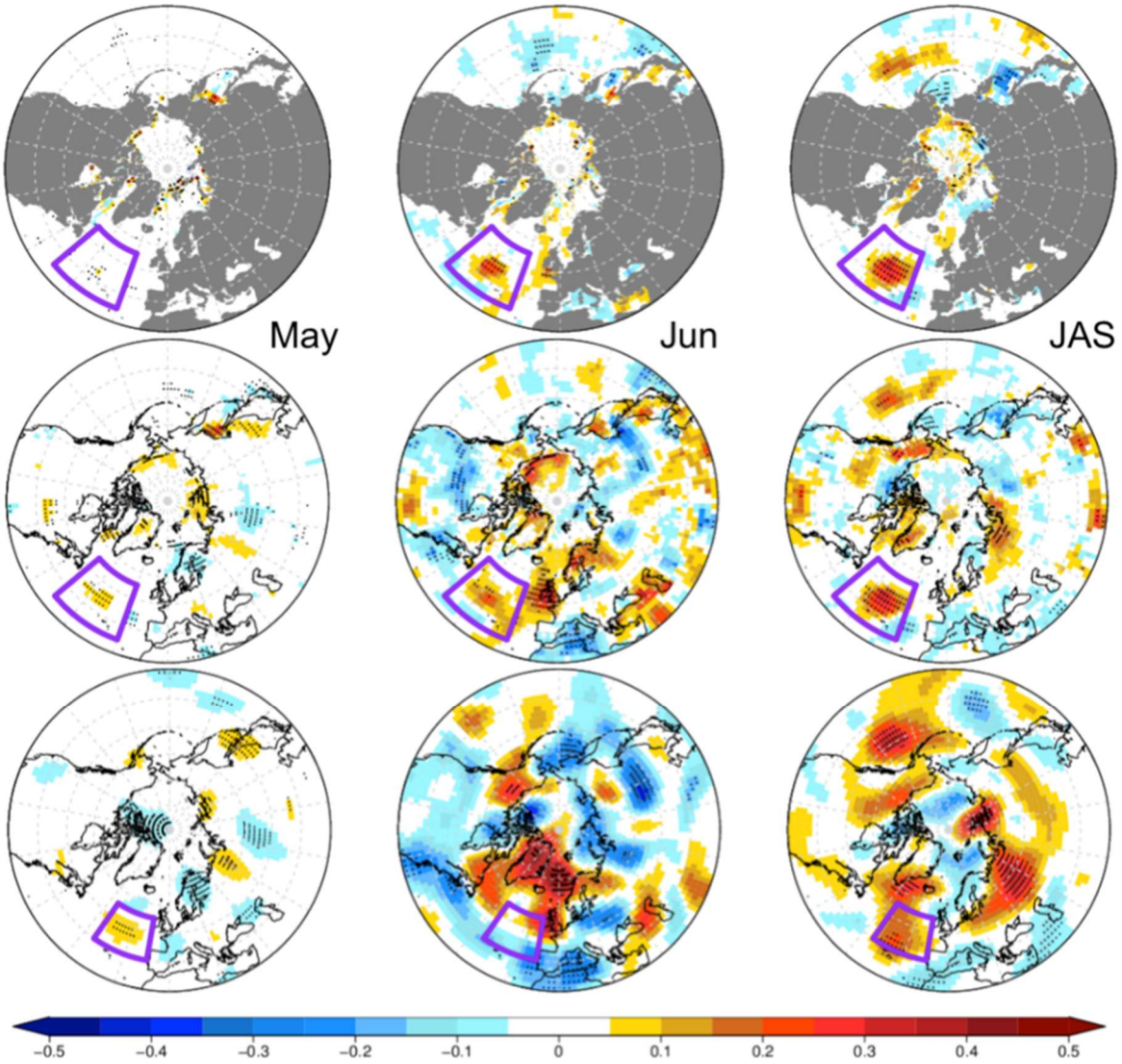

Figure 3.8.3: *The same as in Figure 3.8.2 but for the ACC differences in sea surface temperature (top), 2m air temperature (middle) and the geopotential height at 500m (bottom). In all cases the reference observational dataset is ERA5, to make sure that all observational references are fully physically consistent, and thus facilitate the interpretation of the results.*

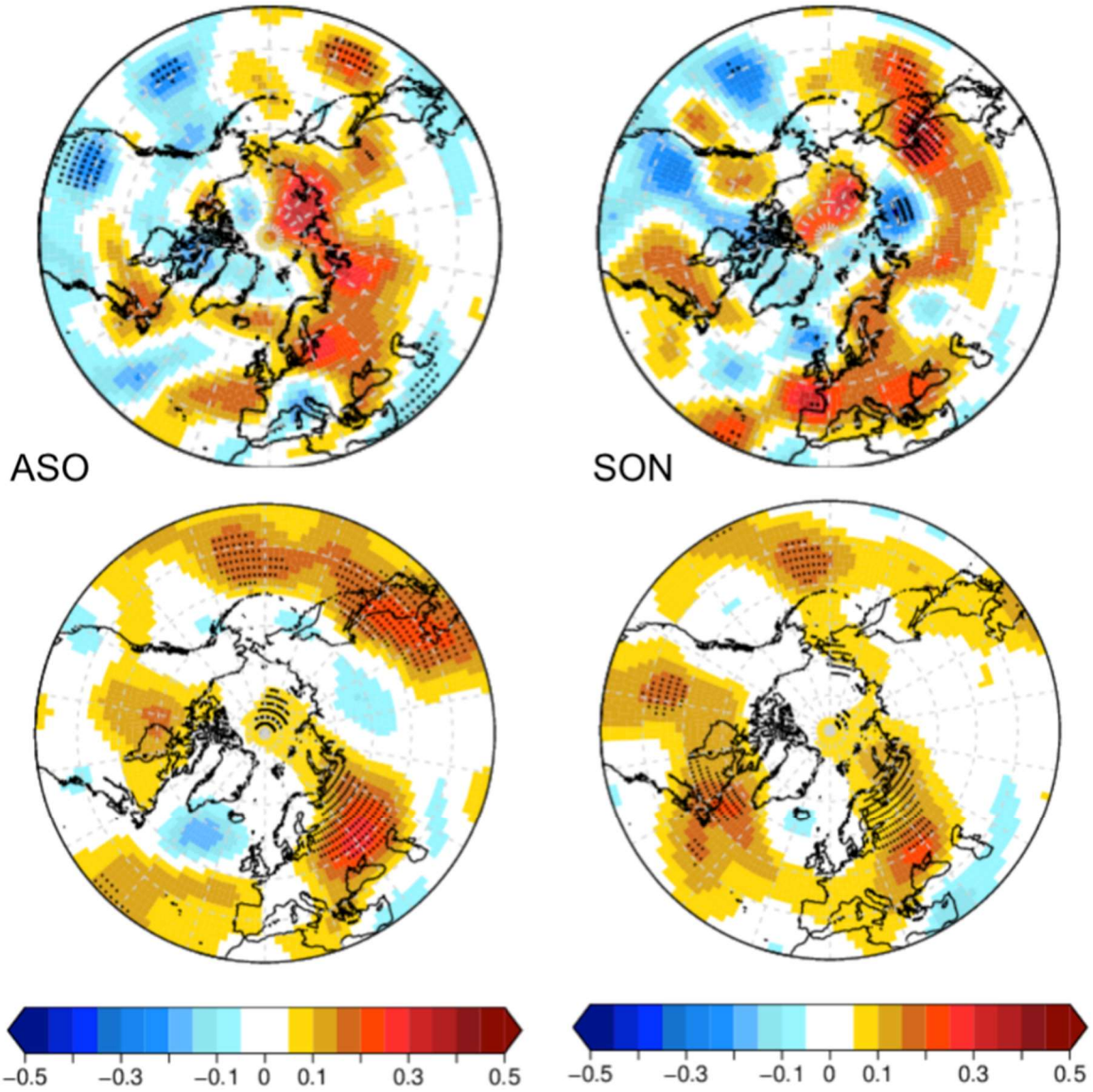

Figure 3.8.4: *(Top) ACC difference for the geopotential height at 500m in August-September-October (left) and September-October-November (right) in the two same reforecast systems of Figure 3.8.2. (Bottom) ACC difference between for the same variable and temporal averages, but in this case between the reforecast system initialised from the enhanced reanalysis, and the same system, but after regressing out the variability of SST in July-August-September averaged over a selected region in the North Atlantic (purple box in Figure 3.8.3 top panel).*

Publications

Acosta-Navarro et al. (2022).

Interactions with the ECVs used in this experiment

There have been good interactions with the CCI ECV teams whose data are being used in this CMUG WP. In particular, Thomas Lavergne (Sea Ice CCI) recommended us the use of OSISAFv2as the most reliable product from the CCI on Sea Ice for the enhanced sea ice reanalysis.

Consistency between data products

We considered three different SIC products to produce the enhanced sea ice reanalysis to be able to explore the sensitivity of the results to the specific product used. No major differences have been observed. Figure 3.8.5 is included as an illustration of the large similarities across products. It shows the integrated ice edge error (a metric designed to measure the errors in predicting the sea ice edge that avoids error compensation) for the whole Arctic basin for three different cases. In each panel, only 10 members from the whole re-forecast system are considered, and correspond to all members that used either ORAS5, OSISAFv2 or CERSAT for assimilation. We can see that in all cases there are large error reductions in the first forecast month, followed by modest reductions in the second month (June). Those assimilating CERSAT seem to have also reduced errors in July, although is hard to tell if this result indicates that the CERSAT product is superior, or if this (and other) differences across products emerges due to the reduced number of members. We have also repeated some of the previous figures separately for the different members, and the main findings appear to be robust (e.g. the increased skill of SST in the North Atlantic with SIC assimilation, and the subsequent improvements in GPH500 skill).

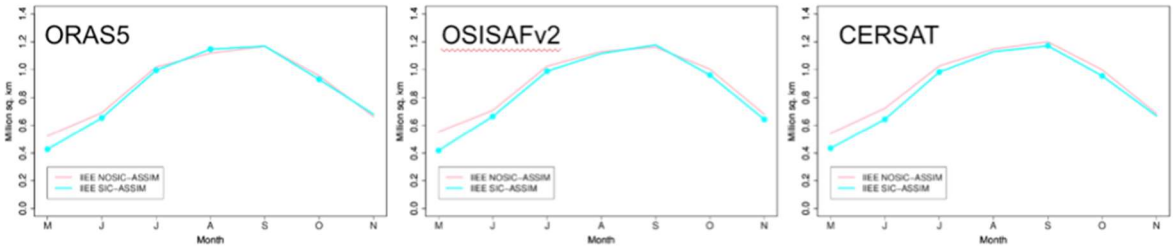

Figure 3.8.5: *Integrated Ice Edge Error as a function of forecast month in the re-forecast systems initialised from the enhanced and baseline reconstructions. Each panel shows the results for the members that are initialised assimilating one of the three different SIC datasets.*

Recommendations to the CCI ECV teams

In order to assess the benefits for predicting the skill in other ECVs, like Sea Surface Salinity, extending current products to cover at least a couple of decades would be needed, so that skill metrics can be estimated more robustly.

3.9 Biophysical feedbacks in the global ocean

Lead partner: Met Office
Authors: David Ford

Aim

The distribution of chlorophyll in the ocean has an impact on light attenuation and therefore ocean heat uptake, changing the ocean physics and sea ice. However, this biophysical feedback is not yet commonly included in climate models or reanalyses. This activity will assess the suitability of CCI ocean colour products to constrain this process when assimilated into coupled physical-biogeochemical ocean reanalyses. Assimilating ocean colour data has been demonstrated to improve the accuracy of 3D model chlorophyll, and it is expected that this will lead to more accurate simulation of light attenuation and ocean heat uptake in reanalyses, when biophysical feedback processes are included. This should then improve consistency with other ECVs.

Furthermore, air-sea CO_2 flux parameterisations typically used in climate models do not use sea surface state as an input, even though this is known to play a role. A further experiment will assess the impact on air-sea gas exchange of including sea state data as an input in the flux parameterisation. A final experiment will assess the impact of using skin rather than foundation SST in the air-sea flux calculations.

It will address the following scientific questions:

1. What is the impact on model physics and biogeochemistry of using chlorophyll constrained by assimilating OC-CCI data in the light attenuation calculations?
2. Does this lead to improved validation against and consistency with other ocean ECVs (SST, SSS, SL, SI) from CCI?
3. How sensitive are modelled air-sea CO_2 fluxes to the inclusion of significant wave height and skin SST in the air-sea flux parameterisation?

Key Outcomes of CMUG Research

1. Two-way physics-biogeochemistry coupling has been implemented in the ocean components of an Earth System model. The impact was to increase SST and decrease ocean heat content, with regional and seasonal variations. Assimilating OC-CCI data enhanced these changes in the model considered.
2. By comparing assimilative and free-running simulations, it was found that the uncertainties due to errors in the model chlorophyll were of a comparable magnitude to the changes introduced by two-way coupling. Models may therefore require further development, or for feedbacks to be constrained by observation data.
3. Modelled air-sea CO_2 fluxes are sensitive to the use of sea state data, and this should be investigated further in climate models.
4. Modelled air-sea CO_2 fluxes are modified by using skin rather than foundation SST, though this may be a spin-up effect and should be investigated further.

Summary of Results

The assimilation of chlorophyll from CCI ocean colour products to constrain the light attenuation and ocean physics builds on work previously performed with precursor GlobColour data, and during the previous phase of CMUG. A paper describing results assessing multivariate consistency of ocean CCI products, from experiments performed during the previous phase of CMUG, has recently been published in a peer-review journal (Ford, 2020, "Assessing the role and consistency of satellite observation products in global physical-biogeochemical ocean reanalysis", https://os.copernicus.org/articles/16/875/2020/). This was followed up by a blog post for EGU highlighting CCI and CMUG (https://blogs.egu.eu/divisions/os/2020/09/22/satellite-data-for-ocean-reanalysis/). A key result from this paper, which will directly inform the work performed in WP3.9, is shown in Fig. 3.9.1. Previous studies have suggested a direct correlation between the timing of the initiation of the spring bloom and that of the annual switch from negative to positive air-sea heat fluxes. Other studies have reached contrasting or mixed conclusions. This may in part be due to some studies looking at chlorophyll concentration, and others at phytoplankton biomass. The reanalyses produced as part of CMUG provided an opportunity to look at this relationship in a long model time series, and the impact of data assimilation. In the free-running model, there was a strong positive correlation between phytoplankton biomass and net air-sea heat flux across much of the ocean, whereas for chlorophyll concentration the correlation with net air-sea heat flux was weaker, and often negative at low latitudes. This suggests that seasonal variations in carbon-to-chlorophyll ratio play an important role, and that studies of phytoplankton bloom initiation based solely on chlorophyll data may not provide a full understanding of the underlying processes.

In WP3.9, experiments have been performed using the ocean and sea ice components of the UKESM1 Earth System model, which contributed to CMIP6. NEMO[2] was used to model ocean physics, MEDUSA[3] for ocean biogeochemistry, and CICE[4] for sea ice. Atmospheric forcing was provided by the ERA5 reanalysis. Data assimilation was performed using the 3D-Var NEMOVAR scheme. Assimilation and validation used v5.0 OC-CCI data, v2.1 SST-CCI data, v1.8 SSS-CCI data, v2.0 SL-CCI data, OSI SAF SI data (as SI-CCI does not provide a gap-free record for the period run), and v1.1 SS-CCI data. This section will first detail experiments focussed on two-way physics-biogeochemistry coupling through the light attenuation, and then detail experiments focused on air-sea CO_2 flux parameterisations.

[2] https://www.nemo-ocean.eu/
[3] https://ukesm.ac.uk/ukesm-component-models/ocean-biogeochemistry/ocean-biogeochemistry-ukesm1/
[4] https://climatemodeling.science.energy.gov/technical-highlights/cice-consortium-model-sea-ice-development

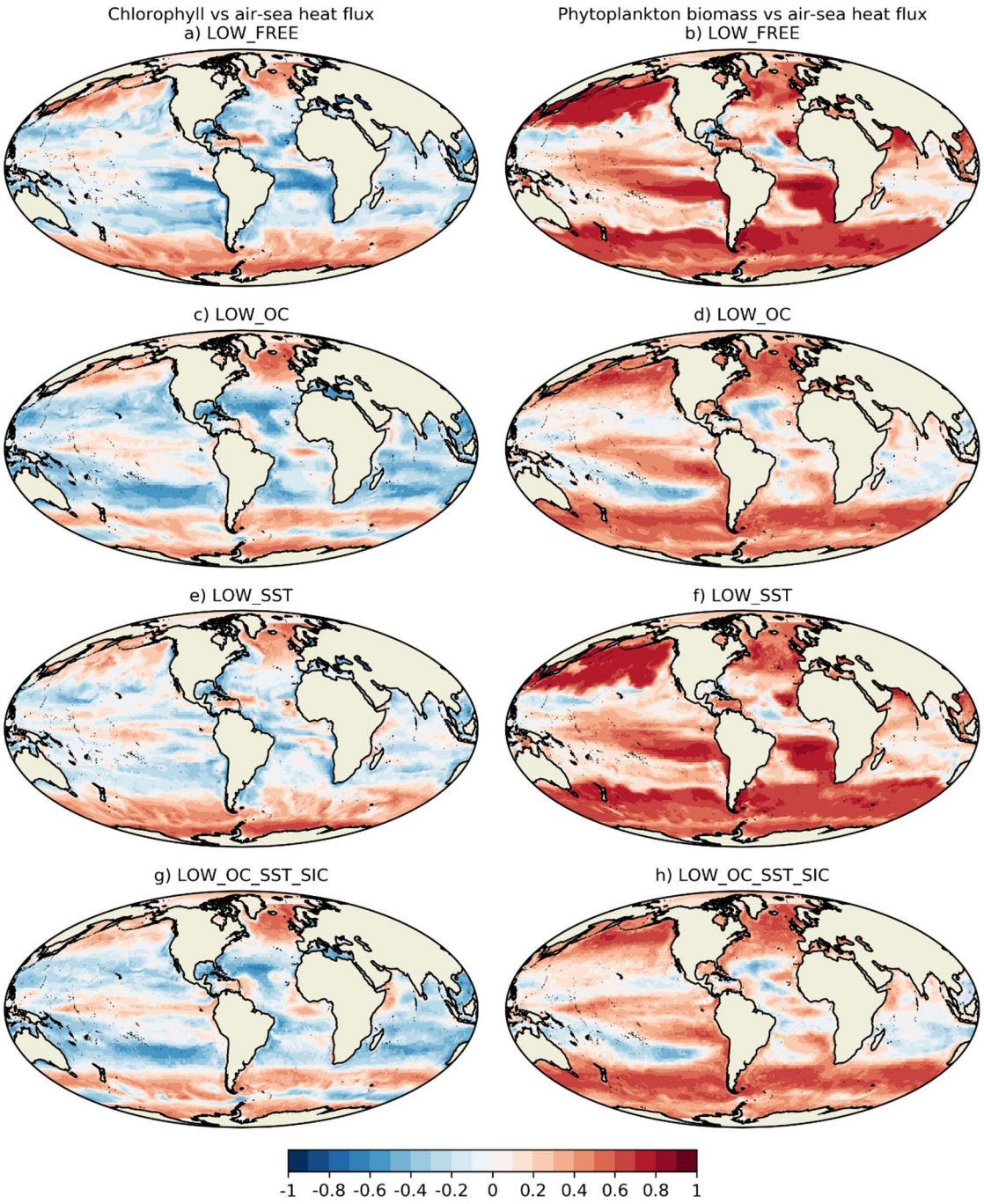

Figure 3.9.1*: Maps of correlation between surface chlorophyll and net air-sea heat flux (left column) and surface phytoplankton biomass and net air-sea heat flux (right column), covering 1998 - 2010 for model runs with (a-b) no data assimilation, (c-d) assimilation of CCI ocean colour, (e-f) assimilation of CCI SST, (g-h) assimilation of CCI ocean colour, SST and sea ice. Taken from Ford (2020).*

Two-way physics biogeochemistry coupling

For the two-way physics-biogeochemistry coupling, some modifications were made to NEMO and MEDUSA. This allowed NEMO and MEDUSA to both use the same light model, that of Lengaigne et al. (2007), used by NEMO in UKESM1. The light model calculates light attenuation coefficients based on chlorophyll concentration. By default, a constant chlorophyll value of 0.05 mg m^{-3} is used in UKESM1. The option was added to instead use 4D-varying chlorophyll from MEDUSA. In NEMO, where the light model is used to calculate heating from solar radiation, some experiments used constant chlorophyll and some MEDUSA chlorophyll, as detailed below. In MEDUSA, where the light model is used to calculate the available light for photosynthesis, MEDUSA chlorophyll was always used. Four main experiments were run, as shown in Table 3.9.1. These used a 1° resolution configuration, covering a ten-year period from 1 Jan 2010 to 31 Dec 2019. Initial conditions were taken from an existing hindcast. *One-way free* and *One-way OC DA* each used the default one-way coupling with NEMO seeing constant chlorophyll, so had identical physics simulations. The runs differed in that *One-way OC DA* assimilated chlorophyll from OC-CCI, changing the biogeochemistry. Equivalent experiments were run with two-way coupling and NEMO seeing the MEDUSA chlorophyll, *Two-way free* and *Two-way OC DA*. This allowed the impact of two-way coupling in the free-running model, and the subsequent difference due to assimilating OC-CCI data, to be assessed.

Additionally, shorter versions of these experiments were run at 1/4° resolution, to better assess spatial features across multiple ECVs. These are discussed in the "Consistency between data products" section below. Furthermore, some sensitivity experiments were run where output from *Two-way OC DA* was used to constrain the light field of NEMO and/or MEDUSA while the biology remained unconstrained by assimilation. This can allow a more detailed understanding of physical-biogeochemical interactions related to bloom initiation. Results are not detailed here but may be explored in a future journal paper.

Table 3.9.1: Main two-way physics-biogeochemistry coupling experiments.

RUN ID	CHLOROPHYLL SEEN BY NEMO	ASSIMILATION
One-way free	Constant (0.05 mg m^{-3})	None
One-way OC DA	Constant (0.05 mg m^{-3})	Ocean colour
Two-way free	Varying (MEDUSA)	None
Two-way OC DA	Varying (MEDUSA)	Ocean colour

Fig. 3.9.2 shows the mean SST in *One-way free*, and the difference to this from *Two-way free* and *Two-way OC DA*. Fig. 3.9.3 shows the same for temperature at 100 m depth. In the free-running model, two-way coupling raises the mean SST across most of the ocean, except the subtropical gyres where SST is reduced. The biggest SST increase is in the tropics. This pattern broadly matches the mean chlorophyll in MEDUSA (not shown). Assimilating OC-CCI data modifies the MEDUSA chlorophyll, including increasing concentrations in the subtropical gyres, and this change is reflected in the SST. At 100 m depth (Fig. 3.9.3), the temperature change introduced by the two-way coupling is mostly opposite in sign to the change at the surface. This is in line with expectations: increasing chlorophyll results in light being absorbed and scattered and penetrating less deeply, so the associated heating is concentrated nearer the surface. An exception in the decadal mean is in the equatorial Pacific in *Two-way OC DA*: despite high chlorophyll concentrations, there is a surface cooling. This is due to the cooler subsurface waters being advected towards the equator and upwelled, counteracting the direct warming effect from the chlorophyll.

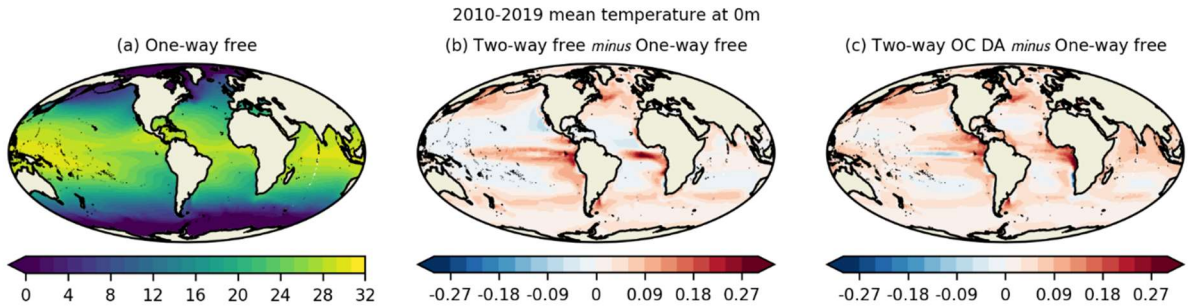

Figure 3.9.2: *Mean SST for 2010-2019. a)* One-way free*, b)* Two-way free *minus* One-way free*, c)* Two-way OC DA *minus* One-way free.

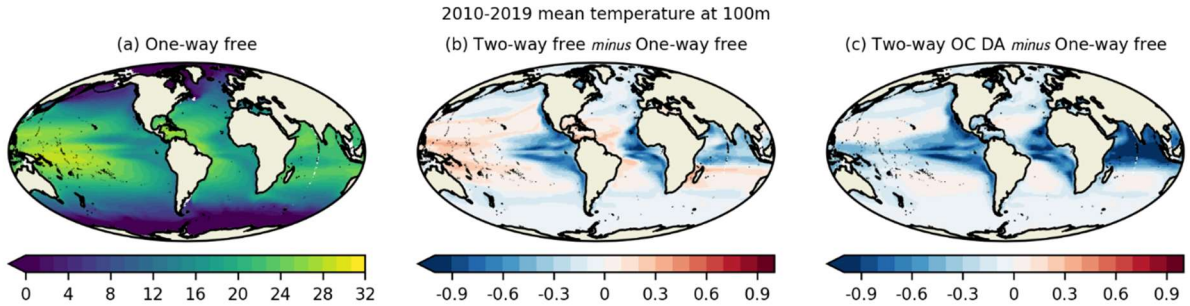

Figure 3.9.3: *Mean temperature at 100 m depth for 2010-2019. a)* One-way free*, b)* Two-way free *minus* One-way free*, c)* Two-way OC DA *minus* One-way free.

Two-way coupling resulted in an average change in the decadal mean SST of ~0.1°C, with a larger subsurface change. This is small compared with overall errors (see "Consistency between data products") but nonetheless significant. Much larger short-term differences occurred though, particularly in the Tropical Pacific, which may have important implications for some applications. The maximum change in SST due to two-way coupling was found to be 4.42°C in *Two-way free* and 4.76°C in *Two-way OC DA*. Across the whole 3D water column, the maximum change was 9.43°C and 9.83°C respectively.

The depth-related changes in temperature can be seen in the Hovmöller plots of global mean temperature in Fig. 3.9.4 and North Atlantic mean temperature in Fig. 3.9.5. In the global mean there is a warming in the upper 50 m, then a cooling down to about 250 m, with a maximum change at about 100 m. In *Two-way OC DA* the surface warming is shallower, and the subsurface cooling much larger in magnitude. It also takes a few years to spin up. The global mean hides various regional differences, an example being the North Atlantic as shown in Fig. 3.9.5. Here, the two-way coupling results in an increase in seasonal variability, with a surface warming in summer and a surface cooling in winter. This is due to cooler subsurface waters being upwelled in winter. This phenomenon is enhanced in *Two-way OC DA*.

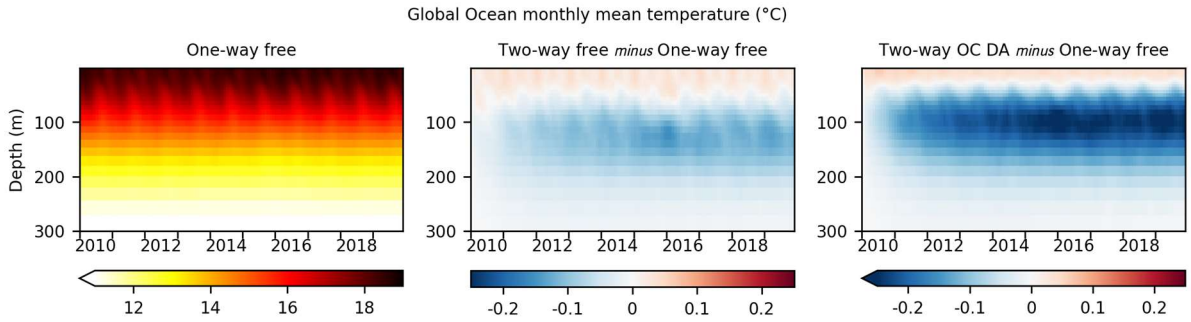

Figure 3.9.4: *Hovmöller plot of global mean temperature for 2010-2019 in the upper 300 m. a)* One-way free*, b)* Two-way free *minus* One-way free*, c)* Two-way OC DA *minus* One-way free.

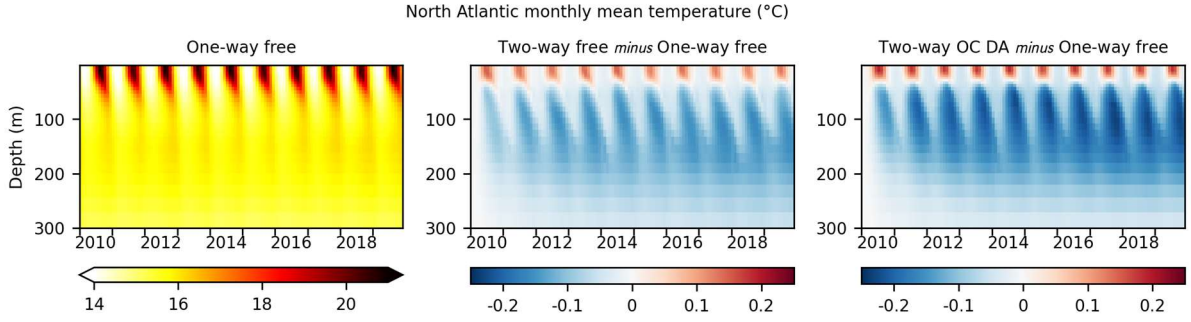

Figure 3.9.5: *Hovmöller plot of North Atlantic mean temperature for 2010-2019 in the upper 300 m. a)* One-way free*, b)* Two-way free *minus* One-way free*, c)* Two-way OC DA *minus* One-way free.

The changes in temperature result in changes to other physics variables such as salinity, mixed layer depth (MLD), sea surface height (SSH), and ocean heat content (OHC). Furthermore, these physics changes result in a cyclical impact back on the biogeochemistry. There is increased stratification and a shallowing of the MLD across most of the ocean. Changes in density and evaporation lead to changes in SSH and salinity, with a complex pattern of salinity changes that develop throughout the water column with time. There is also a marked decrease in OHC. In the final year of simulation, 2019, the globally integrated OHC is 1.99e+22 J lower in *Two-way free* than *One-way free*, and 3.87e+22 J lower in *Two-way OC DA*. The resultant impact on global mean chlorophyll of these changes is to reduce it in the surface 50 m, with a slight increase below this. There is an impact on the magnitude of the North Atlantic spring bloom, but little impact on its timing.

Validation of the experiments against CCI data is shown in the section "Consistency between data products". As well as traditional validation, these experiments can be used to assess the magnitude of the change in SST associated with uncertainty in model chlorophyll, compared with the overall change introduced by two-way coupling. Because assimilating OC-CCI data significantly reduces the error in model chlorophyll, this can be done by calculating the relative change between *Two-way OC DA* and *Two-way free*, compared with that between *Two-way free* and *One-way free*. Across much of the ocean this relative change is ~100%, and higher in the subtropical gyres. This implies that the uncertainty associated with the physics changes when two-way coupling is introduced in the free-running model can be comparable to the magnitude of the changes themselves.

These experiments have confirmed that two-way ocean physics-biogeochemistry coupling is important to consider for climate studies, changing both variability and the mean state. The results also imply caution is needed before simply including two-way coupling in climate projections, due to uncertainties in model chlorophyll. OC-CCI data could play an important role in three ways: 1) constraining chlorophyll in assimilative models, 2) being used as a climatological input field to light attenuation schemes in non-assimilative models, and 3) helping to diagnose model errors, leading to model improvements.

Air-sea CO_2 fluxes

A further set of experiments investigated the role of significant wave height (H_s) and skin SST in air-sea CO_2 flux parameterisations. The experiments used the same model setup as *One-way free* but run at 1/4° resolution from 1 Jan 2010 to 31 Dec 2012. Initial conditions were taken from a UKESM1 OMIP simulation. The runs are detailed in Table 3.9.2.

Table 3.9.2: Air-sea CO_2 flux experiments.

RUN ID	PISTON VELOCITY	SST FOR SURFACE CO_2
Control	Wanninkhof (2014)	Model top-box
Sea State	Deike and Meliville (2018) where H_s available; Wanninkhof (2014) elsewhere	Model top-box
Skin SST	Wanninkhof (2014)	Skin

Air-sea CO_2 flux is calculated as a product of the air-sea CO_2 gradient and the piston velocity *k*. *Control* used the default piston velocity parameterisation of Wanninkhof (2014), which is based solely on wind speed. *Control* also used the default setup of calculating sea surface CO_2 using temperature from the surface model grid cell, which is an average over the top 1 m.

Sea State made use of the alternative piston velocity parameterisation of Deike and Melville (2018), which is based on a combination of wind speed and H_s. As an input, daily level 3 H_s from SS-CCI was used, and upscaled to the model grid. High time resolution was required, hence the use of non-gap filled level 3 data rather than gap-filled monthly level 4 data. Therefore, in grid cells with SS-CCI H_s data available on a given day the parameterisation of Deike and Melville was used, and in other grid cells the parameterisation of Wanninkhof (2014) was used. This allowed the sensitivity of the model to the alternative parameterisation to be assessed.

Skin SST used the piston velocity parameterisation of Wanninkhof (2014), and calculated sea surface CO_2 using skin SST from the model of Artale et al. (2002), as implemented in NEMO by While et al. (2017). Using skin SST, which is typically cooler than the foundation SST more closely represented by the surface model grid cell, should give a more accurate representation of the air-sea flux. In observations, using skin rather than foundation SST has recently been shown to significantly increase calculated ocean carbon uptake (Watson et al., 2020). It is not clear whether this will also be significant in models. To validate the skin SST model, Fig. 3.9.6 shows skin minus foundation SST from the model and from SST-CCI observations, for the final day, month, and year of simulation. Due to differences in foundation SST depth and times of day considered this is not an exact like-for-like comparison, but similar patterns and magnitudes are expected. There is a good match between model and observations, including over different averaging periods.

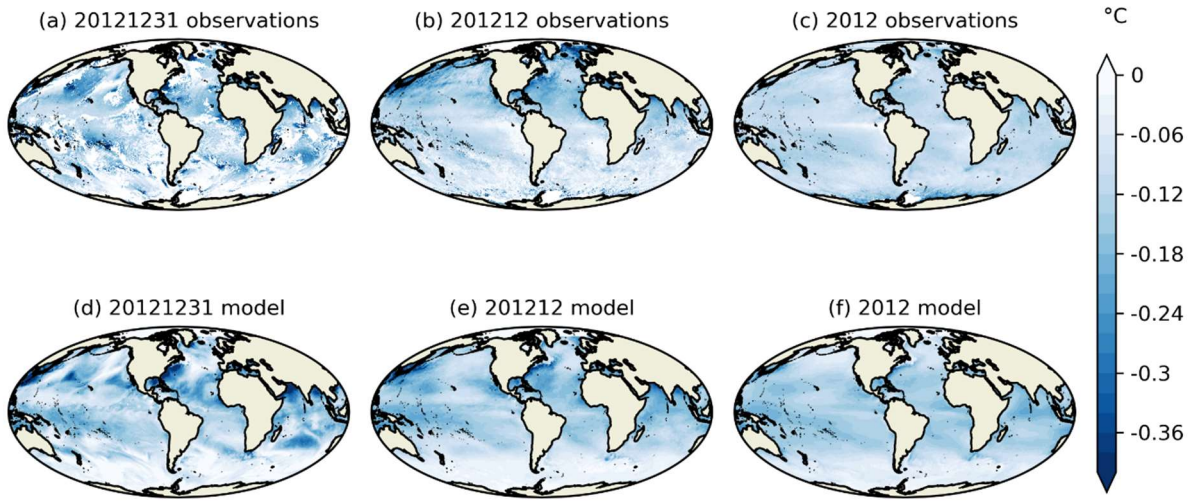

Figure 3.9.6: *Skin minus foundation SST from SST-CCI data (top row) and* Skin SST *(bottom row) for the final day (a, d), month (b, e), and year (c, f) of simulation.*

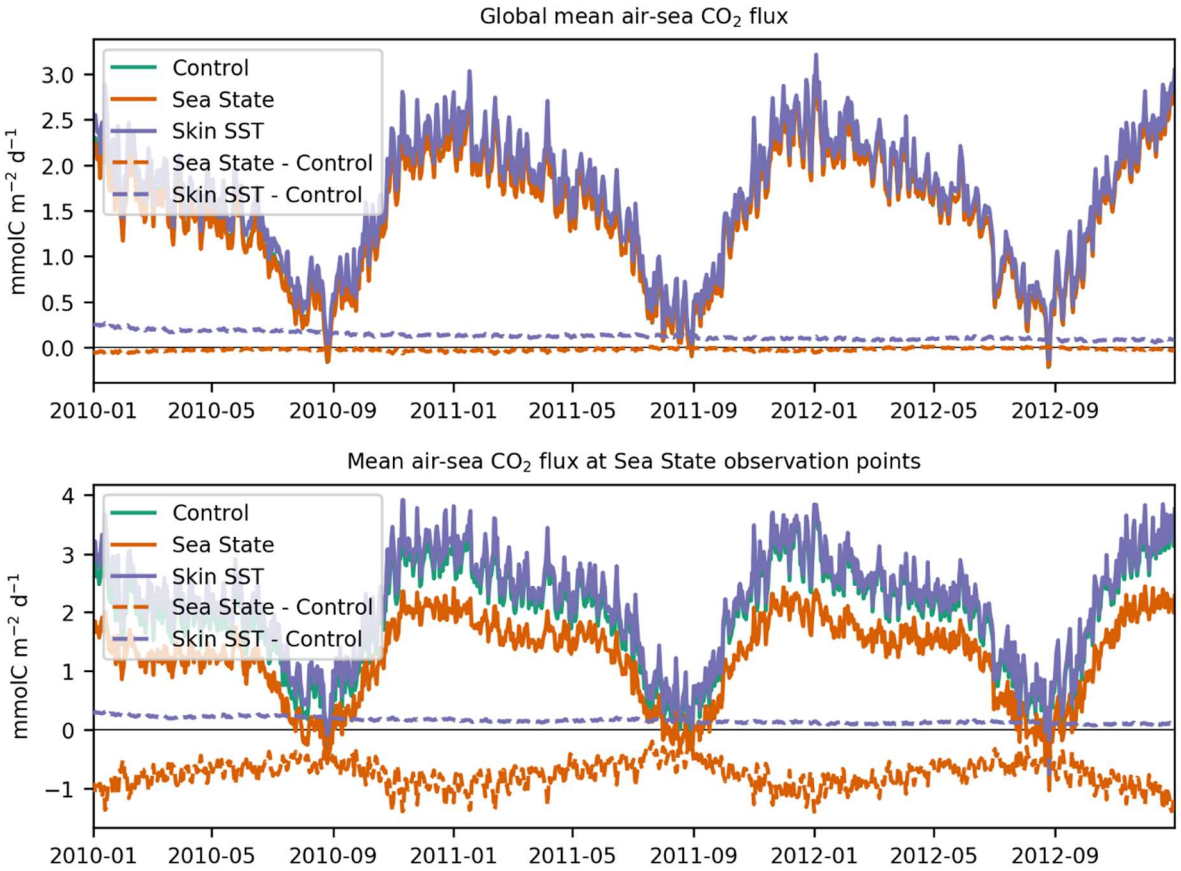

Figure 3.9.7: *Time series of mean air-sea CO_2 flux globally (top) and in grid cells with level 3 SS-CCI data (bottom) from each run and their difference to* Control.

Fig. 3.9.7 shows time series of mean air-sea CO_2 flux from the experiments globally and in model grid cells with SS-CCI data. Compared with *Control*, *Sea State* results in a small decrease in the global

mean air-sea CO_2 flux, which becomes much more significant when the comparison is restricted to points where SS-CCI data was available, and the parametrisation of Deike and Melville (2018) was used. This shows a large sensitivity to the use of H_s, and it is recommended that this be investigated further in future climate model development. H_s could be taken from SS-CCI data, a reanalysis like ERA5, or a coupled wave model. The decrease in air-sea CO_2 flux results in a corresponding decrease in sea surface pCO_2 and increase in pH.

In comparison, *Skin SST* results in an increase in air-sea CO_2 flux compared with *Control*, in line with the conclusions from observations of Watson et al. (2020). The magnitude of this decreases with time though, suggesting it to be a spin-up effect with the flux converging. This is being investigated further in longer runs outside of CMUG. The increased flux results in a corresponding decrease in pH.

Publications

Papers on biophysical feedbacks and the role of skin SST in air-sea CO_2 fluxes are planned.

The following CMUG paper has been published:

Ford, D. A.: Assessing the role and consistency of satellite observation products in global physical–biogeochemical ocean reanalysis, Ocean Sci., 16, 875–893, https://doi.org/10.5194/os-16-875-2020, 2020.

The following paper was published outside of CMUG, but on a related topic, using OC-CCI data, and with contribution from a CMUG scientist:

Skákala, J., Bruggeman, J., Ford, D., Wakelin, S., Akpınar, A., Hull, T., Kaiser, J., Loveday, B. R., O'Dea, E., Williams, C. A. and Ciavatta, S.: The impact of ocean biogeochemistry on physics and its consequences for modelling shelf seas, Ocean Modelling, 172, 101976, https://doi.org/10.1016/j.ocemod.2022.101976, 2022.

Interactions with the ECVs used in this experiment

There have been good interactions with the CCI ECV teams whose data are being used in this CMUG WP.

CMUG has had numerous interactions via email about user requirements and product availability with the marine ECV teams, as well as discussing the work with all relevant teams at the 2018 integration meeting, and reviewing the latest technical documents produced by the ocean colour, SST, sea state and sea level teams. Furthermore, plans and results were presented at a CSWG meeting in October 2020 focusing on SST, SSS and sea ice, with further discussion with the ECV teams present. CMUG also attended a SSS progress meeting in March 2021, and joint SSS-CMUG meeting in May 2021 to discuss working together. Results from the experiments, and plans for the next phase, have been discussed with relevant ECV teams at CCI meetings and by email through 2021 and 2022.

Consistency between data products

Validation of the two-way physics-biogeochemistry coupling runs has been performed against CCI data. Fig. 3.9.8 shows validation against level 4 SST-CCI data, brought up to date with the equivalent C3S data to cover the full period 2010-2019. *One-way free* shows a broad pattern of positive SST bias in low latitudes and negative SST bias elsewhere. *Two-way free* and *Two-way OC DA*, which mostly acted to increase SST, generally increased the error in low latitudes and decreased error elsewhere. The magnitude of the change due to two-way coupling was typically small compared with the overall biases in the original model. Similar validation against level 4 SSS-CCI data is shown in Fig. 3.9.9. This shows a less coherent pattern of errors than for SST, but with similar conclusions: two-way coupling reduces errors in some regions and increases them in others, with the changes introduced typically an order of magnitude smaller than the overall biases. Furthermore, quantitative statistical validation against CCI SST, SSS, and SSH, and OSI SAF sea ice concentration, shows minimal difference in global root mean square errors between the runs.

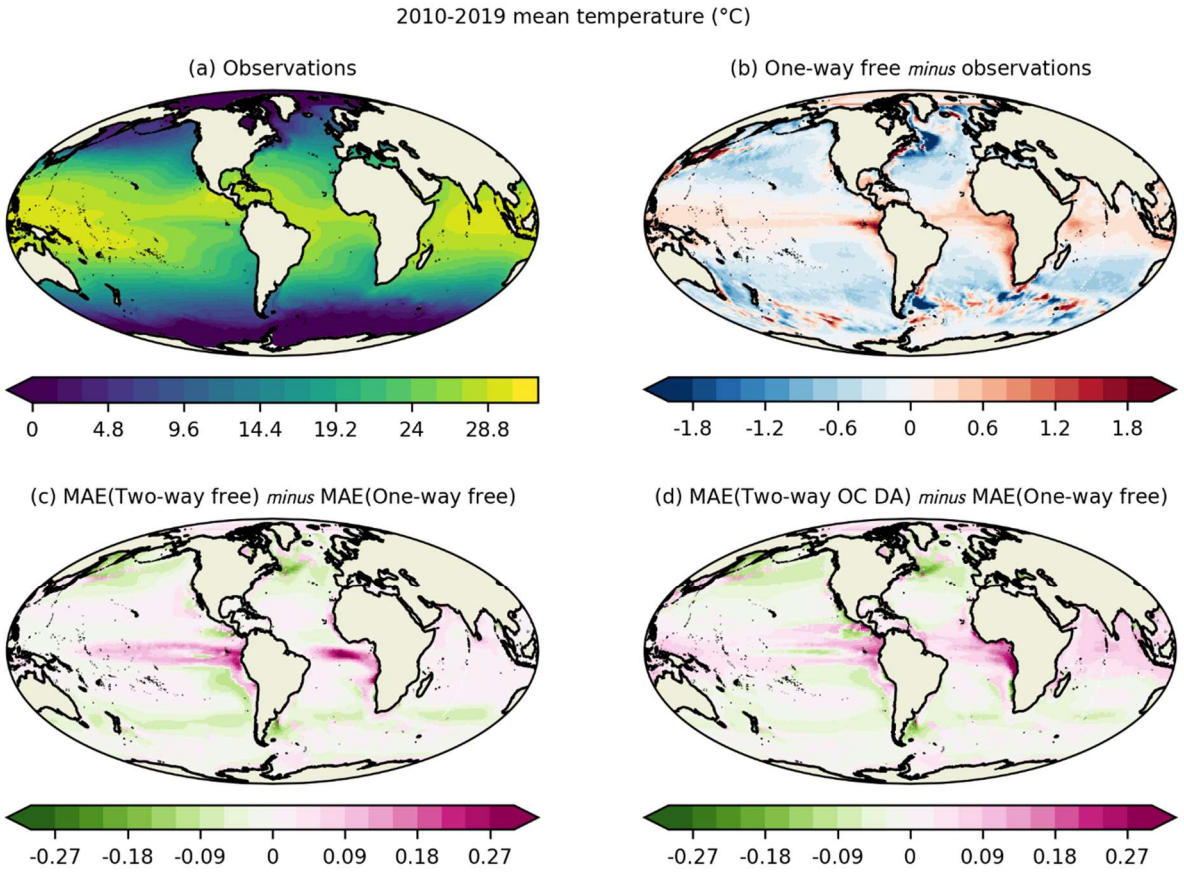

Figure 3.9.8: *a) Mean SST for 2010-2019 from SST-CCI/C3S data. b) Bias in* One-way free *compared with SST-CCI/C3S data. c) Mean absolute error in* Two-way free *compared with SST-CCI/C3S data minus mean absolute error in* One-way free *compared with SST-CCI/C3S data – green (negative) represents a reduction in error due to two-way coupling. d) Mean absolute error in* Two-way OC DA *compared with SST-CCI/C3S data minus mean absolute error in* One-way free *compared with SST-CCI/C3S data – green (negative) represents a reduction in error due to two-way coupling.*

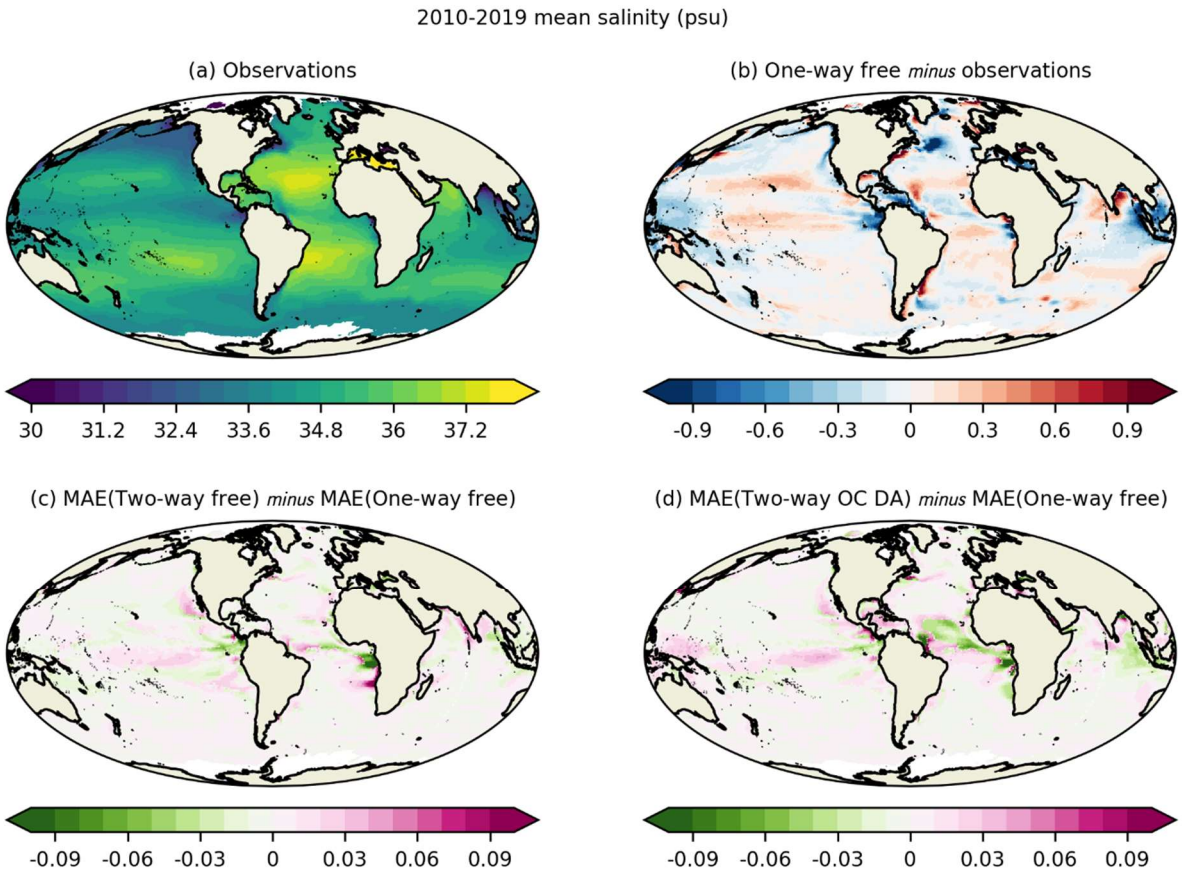

Figure 3.9.9: *a) Mean SSS for 2010-2019 from SSS-CCI data. b) Bias in* One-way free *compared with SSS-CCI data. c) Mean absolute error in* Two-way free *compared with SSS-CCI data minus mean absolute error in* One-way free *compared with SSS-CCI data – green (negative) represents a reduction in error due to two-way coupling. d) Mean absolute error in* Two-way OC DA *compared with SSS-CCI data minus mean absolute error in* One-way free *compared with SSS-CCI data – green (negative) represents a reduction in error due to two-way coupling.*

Validation was also performed against OC-CCI chlorophyll and novel primary production (Kulk et al., 2020) and phytoplankton carbon (Sathyendranath et al., 2020) products (not shown). These products were provided to CMUG by OC-CCI, and were derived from OC-CCI data as part of other ESA projects. Assimilating OC-CCI chlorophyll into *One-way OC DA* reduced errors compared with *One-way free* when validating against the chlorophyll and primary production products but gave a more mixed pattern for phytoplankton carbon. As with SST and SSS, two-way coupling reduced errors in some regions and increased them in others, with the changes small compared with the overall errors.

To assess the consistency of spatial features in different variables, and the impact of two-way coupling on this, 1/4° resolution versions of the experiments were run for 18 months from January 2010. Gradients of SST, SSS, SSH, and $\log_{10}$(chlorophyll) in the Gulf Stream region for May 2011 are shown in Fig. 3.9.10. The gradients were calculated from binned values at observation locations from CCI data and each of the model runs, following Ford (2020). In line with previous CMUG work a good correspondence can be seen between features in the observation products. *One-way free* shows broadly similar features, with some differences to the observation products. These are slightly modified in Two-way free, but with no clear improvement or degradation. The exception is in SSH, where the

eddies in the southwest of the region become more distinct, better matching the SL-CCI data. Interestingly, these then become less distinct in *Two-way OC DA*, despite improvements in the representation of gradients in $\log_{10}$(chlorophyll), and arguably slight improvements in SST and SSS gradients.

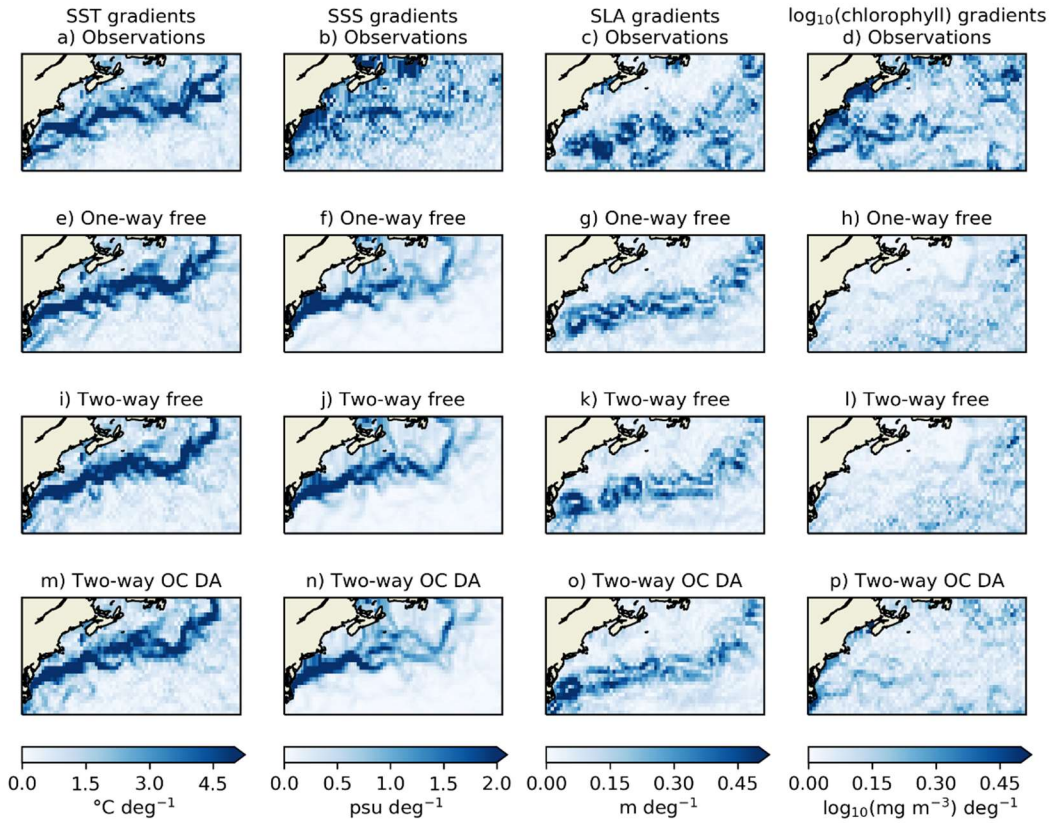

Figure 3.9.10: *Observed and modelled gradients in the Gulf Stream region for May 2011, following Ford (2020). Note SLA stands for Sea Level Anomaly which is the observed quantity and gradients in this variable (in panel c) are equivalent to those in SSH which are shown in panels g, k and o.*

Recommendations to the CCI ECV teams

Primary production and phytoplankton carbon are likely to be useful to modellers and could be considered as official CCI products in future.

3.10 Assessment of the potential of CCI/CCI+ data to constrain mineral dust simulations at the regional scale

Lead partner: BSC
Authors: Enza Di Tomaso, Jeronimo Escribano, Franco Lopez, Oriol Jorba,
Carlos Pérez García-Pando

Aim

This contribution aims at demonstrating the use of CCI/CCI+ data to produce dust analyses at the regional scale. Part of its findings has set the basis for the assessment activity 3.11 on the production of a pilot dust reanalysis, where the impact on dust cycles at a seasonal scale is evaluated.

Key Outcomes of CMUG Research

We have shown the benefit of assimilating CCI IASI retrievals of dust optical depth (using pixel-level uncertainty) by assessing its impact at regional scale in high resolution simulations during a summer period that included an exceptional dust storm in the Eastern Mediterranean. We have shown that the assimilation of the IASI thermal infrared retrievals compares well with the assimilation of MODIS visible retrievals of (coarse) dust optical depth. The MODIS-based analysis, however, is better correlated with independent observations than the IASI-based analysis. Additionally, we have implemented the CCI Medium Resolution Land Cover (LC) in our chemical weather system. We have shown that the CCI LC leads to better short-term forecast of 2 m air temperature and improves night-time surface ozone concentrations simulated over the Iberian Peninsula.

Summary of Results

The work done focused on the preparation of CCI aerosol data for the assimilation system, which included the processing of IASI dust aerosol data to follow the assimilation cycles, and the implementation of an observation operator for the thermal infrared. Assimilation experiments at high resolution were then performed over a regional domain involving relevant dust events.

Compared to a previous case study performed within the phase 2 of the aerosol_cci project, a more advanced assimilation of dust aerosol data was performed during this assessment activity with the aim of better demonstrating the use of CCI/CCI+ data to produce dust analyses at the regional scale. In particular the following novel aspects were introduced:

- Experiments were run on a regional scale to allow for high resolution simulations better representing the smaller features of dust events;
- Dust retrievals were assimilated at Level 2 resolution (circa 10 km) rather than Level 3 (1 degree) to avoid the propagation of observation uncertainties difficult to describe in a Level 3 product;

- Retrievals were assimilated at the original retrieval wavelength in the thermal infrared (10 μm) in order to avoid the introduction of errors due to the conversion to a different wavelength (e.g., in the visible part of the electromagnetic spectrum).

The preparation of the observations and of the assimilation system has involved three main tasks which have seen the contact with the Université Libre de Brussels's (ULB) retrieval team:

- IASI dust optical depth from Metop-A have been downloaded for the summer period of 2015. The period has been selected following the recommendation of the data providers: the most recent years of the IASI dust retrieval benefit of higher quality of the EUMETSAT ancillary data used in the retrieval algorithm.

- Retrievals have been filters using the two flags provided (pre_quality_flag=1 and post_quality_flag=1). The pre-quality flag is set depending on cloud coverage (only cloud free data are processed), while the post-quality flag removes unreliable retrievals.

- The observation operator has been built for dust aerosol optical depth at 10 μm. The operator consists in calculating the model equivalent of the observations, i.e. to map the model background state vector into the observation space. Hence it has two components: the horizontal interpolation component (model tracers are interpolated at the observation location), followed by the calculation of a total column extinction from a model mass concentration profile.

The extinction efficiency factors for 10 μm used in the latter calculation were estimated using the Mie scattering theory assuming dust spherical, non-soluble particles for the 8 model size bins, and, within a bin, a lognormal distribution for dust with geometric radius of 0.2986 μm and standard deviation of 2.0 (Klose et al., 2021). Information on refractive indices was taken from results of an experimental campaign (Di Biagio et al. 2017, 2019) rather than from the more commonly used OPAC database.

High resolution assimilation experiments over a regional domain including Northern Africa, the Middle East and Europe were performed at a 0.1° latitude × 0.1° longitude horizontal resolution and 40 hybrid pressure-sigma model layers. This domain configuration is used operationally to deliver daily forecasts at the World Meteorological Organisation Barcelona Dust Regional Center (https://dust.aemet.es/). IASI analyses were produced using Local Ensemble Transform Kalman Filter (LETKF) data assimilation in the Multiscale Online Non-hydrostatic AtmospheRe CHemistry model (MONARCH; Klose et al., 2021) developed at the Barcelona Supercomputing Center (BSC). We have applied spatial covariance localization by which the influence of an observation on the analysis decays gradually toward zero as the distance from the analysis location increases. The localization factor was set such that the observation influence practically fades to zero before 30 model grid points away from the observation location (in the horizontal plane).

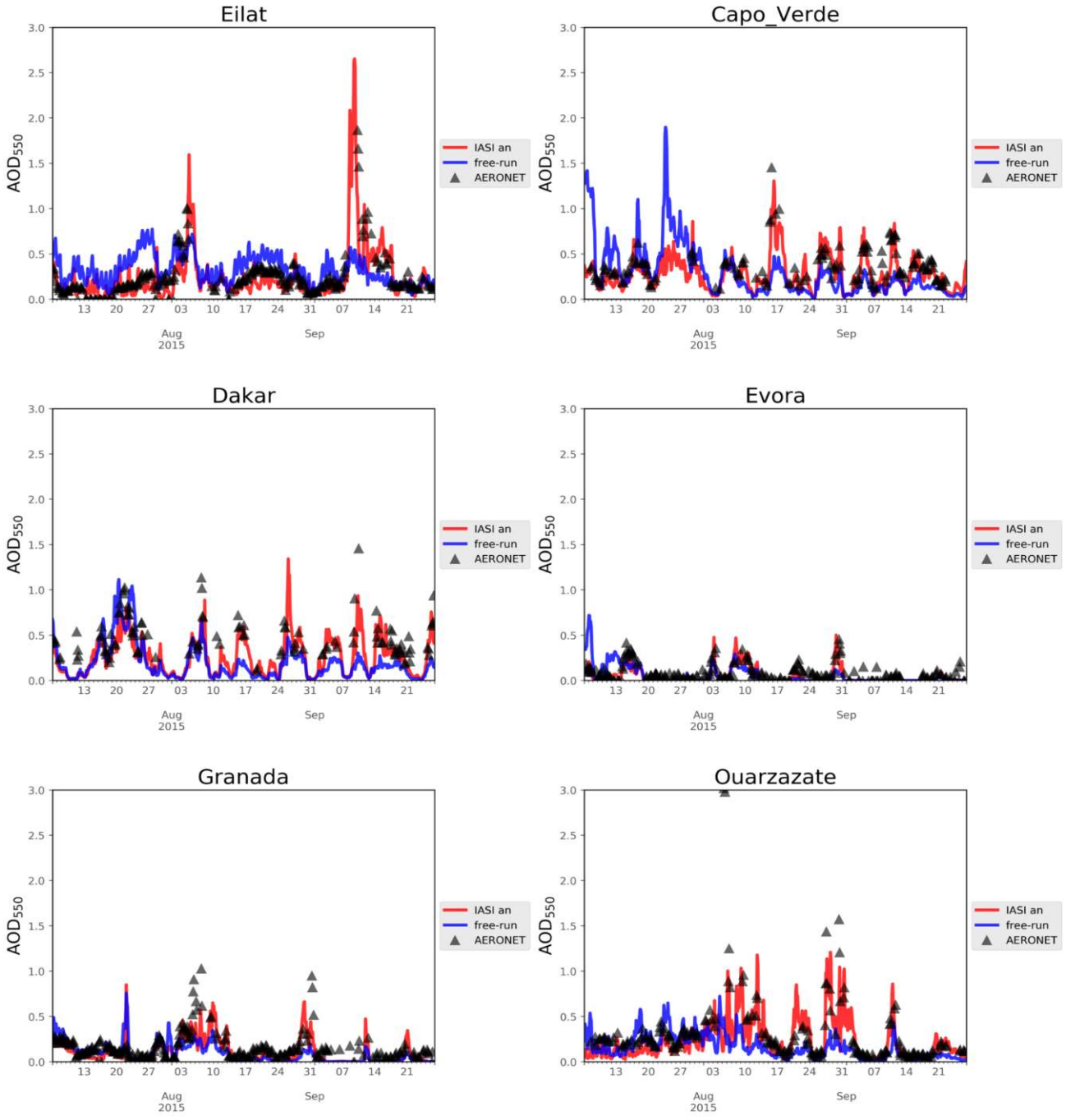

***Figure 3.10.1**: Time series of the dust AOD from the IASI analysis (red), the free-run simulation (blue) and independent ground-based observations (AERONET direct sun; black triangles) for summer of 2015 at Eilat (Israel), Capo Verde (right), Dakar (Senegal), Evora (Portugal), Granada (Spain) and Ouarzazate (Morocco).*

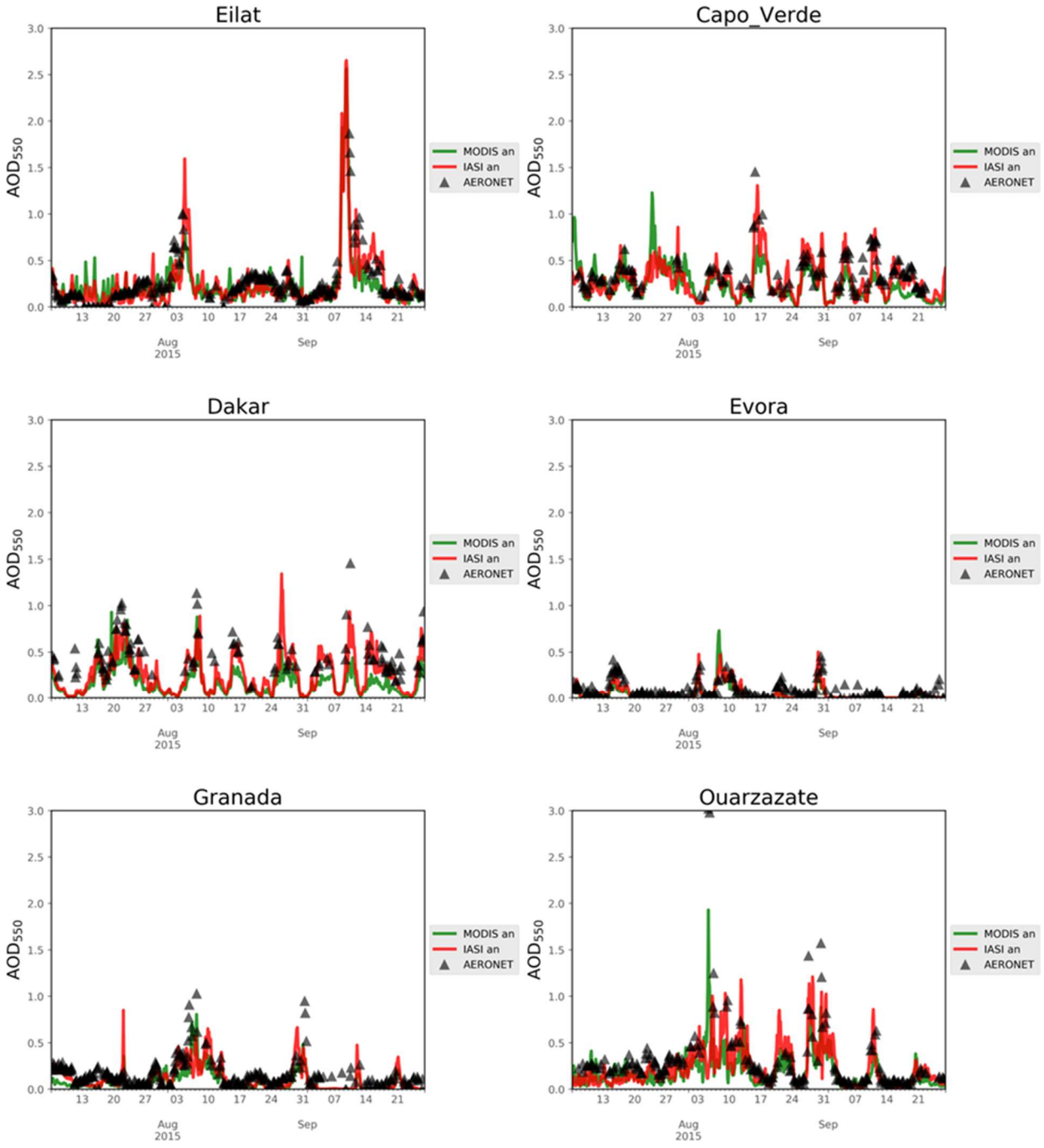

***Figure 3.10.2**: Timeseries of dust AOD from the IASI analysis (red), the MODIS analysis (green) and independent ground-based observations (AERONET direct sun; black triangles) for summer of 2015 at Eilat (Israel), Capo Verde (right), Dakar (Senegal), Evora (Portugal), Granada (Spain) and Ouarzazate (Morocco).*

The control variable is formulated in terms of the total mixing ratio over the 8 model prognostic variables (corresponding to different dust particle size bins) used to simulate the transport of dust in MONARCH. After the estimation of total dust mixing ratio analysis, the analysis increments are partitioned among the dust size bin according to their fractional contribution to the total mixing ratio in the forecast step. Figure 3.10.1 shows the IASI analysis for dust Aerosol Optical Depth (AOD) at 550 nm during a summer period in 2015 together with a free-run simulation (an ensemble simulation with no data assimilation) and with AERONET dust-filtered AOD values from the direct-sun algorithm (version 2, level 2.0) at 6 different locations. While the intensity of some events is underestimated by the IASI analysis, there is a general good agreement between the analysis simulation and the observations in the identification of the dust events both in the short- and long-range dust transport. The study period includes a remarkable dust event that occurred in the Eastern Mediterranean between the 6th and 13th of September 2015 that is well described by the IASI analysis at the Eilat AERONET station in Israel. Figure 3.10.2 shows that the IASI analysis compares well with a MODIS-based analysis produced by BSC with similar settings and resolution than the IASI analysis, with some of the dust events, for example in Granada (Spain) or Capo Verde, better depicted in one or the other analysis. Some of the differences between the two analyses might be due to a different coverage of the IASI and MODIS retrievals. Preliminary verification statistics show a higher correlation of the MODIS analysis (r=0.82) than the IASI analysis (r=0.76) with the AERONET observations shown in Figure 3.10.2 and a comparable root mean square error (RMSE=0.2).

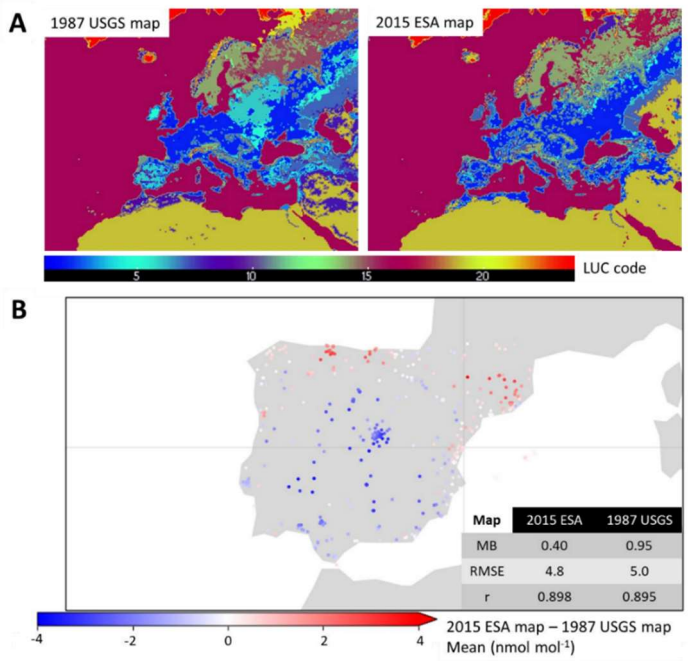

Figure 3.10.3: (A) 1987 USGS and 2015 ESA land cover maps of Europe. USGS 24-category codes were used in the maps. (B) Mean ozone surface concentration difference (nmol mol-1) between MONARCH simulations using the 2015 ESA land cover map and the 1987 USGS land cover map over the Iberian Peninsula EEA Air Quality e-Reporting sites for July 2019. Statistics for the simulation period are shown.

Additionally, we have implemented the CCI Land Cover in the meteorological driver of our MONARCH model. More specifically we have used the medium-resolution land cover CCI product that has been produced at a 300 m resolution (ESA, "Land Cover CCI Product User Guide Version 2", Tech. Rep., Available at: maps.elie.ucl.ac.be/CCI/viewer/download/ESACCI-LC-Ph2-PUGv2_2.0.pdf, 2017). Before this work, a map from the United States Geological Survey (USGS) was used by the meteorological driver of MONARCH.

In order to fulfil the modelling requirements, the CCI product was re-mapped to a 30" resolution map (using the dominant-class criteria), whereas the land use classes (LUCs) were re-mapped to the USGS 24-category codes following an equivalence matrix. This matrix was made by assigning to each of the ESA 37-category LUCs the USGS code that defines the same physical coverage of the surface. Two approaches were followed when no direct LUC code translation was possible, in order to choose a similar surface. For each land use class on a CCI LC map, the match frequency of LUCs on the USGS LC map was calculated. The LUCs with the highest match frequency were considered as the equivalent ones. On the other hand, following Pineda et al. (2004) method, for each LUC on both the CCI LC map and the USGS LC map, 10-day Normalized Difference Vegetation Index (NDVI) means for the year 2000 were calculated using VGT-S10 NDVI data (35 NDVI datasets, each one covering a 10-day period). The Gower's distance coefficient (Gower, 1971) was used to compare the LUCs based on the NDVI. The USGS LUC with the lowest Gower's distance coefficient was chosen as the best match for the CCI LUC.

Over Europe, most of the inland surfaces see a modification in the LUCs classification after updating the land cover map (Figure 3.10.3 - A). Particularly, over the Iberian Peninsula there is a change in the presence of some classes (Cropland/Woodland Mosaic appears in the 1987 USGS map, but it is not present in the 2015 ESA one), as well as a redistribution of classes such as Dryland Cropland and Pasture, Mixed Shrubland/Grassland, and Deciduous Broadleaf Forest. This result is due to both having used land cover information from a more recent year (2015 versus 1987) and the conversion of the ESA 37-category LUC codes into the USGS 24-categories.

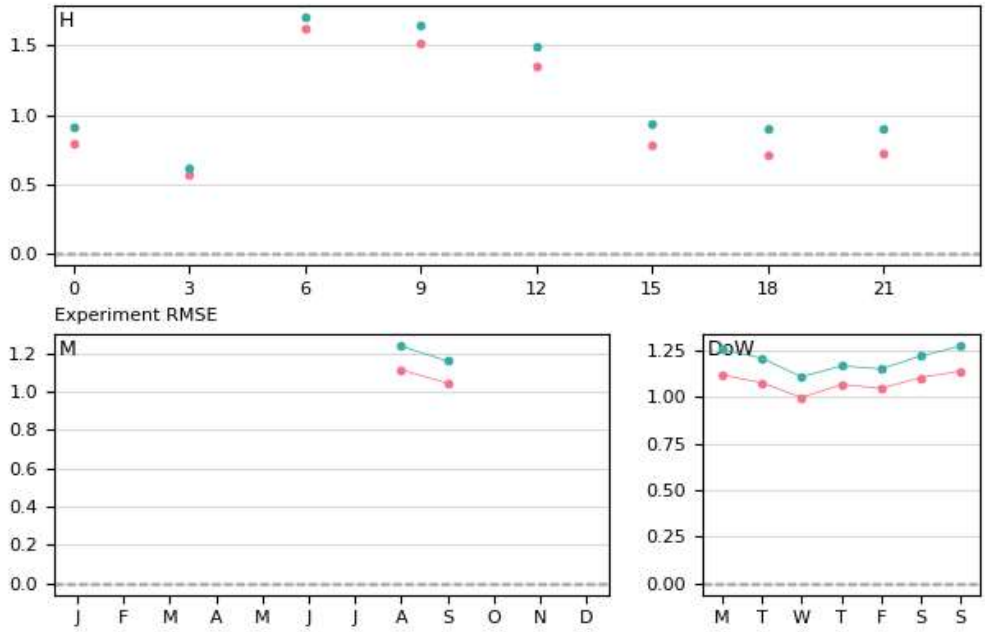

Figure 3.10.4: Evaluation of T2 for the European domain at urban NCDC-ISD stations: RMSE at a 3-hourly (top), monthly (bottom left) and day of the week (bottom right) basis when using the old USGS LC (green) and when using the CCI LC map (red) translated to the current land cover categories (USGS).

We have run MONARCH simulations to see the impact of this change in LC on key geophysical variables. The model was configured at a regional scale over Europe at the 0.2 degree latitude x 0.2 degree longitude horizontal resolution. The 2m air temperature (T2) has been evaluated over the European domain at National Climatic Data Center - Integrated Surface Database (NCDC-ISD) urban stations. Urban sites have been selected as defined by the MODIS MCD12C1 v6 IGBP classification. RMSE statistics are improved on an hourly, weekly and monthly basis when using the CCI LC (Figure 3.10.4). An improvement is seen also in coastal sites (not shown). Changes are seen also in dust aerosol concentration (not shown) but they are not significant when validated against AERONET observations. Please note that the dust emission scheme is only partially affected by this development since it uses additional information about land use which is decoupled from the meteorological driver.

Furthermore, we have looked at the impact of employing an updated land cover map on MONARCH simulations of ozone surface concentration. Modelling ozone surface concentration has several sources of uncertainty, with respect to biogenic and anthropogenic precursors emissions, chemical boundary conditions, chemistry formation, and deposition. Deposition velocity depends on biotic and abiotic parameters that, ultimately, are linked to the land use class. Simulation results for July 2019 show that changes in surface ozone were not homogeneous over the Iberian Peninsula when updating the LC information with the CCI product. Figure 3.10.3 (B) shows the differences of surface ozone between simulations with the new and old LC at European Environment Agency Air Quality e-Reporting (EEA-AQ) sites. Over the northern area there was an increase of the ozone concentration, whereas in the centre and southern areas lower surface concentration was simulated, compared to the simulation using the USGS map. Differences of up to 4 nmol mol-1 are identified in regions where spatial and categorical changes occurred between land cover maps. A better fit of the simulations to independent observations was obtained when using the CCI LC map compared to the USGS one, as found by calculating monthly statistics of mean bias (0.40 vs. 0.95), root mean square error (4.8 vs. 5.0) and correlation coefficient (0.898 vs. 0.895). Overall, the use of the CCI land cover map improved the simulation of ground-level ozone over the Iberian Peninsula. Surface ozone is improved mostly during night-time, most likely through changes in ozone deposition.

Publications

Klose et al. (2021).

Interactions with the ECVs used in this experiment

There have been interactions with Lieven Clarisse from the Université Libre de Brussels (ULB) on the IASI dust aerosol retrievals, and with Thomas Popp (DLR) during Colocation and Integration meetings held during the course of the project.

Consistency between data products

No inconsistencies could be found between the two ECV products considered in this study. We did not detect significant changes in dust aerosol concentrations when updating land cover information in the meteorological driver of our model.

Recommendations to the CCI ECV teams

The recommendation for the CCI LC team is to support future studies on the use of their products directly in dust emission schemes. Such studies are worth to be considered as they could potentially show a significant impact of the ESA LC on dust aerosol concentrations.
Please see recommendations in 3.11 for the aerosol CCI team.

3.11 Production of a pilot dust reanalysis at the regional scale

Lead partner: BSC
Authors: Enza Di Tomaso, Jeronimo Escribano, Carlos Pérez García-Pando, Oriol Jorba

Aim

This contribution aims at producing a pilot dust reanalysis based on CCI/CCI+ data, and at assessing whether their integration in model simulations can improve the monitoring of mineral dust and the characterization of dust cycles.

Key Outcomes of CMUG Research

1. A pilot IASI reanalysis for 1 year (2015) has been produced for a regional domain and at a high spatial resolution;
2. Some of the main features of the dust seasonal cycle are well represented by the IASI analysis during the year considered. However, dust concentrations in the winter months are particularly low when assimilating IASI dust retrievals;
3. The comparison with a MODIS-based reanalysis produced at the same spatial resolution showed that the IASI retrievals weaken the analysis of dust optical depth over some major emission areas;
4. The consistency of the assimilation procedure has been proven by the analysis of simulation departures from assimilated observations.

Summary of Results

This assessment activity is based on the results of the assessment activity 3.10 on the potential of CCI/CCI+ data to constrain mineral dust simulations at the regional scale. Initially, preparatory technical work was necessary on the refinement of the BSC technical infrastructure for high resolution (computationally demanding) IASI assimilation experiments to be run over a regional domain and over the longer (1 year) period of the pilot dust reanalysis, compared to what it is planned for selected dust events in 3.10. As part of this work, advances have been made in the BSC simulation workflow manager in order to improve the automatization of experiments and to optimize the storage of simulations' outputs. Subsequently, the assimilation of IASI dust Level 2 into a high-resolution regional simulation (0.1 x 0.1°) for a full year has been performed to produce a pilot study for a IASI dust reanalysis.

Deviation of plans: the pilot reanalysis is finally based on a dust aerosol CCI product with no use of CCI+ land cover information since high resolution land cover (HRLC) data was not available for this run. The production of a pilot reanalysis at high resolution and with an ensemble-based data assimilation is a computationally intensive task that had to be performed at a specific stage in the work

flow with the available computational resources. Given its restricted spatial availability on a small portion of the domain of interest, the HRLC would have been likely of a very minor impact on the reanalysis. The main features of the dust seasonal cycle are well represented by the IASI analysis and first-guess of Dust Optical Depth (DOD) as shown in Figure 3.11.1 (left and central column): for example, the mobilization of dust in the Taklamakan region in spring and in the Arabian peninsula during summer, the transport of south Saharan dust south-west toward the Gulf of Guinea during winter and spring, the shift toward northern latitudes of the plume originated in Western Africa and transported across the tropical Atlantic during summer, or low dust optical depth simulated everywhere in autumn. The lowest values of dust optical depth of the IASI analysis occur in the winter months, which deserve some further attention due to less accurate IASI dust retrievals in that season, as confirmed by the retrieval team. The analysis increments in Figure 3.11.1 (right column) show the impact of the observations, indicating the correction of some systematic overestimation (blue; in particular over emission source areas) or underestimation (red) of dust concentrations according to the IASI dust retrievals.

Figure 3.11.2 shows model simulation values (first-guess and analysis) collocated with the assimilated observations for IASI (DOD; top) and MODIS (DODcoarse; bottom). Retrievals (and consequently, analysis) of dust optical depth over the major emission areas of the domain, like the Bodélé depression in Chad and the Arabian desert, are considerably lower for IASI than MODIS. This might be due to IASI observations being less sensitive to surface layers of dust, as confirmed by the retrieval team.

Figure 3.11.3 shows that bias and standard deviation of departures from assimilated IASI observations calculated for the whole year of 2015 are reduced in the analysis compared to the first-guess, proving the consistency of our assimilation procedure.

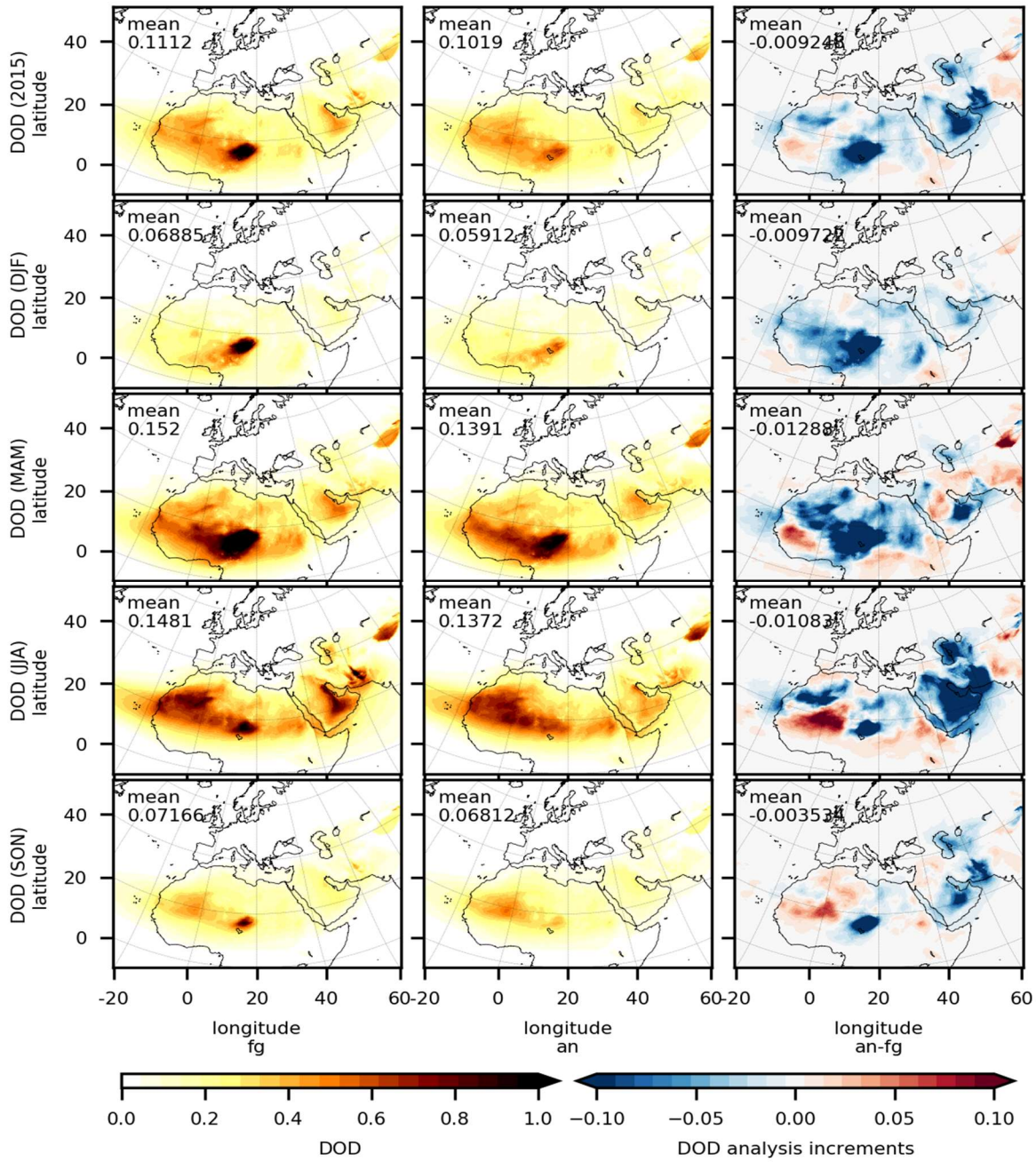

Figure 3.11.1: *Maps of first-guess simulations (left), IASI analysis (centre) and their difference (analysis increments; right) averaged for 2015 (first raw) and for different seasons of that year (raw 2 to 5).*

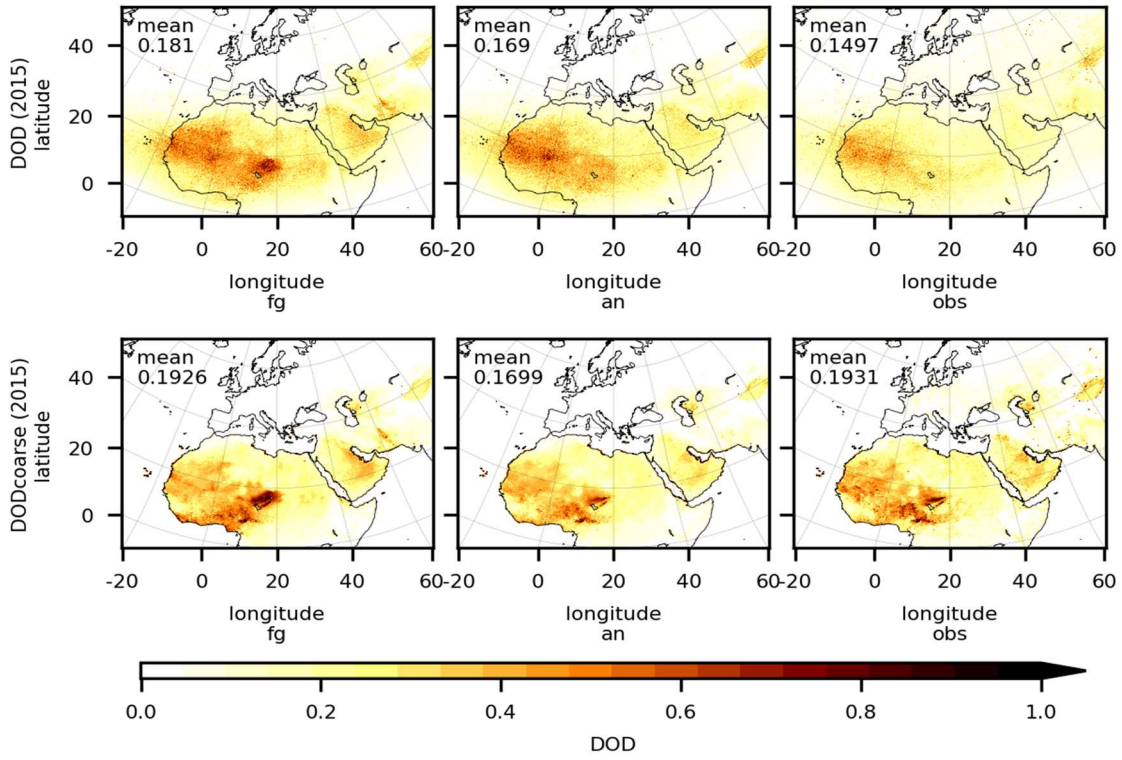

***Figure 3.11.2**: Collocated values of Dust Optical Depth (DOD) for IASI first-guess, analysis and observations (top), and collocated values of coarse Dust Optical Depth (DODcoarse) for MODIS first-guess, analysis and observations (bottom).*

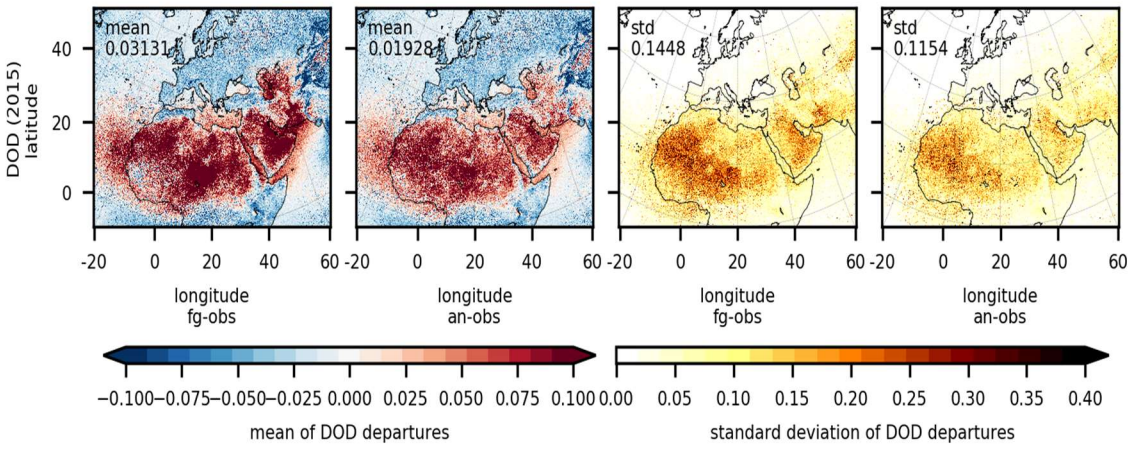

***Figure 3.11.3**: Bias and standard deviation of the departures of IASI assimilated observations from first-guess and analysis.*

Publications

None so far.

Interactions with the ECVs used in this experiment

There have been interactions with Lieven Clarisse from the Université Libre de Brussels (ULB) on the IASI dust aerosol retrievals, and with Thomas Popp (DLR) during Colocation and Integration meetings held during the course of the project.

Consistency between data products

As stated in 3.10, we did not detect significant changes in dust aerosol concentrations when updating land cover information in the meteorological driver of our model.

Recommendations to the CCI ECV teams

The recommendation for the CCI aerosol team is to support further studies on the exploitation of IASI observations for dust data assimilation in particular to deal with two aspects: the fact that IASI observations are less sensitive to surface layers of dust and that less accurate IASI dust retrievals are present in the ULB product in the winter season.

3.12 Integrated assimilation of the CCI+ Sentinel 3 AOD and Sentinel 5P ozone retrievals in the IFS

Lead partner: ECMWF
Authors: Rossana Dragani, Angela Benedetti

Aim

The aim of this research is to assess the impact of assimilating the CCI+ ozone retrievals from Sentinel 5P (S5P) and Aerosol Optical Depth (AOD) from the Sentinel 3 measurements to feed back to the Copernicus Climate Change Service (C3S) and Copernicus Atmosphere Monitoring Service (CAMS) reanalyses. It will address the following scientific questions:

1. Are the CCI+ ozone and aerosol data suitable for constraining a global reanalysis?
2. Assessment of the uncertainty characteristics provided with the CCI data using the ECMWF data assimilation system
3. Assess consistency between the two CCI data records via a data assimilation system and with independent observations
4. Assess consistency of the produced reanalysis with existing global reanalyses.

Summary of Work

S3 SLSTR AOD experiments

The assimilation experiments using the latest release of the SU SLSTR AOD product (v1.14) in the Integrated Forecast System in composition configuration used by CAMS, have been completed. A full report has been submitted to ESA via the AER CCI+ team, under which funding the work was completed. A key result of the study was to show the positive impact of the SLSTR data with respect to a run with no aerosol data assimilation. However, the best configuration as compared to the independent AERONET AOD dataset is still the one which uses MODIS and PMAP AODs in addition to the SLSTR data. Recent work has involved comparing the CISAR and SU SLSTR products to the CAMS reanalysis for 2020. This has been included in the Climate Assessment Report produced by the AER CCI+ team. Qualitative comparisons show that the SU SLSTR product is quite mature and compares relatively well with the CAMS renalysis, apart from some discrepancies already observed in 2019 and reported in previous versions of the CAR. However, the CISAR retrievals show poor agreement with the reanalysis AOD fields, possibly due to the fact that aerosol signal gets aliased into cloud signal in the retrieval.

S5P TCO3 experiments

Experiments were run over the period September-December 2020 to understand the impact of the S5P TCO3 (Total Column Ozone) observations provided by DLR (German Aerospace Center) using the retrieval of BIRA (Belgian Institute for Space Aeronomy) on the NWP configuration of the Integrated Forecast System. More specifically, the following data were used for the runs with the NRT product:

- NRTI data 01_020103 from 01/09/2020 until 02/12/2020
- NRTI data 01_020104 from 02/12/2020 until 30/12/2020

and, for the runs with the offline product,

- OFL data 01_020103 from 12/07/2020 until 29/11/2020

The analysis of the experiments shows a small but tangible impact of using the S5P TCO3 data on the NWP performance. A comparison of one-month assimilation experiments with the CCI+ S5P offline TCO3 product and the NRT (near real-time) TCO3 product shows that the performance of the NRT product is slightly better for certain aspects and slightly worse forothers. Longer experiments might be needed to be able to come to a firmer conclusion. Overall, there is no adverse impact of using the S5P TCO3 data in the NWP and it has been recommended to start using this dataset in the NWP operational configuration as it is done in the CAMS configuration.

This research has benefitted from the work performed within CAMS by Antje Inness and Roberto Ribas who are gratefully acknowledged. In particular, due to the high resolution of the S5P data, a preprocessing called *superobbing* has been put in place in order to be able to exploit these observations at the resolution of the analysis.

Some results are shown in the figures below. Standard scores, show a small but positive (and statistically significant) impact on the NWP resulting in a reduction of root mean square error for upper-level geopotential in the experiment with active S5P (NRT) data at day 1 (T+24) and day 2(T+48). A slight degradation is observed at T+12.

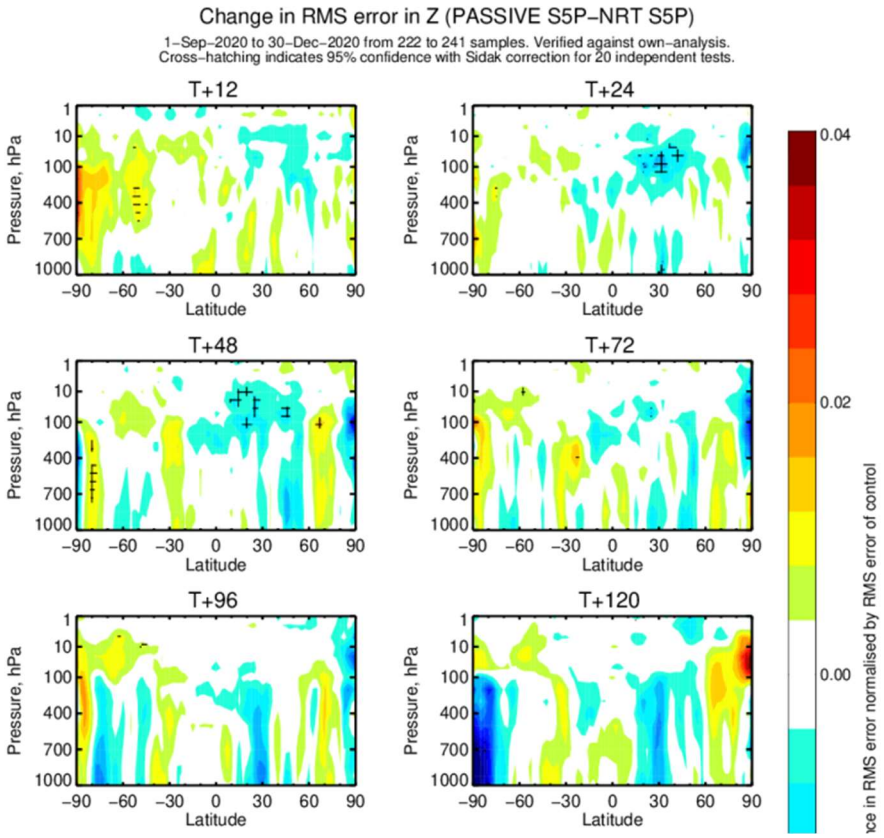

Figure 3.12.1*: Change in RMS error in geopotential for the experiment with passive S5P data compared to active S5P TCO3 data. Blue indicates a reduction in RMSE. Hatched areas are statistically significant at the 95% level.*

When looking at independent observations, particularly the infrared hyperspectral instruments, it is possible to see the role of the S53 TCO3 in improving the fit to the radiance observations at upper-levels. The improvement is mainly due to the Tropics with up to a 4% higher standard deviation in the experiments without S5P TCO3.

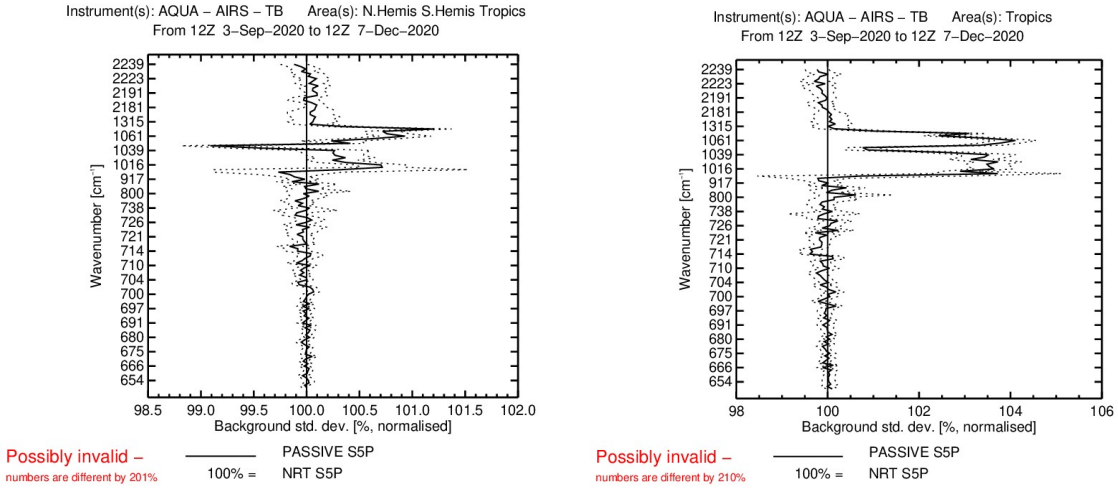

Figure 3.12.2*: Standard deviation of passive S5P TCO3 experiment with respect to NRT S5P TCO3 assimilation experiment (represented by the vertical 100% line). Note the increase of the std deviation at upper levels, particularly at the Tropics in the experiment without S5P TCO3 data.*

Similar plots were analyzed for the experiments with the offline S5P TCO3 CCI+ datasets for the month of September 2020. The impact of the offline dataset seems to be less positive than that of the NRT datasets (picture not show). It might be due to the fact that only one month of data were used and more extended experimentation is needed to come to final conclusions regarding the relative merits of the offline versus the NRT S5P TCO3 dataset. It is envisaged that the next CAMS reanalysis, scheduled to start at the beginning of 2024, will use the offline dataset rather than the NRT one. Datasets will have to be ready by mid-2023. Regarding the plans for the next meteorological reanalysis, ERA6, it is anticipated that the same data product will also be used. ERA6 production will start early 2024.

Publications

An article on the use of CCI data at ECMWF has appeared in the ECMWF Spring Newsletter. It can be found following this link: https://www.ecmwf.int/en/newsletter/171/news/use-esa-climate-change-initiative-data-ecmwfs-earth-system-model.

Interactions with the ECVs used in this experiment

During this phase of CMUG work there have been continuous interactions with the Aerosol and Ozone CCI ECV teams at the quarterly CSWG meetings and the Integration meetings and by personal contact, attendance at ECV project meeting, and email exchanges.

Consistency between data products

No inconsistencies were found for the S5P TCO3 datasets. Inconsistencies were found for the SLSTR AOD products: those have been reported in the latest version of the AER CCI+ CAR report.

Recommendations to the CCI ECV teams

Regarding the S5P TCO3, the differences in the offline and online versions of the datasets observed in the one-month experiments are not significant and no specific recommendations can be made. The offline dataset will be tested next year for inclusion in the next CAMS reanalysis which will start at the beginning of 2024. There are also plans to include the same product in ERA6. No problems are anticipated with the use of the S5P TCO3 products as those are very stable and consistent data records.

Regarding the SLSTR AOD datasets, feedback has been given directly to the AER team. It appears that the SLSTR SU v1.14 product is of good quality and compares qualitatively well with the CAMS reanalysis AOD. Some discrepancies were observed particularly in areas affected by anthropogenic pollution such as East Asia. Newer versions were not available for evaluation. It is not clear whether the SU SLSTR products will be used in the next CAMS reanalysis. EUMETSAT has developed a new retrieval algorithm based on the SU one and will provide NRT AOD data from SLSTR which are going to be tested both for the operational run and for the reanalysis. The CISAR SLSTR product needs refinements before it can be considered for validation of the CAMS system. In particular, the aerosol signal seems to be aliased into the cloud signal in the current version of the algorithm. While it is valuable that there is consistency between cloud and aerosol products derived from the same instrument, this aspect represents a challenge. More work is recommended on this new algorithm.

4. References

Acosta-Navarro JC, Ortega P, García-Serrano J, et al (2019) December 2016: Linking the Lowest Arctic Sea-Ice Extent on Record with the Lowest European Precipitation Event on Record. Bull Am Meteorol Soc 100:S43–S48. https://doi.org/10.1175/BAMS-D-18-0097.1.

Acosta-Navarro, J C, García-Serrano J, Lapin, V. and Ortega, P.: Added value of assimilating springtime Arctic sea ice concentration in summer-fall climate predictions, Environ. Res. Lett. 17, 064008, https://doi.org/10.1088/1748-9326/ac6c9b, 2022.

Ait-Mesbah,S. F. Cheruy , J.L. Dufresne F. Hourdin, On the representation of surface temperature in semi-arid and arid regions, Geophys. Res. Lett., 42(18), pp. 7572–7580, 2015, https://doi.org/10.1002/2015GL065553.

Albergel, C., Zheng, Y., Bonan, B., Dutra, E., Rodríguez-Fernández, N., Munier, S., Draper, C., de Rosnay, P., Muñoz-Sabater, J., Balsamo, G., Fairbairn, D., Meurey, C., and Calvet, J.-C.: Data assimilation for continuous global assessment of severe conditions over terrestrial surfaces, Hydrol. Earth Syst. Sci., 24, 4291–4316, https://doi.org/10.5194/hess-24-4291-2020, 2020.

Bellprat, O., F. Massonnet, S. Siegert, C. Prodhomme, D. Macias-Gómez, V. Guemas, F. Doblas-Reyes (2017) Uncertainty propagation in observational references to climate model scales. Remote Sensing of Environment. Volume 203, 15 December 2017, Pages 101-108. https://doi.org/10.1016/j.rse.2017.06.034.

Betts, A. K., Reid, D., & Crossett, C. (2020). Evaluation of the FLake Model in ERA5 for Lake Champlain. *Frontiers in Environmental Science*, *8*. https://doi.org/10.3389/fenvs.2020.609254

Cheruy F., A. Ducharne, F. Hourdin, I. Musat,, E. Vignon, G. Gastineau, V. Bastrikov. N. Vuichard, B. Diallo, J.L. Dufresne, J. Ghattas, J.Y. Grandpeix, A. Idelkadi, L. Mellul, F. Maigna, M. nenegoz, C. Ottlé, P. Peylin, F. Wang, Y. Zhao, Improved near surface continental climate in IPSL-CM6A-LR by combined evolutions of atmospheric and land surface physics. Journal of Advances in Modeling Earth System, 12, e2019MS002005, https://doi.org/10.1029/2019MS002005, 2020.

Cornes, R. C., van der Schrier, G., van den Besselaar, E. J. M., & Jones, P. D. (2018). An Ensemble Version of the E-OBS Temperature and Precipitation Data Sets. *Journal of Geophysical Research: Atmospheres*, *123*(17), 9391–9409. https://doi.org/10.1029/2017JD028200.

Dee, D. P., Uppala, S. M., Simmons, A. J., Berrisford, P., Poli, P., Kobayashi, S., Andrae, U., Balmaseda, M. A., Balsamo, G., Bauer, P., Bechtold, P., Beljaars, A. C. M., van de Berg, L., Bidlot, J., Bormann, N., Delsol, C., Dragani, R., Fuentes, M., Geer, A. J., … Vitart, F. (2011). The ERA-Interim reanalysis: configuration and performance of the data assimilation system. *Quarterly Journal of the Royal Meteorological Society*, *137*(656), 553–597. https://doi.org/10.1002/qj.828

Deike, L., & Melville, W. K. (2018). Gas transfer by breaking waves, Geophysical Research Letters, 45, 10,482– 10,492. https://doi.org/10.1029/2018GL078758.

Di Biagio, C., Formenti, P., Balkanski, Y., Caponi, L., Cazaunau, M., Pangui, E., Journet, E., Nowak, S., Caquineau, S., Andreae, M. O., Kandler, K., Saeed, T., Piketh, S., Seibert, D., Williams, E., and Doussin, J.-F. (2017). Global scale variability of the mineral dust long-wave refractive index: a new dataset of in situ measurements for climate modeling and remote sensing, Atmos. Chem. Phys., 17, 1901–1929, https://doi.org/10.5194/acp-17-1901-2017

Di Biagio, C., Formenti, P., Balkanski, Y., Caponi, L., Cazaunau, M., Pangui, E., Journet, E., Nowak, S., Andreae, M. O., Kandler, K., Saeed, T., Piketh, S., Seibert, D., Williams, E., and Doussin, J.-F. (2019). Complex refractive indices and single-scattering albedo of global dust aerosols in the shortwave spectrum and relationship to size and iron content, Atmos. Chem. Phys., 19, 15503–15531, https://doi.org/10.5194/acp-19-15503-2019

Ford, D. A.: Assessing the role and consistency of satellite observation products in global physical–biogeochemical ocean reanalysis, Ocean Sci., 16, 875–893, https://doi.org/10.5194/os-16-875-2020, 2020.

Gordon, H. B.; Rotstayn, L. D.; McGregor, J. L.; Dix, M. R.; Kowalczyk, E. A.; O'Farrell, S. P.; Waterman, L. J.; Hirst, A. C.; Wilson, S. G.; Collier, M. A.; Watterson, I. G.; Elliott, T. I. (2002). The CSIRO Mk3 Climate System Model. *Aspendale: CSIRO Atmospheric Research*. https://doi.org/10.4225/08/585974a670e09

Gower, J. C. (1971). A General Coefficient of Similarity and Some of Its Properties. Biometrics 27, no. 4: 857–71. https://doi.org/10.2307/2528823

Jacob, D., Petersen, J., Eggert, B., Alias, A., Christensen, O. B., Bouwer, L. M., Braun, A., Colette, A., Déqué, M., Georgievski, G., Georgopoulou, E., Gobiet, A., Menut, L., Nikulin, G., Haensler, A., Hempelmann, N., Jones, C., Keuler, K., Kovats, S, P. (2014). EURO-CORDEX: New high-resolution climate change projections for European impact research. *Regional Environmental Change, 14(2), 563–578*. https://doi.org/https://doi.org/10.1007/s10113-013-0499

Klose, M., Jorba, O., Gonçalves Ageitos, M., Escribano, J., Dawson, M. L., Obiso, V., Di Tomaso, E., Basart, S., Montané Pinto, G., Macchia, F., Ginoux, P., Guerschman, J., Prigent, C., Huang, Y., Kok, J. F., Miller, R. L., and Pérez García-Pando, C. (2021). Mineral dust cycle in the Multiscale Online Nonhydrostatic AtmospheRe CHemistry model (MONARCH) Version 2.0, Geosci. Model Dev., 14, 6403–6444, https://doi.org/10.5194/gmd-14-6403-2021.

Kotlarski, S., Keuler, K., Christensen, O. B., Colette, A., Déqué, M., Gobiet, A., Goergen, K., Jacob, D., Lüthi, D., van Meijgaard, E., Nikulin, G., Schär, C., Teichmann, C., Vautard, R., Warrach-Sagi, K., & Wulfmeyer, V. (2014). Regional climate modeling on European scales: a joint standard evaluation of the EURO-CORDEX RCM ensembleNo Title. *Geoscientific Model Development, 7(4), 1297–1333.* https://doi.org/10.5194/gmd-7-1297-2014

Kotlarski, S., Szabó, P., Herrera, S., Räty, O., Keuler, K., Soares, P. M., Cardoso, R. M., Bosshard, T., Pagé, C., Boberg, F., Gutiérrez, J. M., Isotta, F. A., Jaczewski, A., Kreienkamp, F., Liniger, M. A., Lussana, C., & Pianko-Kluczyńska, K. (2019). Observational uncertainty and regional climate model evaluation: A pan-European perspective. *International Journal of Climatology*, *39*(9), 3730–3749. https://doi.org/10.1002/joc.5249

Kulk G, Platt T, Dingle J, Jackson T, Jönsson BF, Bouman HA, Babin M, Brewin RJW, Doblin M, Estrada M, Figueiras FG, Furuya K, González-Benítez N, Gudfinnsson HG, Gudmundsson K, Huang B, Isada T, Kovač Ž, Lutz VA, Marañón E, Raman M, Richardson K, Rozema PD, Poll WHvd, Segura V, Tilstone GH, Uitz J, Dongen-Vogels Vv, Yoshikawa T, Sathyendranath S. Primary Production, an Index of Climate Change in the Ocean: Satellite-Based Estimates over Two Decades. Remote Sensing. 2020; 12(5):826. https://doi.org/10.3390/rs12050826.

Layden, A., Merchant, C., & MacCallum, S. (2015). Global climatology of surface water temperatures of large lakes by remote sensing. *International Journal of Climatology*, *35*(15). https://doi.org/10.1002/joc.4299

Lengaigne, M., Menkes, C., Aumont, O., Gorgues, T., Bopp, L., André, J. M., & Madec, G. (2007). Influence of the oceanic biology on the tropical Pacific climate in a coupled general circulation model. Climate Dynamics, 28(5), 503-516, https://doi.org/10.1007/s00382-006-0200-2.

MacCallum, S. N., & Merchant, C. J. (2012). Surface water temperature observations of large lakes by optimal estimation. *Canadian Journal of Remote Sensing*, *38*(1), 25–45. https://doi.org/10.5589/m12-010

Mallard, M. S., Nolte, C. G., Spero, T. L., Bullock, O. R., Alapaty, K., Herwehe, J. A., Gula, J., & Bowden, J. H. (2015). Technical challenges and solutions in representing lakes when using WRF in downscaling applications. *Geosci. Model Dev.*, *8*(4), 1085–1096. https://doi.org/10.5194/gmd-8-1085-2015

Merchant, C. J., Embury, O., Rayner, N. A., Berry, D. I., Corlett, G. K., Lean, K., Saunders, R. (2012). A 20 year independent record of sea surface temperature for climate from Along-Track Scanning Radiometers. *Journal of Geophysical Research*, *117*(C12), C12013. https://doi.org/10.1029/2012JC008400.

Pineda, N., O. Jorba, J. Jorge and J. M. Baldasano (2004) Using NOAA AVHRR and SPOT VGT data to estimate surface parameters: application to a mesoscale meteorological model, International Journal of Remote Sensing, 25:1, 129-143, https://doi.org/10.1080/0143116031000115201

Rouse, W. R., Blanken, P. D., Duguay, C. R., Oswald, C. J., & Schertzer, W. M. (2008). Climate-Lake Interactions. In *Cold Region Atmospheric and Hydrologic Studies. The Mackenzie GEWEX Experience* (pp. 139–160). Springer Berlin Heidelberg. https://doi.org/10.1007/978-3-540-75136-6_8

Reynolds, R. W., Rayner, N. A., Smith, T. M., Stokes, D. C., Wang, W., Reynolds, R. W., Rayner, N. A., Smith, T. M., Stokes, D. C., & Wang, W. An Improved In Situ and Satellite SST Analysis for Climate. https://doi.org/10.1175/1520-0442(2002)015<1609:AIISAS>2.0.CO;2, 2002.

Ruggieri P, Buizza R, Visconti G (2016) On the link between Barents-Kara sea ice variability and European blocking. J Geophys Res Atmospheres 121:5664–5679. https://doi.org/10.1002/2015JD024021.

Sathyendranath, S., Platt, T., Kovač, Ž., Dingle, J., Jackson, T., Brewin, R.J., Franks, P., Marañón, E., Kulk, G. and Bouman, H.A., 2020. Reconciling models of primary production and photoacclimation. *Applied Optics*, *59*(10), pp.C100-C114., https://doi.org/10.1364/AO.386252

Sevruk, B. (1985). Correction of precipitation measurements summary report. In: Correction of Precipitation Measurements. *Züricher Geographische Schriften, Vol. 23. Zürich: Geographisches Institut, Eidgenössische Technische Hochschule Zürich, Pp. 13– 23*.

Smith, D.M., Screen J.A., Deser C., et al (2019) The Polar Amplification Model Intercomparison Project (PAMIP) contribution to CMIP6: investigating the causes and consequences of polar amplification. Geosci Model Dev 12:1139–1164. https://doi.org/10.5194/gmd-12-1139-2019.

Tucker, S. O., Kendon, E. J., Bellouin, N., Buonomo, E., Johnson, B., Murphy, J. M. (2021). *Evaluation of a new 12km regional perturbed parameter ensemble over Europe (submitted)*.

Walters, D., Baran, A., Boutle, I., Brooks, M., Earnshaw, P., Edwards, J., Furtado, K., Hill, P., Lock, A., Manners, J., Morcrette, C., Mulcahy, J., Sanchez, C., Smith, C., Stratton, R., Tennant, W., Tomassini, L., Van Weverberg, K., Vosper, S., … Zerroukat, M. (2017). The Met Office Unified Model Global Atmosphere 7.0/7.1 and JULES Global Land 7.0 configurations. *Geoscientific Model Development Discussions*, 1–78. https://doi.org/10.5194/gmd-2017-291.

Wang, F., Cheruy F., Vuichard N., Hourdin, F., 2016 The impact of heat roughness length on surface meteorology in IPSL - CM model , AMA (Ateliers de Modélisation Atmosphérique), Toulouse, 18-22 Jan. 2016.

Wanninkhof, Rik, (2014), Relationship between wind speed and gas exchange over the ocean revisited, *Limnol. Oceanogr. Methods*, 12, https://doi.org/10.4319/lom.2014.12.351.

Watson, A.J., Schuster, U., Shutler, J.D. *et al.* Revised estimates of ocean-atmosphere CO_2 flux are consistent with ocean carbon inventory. *Nat Commun* **11,** 4422 (2020). https://doi.org/10.1038/s41467-020-18203-3.

While, J., Mao, C., Martin, M. J., Roberts-Jones, J., Sykes, P. A., Good, S. A., & McLaren, A. J. (2017). An operational analysis system for the global diurnal cycle of sea surface temperature: implementation and validation. *Quarterly Journal of the Royal Meteorological Society*, *143*(705), 1787-1803, https://doi.org/10.1002/qj.3036.